UTS UNIVERSITY OF TECHNOLOGY SYDNEY

Experimental and Numerical Study of Rubber Intermixed Ballast System Subjected to Monotonic and Cyclic Loading

by Chathuri Madhusanka Kulappu Arachchige

Thesis submitted in fulfilment of the requirements for the degree of

Doctor of Philosophy

under the supervision of Dr. Yujie Qi and Distinguished Professor Buddhima Indraratna

University of Technology Sydney
Faculty of Engineering and Information Technology

September 2022

CERTIFICATE OF ORIGINAL AUTHORSHIP

I, *Chathuri Madhusanka Kulappu Arachchige* declare that this thesis, is submitted in fulfilment of the requirements for the award of *Doctor of Philosophy*, in the *School of Civil and Environmental Engineering, Faculty of Engineering and Information Technology* at the University of Technology Sydney.

This thesis is wholly my own work unless otherwise referenced or acknowledged. In addition, I certify that all information sources and literature used are indicated in the thesis.

This document has not been submitted for qualifications at any other academic institution.

This research is supported by the Australian Government Research Training Program.

Signature:

Date:

ACKNOWLEDGEMENTS

I would like to express my enormous gratitude to Distinguished Professor Buddhima Indraratna for his excellent guidance and tireless supervision throughout the research. His support, patience, and encouragement truly helped me believe in myself and develop my skills.

I would also like to express my sincere acknowledgment to my principal supervisor Dr. Yujie Qi for her guidance, encouragement, and continual support throughout this research. Her constructive feedback, suggestions, and friendship have been invaluable during the course of my study. I also extend my sincere gratitude to Associate Professor Vinod Jayan and Professor Cholachat Rujikiatkamjorn for the kind support, suggestions and comments provided during my candidature.

Many thanks to the technical staff at University of Wollongong and University of Technology Sydney for providing technical support during the laboratory works and the field trial. I am also grateful to Bill Clayton for the professional editing of this thesis.

I thank my friends and colleagues at Transport Research Centre UTS for helping me professionally and personally whenever I need. I especially need to acknowledge my friends from Sri Lanka for their friendship, support, and company which helped me in many ways to make this journey easier and happier.

I extend my gratitude to Australian Research Council, ARC Industry Transformation Training Centre for Advanced Rail Track Technologies (ITTC-Rail) for the financial assistance. In addition, financial and technical assistance provided by the industry partners, including Bridgestone, Australasian Centre for Rail Innovation (ACRI), and Sydney Trains is gratefully acknowledged.

Particularly, I am indebted to my husband Amith Bodha Hanandige for his love, encouragement and support throughout the period of my studies. During the same time, we were blessed to have our son Kinneth Bodha Hanandige; since then, he has been there for me, helping myself to enjoy the ride a bit more. Finally, my heartfelt gratitude goes to my parents for their sacrifices, love and the support extended from the beginning.

LIST OF SYMBOLS

Letters

A	=	shift in the PSD curve after the test
A_L	=	area of the hysteresis loop
A_T	=	area of the triangle
B	=	area between the arbitrary boundary and the final PSD curve
a, b	=	Duncan and Chang model parameters
a_1, b_1	=	parameters associated with E_i
B_g	=	Marsal's breakage index
c	=	cohesion
C_c	=	coefficient of curvature
C_u	=	coefficient of uniformity
D	=	damping ratio
D_{max} , D_{min}	=	maximum and minimum particle size
D_r	=	relative density
d	=	dilatancy
E	=	secant modulus
E_i	=	initial tangent modulus
E_t	=	tangent modulus
E_{ur}	=	unloading modulus
E_{50}	=	secant modulus at 50% of the q_{peak}
E_d	=	strain energy density
$\hat{E}_d$	=	normalised strain energy density
E'_d	=	dissipated energy per cycle
e	=	void ratio
e_f	=	void ratio after the end of the test
e_i	=	void ratio at the beginning of the test
e_0	=	void ratio after the conditioning phase
F	=	Mohr-Coulomb failure envelope
f	=	frequency
F_s	=	shear yield function
G	=	specific gravity
G_B, G_R, G_s,	=	specific gravities of ballast, rubber, and RIBS respectively
G_f	=	specific gravity of fouling material
g	=	plastic potential
k_1, k_2	=	parameters associated with R_m

L	=	distance between two axles
M	=	mass
M_b	=	mass of ballast
M_c	=	critical state stress ratio
M_f	=	mass of fouling material
M_R	=	resilient modulus
m_s	=	mass of solids
N	=	number of cycles
P_4	=	percentage passing through 4.75 mm sieve (No 4)
P_{200}	=	percentage passing through 0.075 mm sieve (No 200)
p'	=	mean effective stress
q	=	deviator stress
q_{cyc}	=	cyclic deviator stress
$q_{cyc,max}$	=	maximum cyclic deviator stress
$q_{cyc,min}$	=	minimum cyclic deviator stress
q_f	=	deviator stress at failure
q_{peak}	=	peak deviator stress
q_{ult}	=	ultimate deviator stress
R_b	=	rubber content
R_f	=	ratio between q_f and q_{ult}
R_m	=	modification factor of hardening soil model
T	=	tonne
t	=	time
t_1, t_2	=	parameters associated with the permanent axial deformation model
U	=	distortional energy
V	=	train speed
V	=	total volume of the specimen
$V_{f'}$	=	volume of fouling material
V_{vb}	=	volume of voids
W_{ki}	=	percentage retained by weight in each sieve before test
W_{kf}	=	percentage retained by weight in each sieve after test

Greek letters

α, β	=	parameter associated with φ_p model
$\alpha_1, \alpha_2, \beta_1, \beta_2$	=	parameters associated with $k_1$and k_2
α', β'	=	parameter associated with distortional energy model
γ	=	shear strain
γ_d	=	dry unit weight
γ_f	=	shear strain up to the peak shear stress
γ_w	=	unit weight of water
γ^p	=	hardening parameter
$\dot{\gamma^p}$	=	rate of plastic shear strain
ε_1	=	Total permanent axial deformation
ε_1^e	=	elastic axial strain
ε_1^p	=	plastic axial strain
$\varepsilon_2^e, \varepsilon_3^e$	=	elastic lateral strains
$\varepsilon_a, \varepsilon_v, \varepsilon_r$	=	axial, volumetric and radial strains respectively
$\varepsilon_{a,1}$	=	axial deformation after first loading cycle
ε_i	=	axial deformation after monotonic conditioning phase
ε_q	=	deviator strain
ε_{rec}	=	recoverable strain
ε_v^p	=	plastic volumetric strain
$\dot{\varepsilon}_v^p$	=	rate of plastic volumetric strain
η	=	stress ratio
η_{peak}	=	peak deviator stress ratio
λ, μ	=	parameter associated with φ_p model
ν	=	poisson's ratio
σ	=	normal stress
σ_3'	=	effective confining pressure
τ	=	shear stress
φ	=	friction angle
φ_{cv}	=	critical state friction angle
$\varphi_{d=0}$	=	friction angle at phase transformation state
φ_{ef}	=	effective friction angle
φ_m	=	mobilised friction angle
φ_p	=	peak friction angle
ψ	=	dilation angle
ψ_m	=	mobilised dilation angle
ψ_p	=	dilation angle at peak stress ratio

Abbreviations

AC	=	Aggregate Crushing value
ARTC	=	Australian Rail Track Corporation
AREMA	=	American Railway Engineering and Maintenance of Way Association
BBI	=	Ballast Breakage Index
DAQ RIBS	=	Data Acquisition of RIBS Section
DAQ REF	=	Data Acquisition of Reference Section
DEM	=	Discrete Element Modeling
ELT	=	End-of-Life Tyres
FI	=	Fouling Index
FEM	=	Finite Element Modeling
IMRT	=	Iran Ministry of Roads and Transportation
LAA	=	Loss Angeles Abrasion value
LVDT	=	Linear Variable Differential Transducer
MDD	=	Maximum Dry Density
MGT	=	Million Gross Tons
NSW	=	New South Wales
PSD	=	Particle Size Distribution
PTZ	=	Pan-Tilt-Zoom
RC	=	Rubber Crumbs
RIBS	=	Rubber Intermixed Ballast System
R & D	=	Research and Development
T5	=	Traffic Classification T5
TDA	=	Tyre Derived Aggregates
TfNSW	=	Transport for New South Wales
USP	=	Under Sleeper Pads
VCI	=	Void Contamination Index
WA	=	Wet Attrition value

TABLE OF CONTENTS

CERTIFICATE OF ORIGINAL AUTHORSHIP i
ACKNOWLEDGEMENTS ii
LIST OF SYMBOLS iv
TABLE OF CONTENTS viii
LIST OF FIGURES xii
LIST OF TABLES xvi
LIST OF PUBLICATIONS xvii
ABSTRACT xix
1 INTRODUCTION 1
1.1 General Background 1
1.2 Research Motivation 5
1.3 Objectives and Scope 7
1.4 Thesis Outline 8
CHAPTER TWO 12
2 LITERATURE REVIEW 12
2.1 Introduction 12
2.2 End-of-Life Tyres (ELT) 13
2.2.1 Scrap Tyre Products 14
2.3 Ballast 15
2.3.1 Factors affecting ballast behaviour 16
2.3.2 Ballast fouling 17
2.4 Behaviour of Granular/Ballast Material under Monotonic Loading 19
2.5 Behaviour of Granular/Ballast Material under Cyclic Loading 24
2.6 Use of Elastic Tyre Aggregates in Railway Substructure 28
2.7 Constitutive Modelling 38

2.8 Field Testing for Mixtures of Ballast and Granular Rubber.....41
2.9 Chapter Summary.....42
CHAPTER THREE ..... **Error! Bookmark not defined.**
3 MATERIALS AND TESTING PROGRAMME.....44
3.1 Introduction 44
3.2 The Sizes of Rubber Granules.....44
3.2.1 Particles prone to breakage 45
3.2.2 Shape of rubber particles.....48
3.2.3 Criteria for assessing durability 50
3.3 Test Materials and Laboratory Test Plan.....50
3.4 Sample Preparation and Test Setup.....55
3.5 Monotonic Shearing 59
3.6 Cyclic Loading 60
3.7 Chapter Summary.....61
CHAPTER FOUR ..... **Error! Bookmark not defined.**
4 BEHAVIOUR OF RIBS MIXTURES UNDER MONOTONIC LOADING 63
4.1 Introduction 63
4.2 Stress-Strain Response 63
4.3 Dilatancy Behaviour.....66
4.4 Modulus Degradation 70
4.5 Friction Angle and Dilation Angle 74
4.6 Ballast Breakage.....80
4.7 Energy Absorption 83
4.7.1 Strain energy density.....83
4.7.2 Effect of replaced rubber and distortional energy.....86
4.8 Critical State Behaviour 88
4.9 Chapter Summary.....91
CHAPTER FIVE ..... **Error! Bookmark not defined.**
5 BEHAVIOUR OF RIBS MIXTURES UNDER CYCLIC LOADING 92

5.1 Introduction 92
5.2 Loading Procedure 93
5.3 Void Ratio 95
5.4 Permanent Deformation Behaviour 97
5.4.1 Axial strain 97
5.4.2 Volumetric strain 103
5.5 Resilient Modulus 105
5.6 Damping Ratio and Energy Dissipation Capacity 107
5.7 Ballast Degradation under Cyclic Loading 109
5.8 Chapter Summary 111
CHAPTER SIX 113
6 ASSESSING THE OPTIMAL RUBBER CONTENT 113
6.1 Introduction 113
6.2 Conventional Ballast as the Reference 114
6.3 Proposed Acceptance Criteria for RIBS 116
6.4 Optimising the Amount of Rubber 117
6.5 Justifying the Optimal $R_b\%$ in RIBS Mixture under Cyclic Loading 122
6.6 Drainage Potential 123
6.7 Initial Compaction Characteristics 124
6.8 Chapter Summary 125
CHAPTER SEVEN 127
7 CONSTITUTIVE MODELLING OF BALLAST-RUBBER MIXTURES 127
7.1 Introduction 127
7.2 Strain Softening/Hardening Model 128
7.2.1 Hardening soil model 129
7.2.2 Shear hardening 133
7.2.3 Flow rule and plastic potential 134
7.3 Model Validation 138
7.3.1 Model parameters and calibration 138

7.3.2 Model validation using test data 141
7.4 Model Limitations 146
7.5 Chapter Summary 146
CHAPTER EIGHT 147
8 PRACTICAL APPLICATIONS AND LIMITATIONS 147
8.1 Introduction 147
8.2 Practical Application of RIBS in a Trial Track 147
8.2.1 Design of track 148
8.2.2 Construction of track 153
8.2.3 Observations and considerations during construction 158
8.2.4 Monitoring and test outcomes 159
8.3 Limitations of RIBS 159
8.4 Chapter Summary 161
CHAPTER NINE ..... **Error! Bookmark not defined.**
9 CONCLUSIONS AND RECOMMENDATIONS 162
9.1 Introduction 162
9.2 Geotechnical Characteristics of RIBS under Static Loading 162
9.3 The Response of RIBS under Cyclic Loading 164
9.4 Optimal Amount of Rubber in RIBS Mixtures 166
9.5 Constitutive Modelling 166
9.6 Practical Applications and Limitations 167
9.7 Recommendations for Future Works 169
REFERENCES 171
APPENDIX A: Calculation of Material Quantities for the Specimens 185
APPENDIX B: Design Calculations of RIBS Track 187

LIST OF FIGURES

Figure 2.1 The influence of confining pressure on the angle of internal friction (adopted from Indraratna et al., (1998)).....20

Figure 2.2 Ballast Breakage Index (Indraratna et al., 2005).....22

Figure 2.3 The effect of particle breakage, dilatancy and confining pressure on the friction angle of latite basalt, as investigated by Indraratna and Salim (2002).....23

Figure 2.4 Strain response under cyclic loading (adopted from Sun et al., 2016).....26

Figure 2.5 An example of the shakedown mechanism (adopted from Sun et al., 2016) 27

Figure 2.6 Definition of the resilient modulus, M_R.....27

Figure 2.7 Particle size distribution of ballast mixed with rubber that was used in the study by Sol-Sanchez et al., (2015).....30

Figure 2.8 Settlements and energy dissipation capacity (adopted from Sol-Sanchez et al., 2015).....31

Figure 2.9 Stiffness modulus and damping ratio with diverse % of TDA (data source Esmaeili et al., 2016).....32

Figure 2.10 Settlement of ballast with different R_b% under cyclic loading (after Fathali et al., 2016 and Sol-Sanchez et al., 2015).....33

Figure 2.11 Comparison of particle breakage for ballast with different R_b% (adopted from Fathali et al., 2016).....34

Figure 2.12 Rate of energy consumption against the rate of particle breakage (Adopted from Indraratna and Salim (2002).....40

Figure 3.1 Marsal's breakage index, ($B_g = \Delta Wk > 0$) for pure ballast (latite basalt)..46

Figure 3.2 Different size rubber granules.....49

Figure 3.3 Evaluation of best particle size for rubber granules.....49

Figure 3.4 Particle size distribution of RIBS and rubber granules.....52

Figure 3.5 Ballast material preparation (a) vibrating shaker, (b) washing, (c) drying, and (d) prepared ballast.....53

Figure 3.6 Ballast mixed with rubber, (a) conventional Ballast, (b) rubber granules, and (c) RIBS with R_b=5%.....54

Figure 3.7 Laboratory testing program.....55

Figure 3.8 Schematic illustration of the large-scale triaxial testing system (modified after Sun, 2015).....56

Figure 3.9 Sample preparation and test setup: (a) prepared RIBS material (R_b=5%), (b) 7mm membrane supported by two split moulds, (c) compacting the layers with a vibrating plate, (d) last layer of RIBS (R_b=5%), (e) prepared sample, (f) a sample is placed inside the outer cell chamber, and (g) setup of the large scale triaxial apparatus. 58

Figure 4.1 Effect of the rubber on: (a-c) deviator stress-axial strain curves; (d-f) volumetric-axial strain curves 64

Figure 4.2 Variation of deviatoric stress ratio with axial strain 68

Figure 4.3 (a–c) Dilation-stress ratio responses of RIBS under different effective confining pressures: (a) 10 kPa, (b) 30 kPa and (c) 60 kPa; (d) maximum dilatancy with rubber content 69

Figure 4.4 Hyperbolic approximation (after Duncan and Chang (1970)) 70

Figure 4.5 Initial tangent modulus,E_i 71

Figure 4.6 (a) Secant modulus degradation of pure ballast and RIBS (σ_3' = 60 kPa); (b) secant modulus degradation of RIBS at $\eta peak$ against the rubber content 73

Figure 4.7 Effect of the rubber on (a) effective friction angle (φ_{ef}), friction angle at $\eta peak$ (φ_p) (b) dilation angle ψ at η_{peak} 76

Figure 4.8 Effect of confining pressure (σ_3') on φ_p of pure ballast (R_b=0) 77

Figure 4.9 (a) Effect of rubber content (R_b) on φ_p of RIBS (R_b >0) (b) Relationship of α/β with confining pressure, ($R_b > 0$) 78

Figure 4.10 Comparison of peak friction angle, φ_p from the current study with a previous study by Indraratna et al., (1998). 79

Figure 4.11 Influence of R_b on ballast breakage index (BBI) 81

Figure 4.12 Influence of R_b on Marsal's breakage index, $B_g = \Delta W_k > 0$ 82

Figure 4.13 Particles passed through 4.75 mm sieve (after the shearing test at $\sigma 3' = 30\ kPa$) 83

Figure 4.14 (a) Shear strain versus shear stress σ_3'= 10 kPa, and (b) normalised strain energy densities variation against the rubber content. 85

Figure 4.15 Incremental distortional energy (ΔU) 86

Figure 4.16 Distortional energy (U) due to R_b% replaced with the same size of ballast particles at a given deviator strain (ε_q^*) 87

Figure 4.17 The relationship of α' and β' in terms of R_b% for the specimens tested at (a) $\sigma_3' = 30\ kPa$ and (b) $\sigma_3' = 60\ kPa$ 88

Figure 4.18 Estimation of the critical state stress ratio employing the stress ratio and dilatancy 89

Figure 4.19 Estimation of the critical state stress ratio employing the stress ratio and volumetric strain.....90

Figure 4.20 3D surface plot of the critical stress ratio, M_c 91

Figure 5.1 Vertical cyclic stresses, q_{cyc} transmitted to the ballast layer underneath the rail by 25 t axle load coal train with wagons (adopted from Indraratna et al., 2010) 93

Figure 5.2 Details of the loading procedure.....95

Figure 5.3 Void ratio (e) of the specimens at the beginning of the test e_i, after the conditioning phase e_0 and at the end of the test e_f 96

Figure 5.4 Permanent axial deformation after the monotonic conditioning phase εi 97

Figure 5.5 (a-b) Axial strain response of RIBS mixtures under effective confining pressures: (a) 30 kPa (b) 60 kPa; (c-d) rate of axial strain variation of RIBS mixtures under effective confining pressures: (c) 30 kPa (d) 60 kPa 99

Figure 5.6 Empirical modelling for permanent axial deformation under cyclic loads .102

Figure 5.7 (a-b) Volumetric strains (dilation) of RIBS mixtures under effective confining pressures: (a) 30 kPa (b) 60 kPa; (c-d) volumetric strain rates with respect to number of cycles under effective confining pressures: (c) 30 kPa (d) 60 kPa 104

Figure 5.8 Variation of M_R of RIBS mixtures against the rubber content, $R_b\%$ 105

Figure 5.9 Variation of resilient modulus of RIBS mixtures against the number of cycles under effective confining pressures: (a) 30 kPa (b) 60 kPa 106

Figure 5.10 Definition of the damping ratio and the dissipated energy per cycle 108

Figure 5.11 (a-b) Variation of the damping ratio against the number of cycles under effective confining pressures: (a) 30 kPa, (b) 60 kPa; (c-d) variation of dissipation energy against the number of cycles under effective confining pressures: (c) 30 kPa, (d) 60 kPa 108

Figure 5.12 Influence of R_b on Ballast Breakage Index, BBI 110

Figure 5.13 Patterns of ballast breakage 111

Figure 6.1 Typical ballasted track cross-section.....115

Figure 6.2 Effective friction angle of rubber -ballast mixtures.....118

Figure 6.3 Optimisation of the rubber content according to the ballast breakage index and associated axial strain.....119

Figure 6.4 Higher E/E_i at η_{peak} compared to the pure ballast.....120

_Toc103895203Figure 6.5 Higher energy absorption in RIBS compared to pure ballast 121

_Toc103895204Figure 6.6 Optimisation of the rubber content according to the resilient modulus and energy dissipation per cycle 123

_Toc103895205Figure 7.1 Hyperbolic approximation for non-linear stress–strain relationship of soils 129

_Toc103895206Figure 7.2 Effect of the rubber content (R_b) on $E_i/\sigma_3^{'}$: (a) data from the current study, and (b) data from Song et al., 2019 132

Figure 7.3 (a) The linear variation of $k1$ against R_b (b) The linear variation of $k2$ against σ_3' 137

Figure 7.4 Predicted E_i versus E_i from tests 139

Figure 7.5 Deviator stress-axial strain curves from the test results and model predictions for pure ballast and RIBS with different R_b contents: (a) σ_3' =10 kPa; (b) σ_3' =30 kPa; (c) σ_3' =60 kPa. 142

Figure 7.6 Deviator stress-axial strain curves from the test results and model predictions for pure ballast and rubber-ballast mixtures with different R_b contents (test data from: Song et al., 2019) (a) σ =50 kPa; (b) σ =100 kPa; (c) σ =150 kPa. 143

Figure 7.7 Volumetric strain-axial strain curves from the test results and model predictions for pure ballast and RIBS with different R_b contents: (a) σ_3' =10 kPa; (b) σ_3' =30 kPa; (c) σ_3' =60 kPa. 144

Figure 7.8 Volumetric strain- axial strain curves from the test results and model predictions for pure ballast and rubber-ballast mixtures with different R_b contents (test data from: Song et al., 2019): (a) σ =50 kPa; (b) σ =100 kPa; (c) σ =150 kPa. 145

Figure 8.1 Soil sampling refusal at proposed RIBS section of track 149

Figure 8.2 Plan view and cross-section of instrumentation 151

Figure 8.3 Mixing the ballast and rubber granules at the site (a) the materials before mixing, and (b) volumetric mixer while producing RIBS 153

Figure 8.4 Ground preparation (a) excavation starts from the centreline of the track, and (b) the drainage layer on top of the subgrade is separated by a non-woven geotextile 154

Figure 8.5 Particle size distribution of capping material 155

Figure 8.6 Non-destructive density testing for the capping layer 156

Figure 8.7 Data acquisition system 156

Figure 8.8 Stages of RIBS track construction 158

Figure 8.9 Particle size distribution of RIBS in the field trial 161

LIST OF TABLES

Table 2.1 The specific gravity of tyre derived aggregates 15

Table 2.2 Ballast grading requirements AS 2758.7(2015) 17

Table 2.3 Fouling classification (Selig and Waters, 1994) 18

Table 2.4 Empirical models developed to determine the permanent axial strain after any number of cycles 25

Table 2.5 Summary of previous studies for ballast-rubber mixtures under cyclic loads 37

Table 3.1 Particle sizes most likely to break 47

Table 3.2 Characteristics of Latite Basalt (after Indraratna et al., (1998)) 51

Table 3.3 Basic properties of RIBS 59

Table 3.4 Monotonic loading triaxial program 60

Table 3.5 Cyclic loading triaxial program 61

Table 4.1 Effective friction angle of pure ballast and RIBS 74

Table 5.1 Empirical parameters of the model for permanent axial deformation 103

Table 7.1 Model parameters used for the validation 140

Table 8.1 List of the instruments 152

LIST OF PUBLICATIONS

A. Journal Papers

Arachchige, C.M.K, Indraratna, B., Qi, Y., Vinod, J.S. and Rujikiatkamjorn, C. (2021). "Geotechnical characteristics of a Rubber Intermixed Ballast System." *Acta Geotechnica*, pp.1-12. doi:10.1007/s11440-021-01342-2

Indraratna, B., Qi, Y., Jayasuiya, C., Rujikiatkamjorn, C. and Arachchige, C.M.K. (2021). "Use of recycled rubber inclusions with granular waste for enhanced track performance." *Transportation Engineering*, vol.6. doi:10.1016/j.treng.2021.100093

Arachchige, C.M.K, Indraratna, B., Qi, Y., Vinod, J.S. and Rujikiatkamjorn, C. (2022). "Deformation and degradation behaviour of Rubber Intermixed Ballast System under cyclic loading." *Engineering Geology*, vol. 7. doi.org/10.1016/j.enggeo.2022.106786.

B. Conference Proceedings

Qi, Y., Indraratna, B., Heitor, A., Vinod, J.S. and Arachchige, C.M.K. (2021). "The behaviour of granular medium with rubber particles under cyclic loading for transport infrastructure." *International Conference of Geotechnical Engineering 2020,* Colombo, Sri Lanka.

Indraratna, B., Qi, Y., Navaratnarajah, S.K., Arachchige, C.M.K., Mehmood, F. and Rujikiatkamjorn, C. (2022). "Innovative use of waste materials including recycled rubber in rail infrastructure." *7th International conference on road and rail infrastructure, (2022)*, Pula, Croatia.

Arachchige, C.M.K, Indraratna, B., Qi, Y. and Rujikiatkamjorn, C. (2023). "Experimental study of rubber intermixed ballast stratum subjected to monotonic and cyclic loads." In *Geo-Congress*, Los Angeles, USA. (Accepted).

C. Awards

- Bright Spark Lecture on 'Use of Rubber Intermixed Ballast Stratum (RIBS) for enhanced longevity of rail infrastructure', Award issued by ISSMGE on the 3rd International Conference on Geotechnical Engineering (ICGE-Colombo, Sri Lanka. Dec 2021)

- Runner-up award at AGS NSW 2022 Research Award 2022 offered by Australian Geomechanics Society for research in Geotechnical Engineering or Engineering Geology from universities in the New South Wales, Australia.

ABSTRACT

Quarried natural rock aggregates are the most demanded type of railway ballast worldwide, attributed to their favourable physical, geotechnical and mechanical properties. After a certain period of operation and fatigue under repeated loading, degraded ballast requires replenishment with freshly quarried ballast, which is one of the most expensive items in track maintenance schemes. Given the current environmental issues, as well as the challenges in obtaining very large quantities of ballast, railway authorities have now looked for other alternatives.

This doctoral study promotes the concept of using rubber granules from waste tyres as elastic aggregates appropriately blended with traditional ballast aggregates for enhanced performance of rail tracks, i.e., a Rubber Intermixed Ballast Stratum (RIBS). During the course of this study, large-scale laboratory experiments were conducted to examine the geotechnical characteristics of RIBS under monotonic loads, and an acceptance criterion was established to determine the rubber content required to optimise the performancep. The outcomes demonstrate that the proximity of 10% rubber granules by weight in the blended assembly, can significantly reduce dilation, control the degradation of the deformation modulus as well as reduce the breakage of natural rock aggregates. However, much higher rubber contents (>15%) may overly reduce the shear strength of the granular mix and also induce relatively large initial settlements. More significantly, replacing the ballast size fraction with rubber particles ranging from 9.5 to 19 mm with similar

angularity is certainly advantageous as they also reduce the breakage of load-bearing coarse aggregates, thus effectively controlling ballast fouling.

The study was further extended to evaluate the characteristics of RIBS subjected to typical cyclic loads by conducting large-scale triaxial tests following a monotonic conditioning phase. The results indicate that irreversible rearrangement of grain configurations during the conditioning phase was pronounced in RIBS leading to a reduction in deformation during cyclic loading. It was also demonstrated that RIBS increases the energy absorption capacity and damping properties compared to fresh ballast, and reduces ballast breakage while maintaining an adequate resilient modulus. Moreover, a constitutive model for rubber-mixed ballast has been developed to explain fundamentally the stress-dilatancy behaviour of RIBS. In a practical perspective, the application of RIBS in real-life tracks is elucidated to encourage railway asset owners and R&D stakeholders to adopt and implement RIBS given its proven sound geotechnical and mechanical properties. Finally, salient considerations of track design and construction are discussed in relation to the use of RIBS while recognising its limitations.

CHAPTER ONE

1 INTRODUCTION

1.1 General Background

There are miles and miles of ballasted tracks that have been laid down on ground where they are subjected to heavier dynamic loads. Crushed aggregate is one of the most used railway ballast across the world because its mechanical properties play a major role in track stability and drainage, as well as providing safe, reliable, and continuous operations. After millions of loading cycles, ballast degradation becomes more significant and track maintenance is required when the total plastic deformation of all the layers exceeds the allowable limit. Ballast deformation and degradation is a significant contributor to track deformation, which means the corresponding maintenance is the major cost associated with ballasted railway tracks (e.g., Abadi et al., 2016; Indraratna et al., 2018). Ballast replacement has outdistanced the supply of fresh ballast available due to the preservation of natural resources and cost concerns, hence, the use of limited materials modified with enhancers could be the best option to cater for future demands.

A study on end-of-life tyres (ELT) management (Deloitte, 2019) reveals that globally over 30 million tons of tyres reach their end of life every year but sufficient cost-effective and environmentally friendly approaches for managing ELT have not been developed in many countries. For instance, globally, around 29% (more than 60% in China) of ELT

are collected with undetermined end-use, while another 12% of ELT are either landfilled, stockpiled, or unknown. Improperly discarded ELT are associated with serious impacts on the environment and public health through diseases transmitted by mosquitos, fire hazards, or extreme temperatures and toxic gases, etc.

In recent years, there has been an increasing interest in the use of elastic elements in track substructures to reduce noise and vibration and decrease ballast deformation and track degradation. Three types of energy-absorbing layers have been studied for use in rail tracks: i) rail pads at rail-sleeper interface, ii) under sleeper pads (USP) (Ho et al., 2013; Costanzo et al. 2016; Jayasuriya et at., 2018; Carrascal et al. 2010), and iii) under ballast mats (Navaratnarajah and Indraratna 2017; Wettschureck et al., 1997; Müller 2008). Elastomeric particles bounded with polymer matrix resin have already been studied in order to reduce ballast degradation and associated track maintenance: i) Neoballast (Fontserè et al., 2016), ii) Resiliency bound ballast (Ho et al., 2013), and iii) XiTRACK (Kennady et al., 2013). However, by binding the particles with polyurethane or resilient epoxy binder can compromise the permeability of ballast. In fact, one common drawback with these methods is that they are not economically interesting at the beginning.

In recent years, researchers have been investigating various approaches to utilise unbounded shredded or crumbed used tyres in railway substructures as alternatives to traditional ballast and subballast material. Qi et al., (2018) proposed using shredded or crumbed rubber blended with steel furnace slag and coal wash in the subballast, while Fathali et al., (2016); Esmaeili et al., (2016) and Sol-Sanchez et al., (2015) tested ballast mixed with aggregates derived from tyres.

Some previous studies for ballast mixed with rubber agregates (Fathali et al., 2016; Sol-Sanchez et al., (2015); Song et al., 2019) attempted to evaluate the impact of adding rubber granules in ballast employing uniaxial compression tests and direct shear tests under dynamic loading. The most notable findings to emerge from the literature imply that rubber added to a ballast assembly could reduce ballast breakage and damage to track elements by increasing the capacity of the ballast layer to retain more strain energy (Fathali et al., 2016; Sol-Sanchez et al., 2015). The addition of rubber reduces the shear strength and stiffness of the ballast and increases its total settlement (Song et al., 2019). This is primarily attributed to the elastic modulus of rubber granules which is significantly lower than that of rock aggregates. In previous studies, the particle size distribution of rubber granules has generally followed the same shape of ballast gradations for compatibility of intermixing (Esmaeili et al., 2018; Fathali et al., 2016; Song et al., 2019). The study by Esmaeili et al. (2016), investigated the dynamic properties of rail ballast mixed with tyre-derived aggregates (TDA) in a modal shaker test, and they found a significant decrease in overall stiffness associated with an increase in the damping ratio as the amount of TDA increased (e.g. 22% of TDA in the ballast mixture decreased the stiffness more than 90% and increased the damping ratio more than 60%). A follow-up study by the same author (Esmaeili et al., 2018) found that 10% by volume of TDA could reduce the stiffness of pure ballast to one-fourth. This confirms that the overall behaviour of ballast and rubber mixtures is directly influenced by the rubber particles. Some researchers (Sol-Sanchez et al., 2015) suggest mixing rubber granules that are considerably smaller than the ballast particle sizes (8–22.4 mm), but this may not be a practical option, because, relatively smaller rubber particles can contribute to ballast fouling (void filling) and segregation rather than improving the energy absorbing capability of a well-interlocked matrix. Sol-Sanchez et al. (2015) and Esmaeili et al.

(2016) suggested that 10% of rubber granules by volume could reduce ballast degradation and increase the capacity of the ballast to absorb energy and also maintain an acceptable level of stiffness of the matrix. Fathali et al., (2018) proposed 10% by weight as a suitable amount of rubber granules based on the combined effects of physical and mechanical properties, while Gong et al. (2019) and Guo et al. (2019) also proposed the same recommendation of 10% by weight, considering particle breakage. Considering various available ballast standards, Song et al. (2019) suggested the addition of about 5% of rubber particles by volume, in relation to the acceptable mechanical and damping properties expected of a high quality ballast. All these experimental and numerical studies found in the literature so far have focussed on the dynamic properties of railway ballast mixed with rubber granules, and they did not offer consistent and convincing explanations regarding the optimum amount or the size of rubber particles to be utilised. Since all these studies were conducted using either a ballast box, a direct shear test, or a modal shaker, there is a knowledge gap in the performance of this material under controlled confining pressures (σ'_3) that represent typical rail tracks, when selecting the optimum amount of rubber. Furthermore, none of these studies took place in the triaxial space to evaluate the relevant behaviour during the shearing process.

Therefore, this proposed research involves the study of the physical and mechanical characteristics of a Rubber Intermixed Ballast System (RIBS) and its effect on stiffness and damping, by carrying out large-scale laboratory triaxial tests for static and cyclic loading under changing confining pressures.($\sigma'_3 = 10 - 60kPa$). The target isotropic effective confining pressures (i. e. σ'_3 = 10, 30 and 60 kPa) were selected to represent the actual field conditions for conventional tracks (Suiker, 2002). The optimal amount and size of the rubber particles for the RIBS mixture will be determined through a

comprehensive approach considering how this material responds under static and cyclic loads. Moreover, the constitutive relationships of RIBS mixtures incorporating the influence of rubber are also studied and a field trial was constructed using RIBS with the concluded optimal rubber content, R_b.

1.2 Research Motivation

From an environmental perspective, the use of rubber inclusions in rail tracks has proven to be beneficial, but the lack of examples of successful stories indicates the struggle of utilising end of life tyres due to the relatively higher initial cost of the modifications needed, and a lack of attention to the profits from increased longevity. Therefore, one of the motivations for this study is to encourage stakeholders that using rubber granules made from waste tyres in ballast as a sustainable and economical way of enhancing track longevity.

Previous research studies carried out to understand the behaviour of ballast mixed with tyre derived rubber aggregates utilised ballast box test apparatus (Fathali et al., 2016; Sol-Sanchez et al., 2015), direct shear test apparatus (Song et al., 2019; Gong et al., 2019), and modal shaker (Esmaeili et al., 2016). All of these experimental and numerical studies found in literature so far focussed on the dynamic properties of railway ballast mixed with rubber granules, they did not offer consistent and convincing explanations regarding the optimal amount or size of rubber particles to be utilised. Since all these studies were carried out using either a ballast box, a direct shear test, or a modal shaker, none of the authors considered the roles of stress ratio, modulus degradation, and the compression/dilatancy, response to changing confining pressures (σ'_3), when selecting the optimal rubber content. Furthermore, none of these studies took place in a triaxial

space to evaluate their behaviour during the shearing process. Therefore, another motivation for this study is to evaluate the performance of RIBS where the percentages of rubber (R_b) range from 0 to 15% (by weight) under static loads and changing confining pressures ($\sigma'_3 = 10 - 60\ kPa$).

The resilient modulus (M_R) is an essential parameter in track design because it indicates the elastic response of granular material under repeated loads. Railway ballast is subjected to repeated loads so there is a relationship between the M_R and particle breakage (Indraratna et al., 2009). Therefore the M_R of this new rubber mixed ballast material must be examined because it is a key design parameter in design of track foundations and the thickness of the granular layer. The resiliency of ballast with tyre-derived aggregates has not yet been studied, and the influence of rubber on M_R is worthy of scholarly attention. Hence, another motivation for this study is to investigate the influence of rubber aggregates on the resiliency of RIBS material.

Although a lot of research has been carried out on ballast mixed with rubber aggregates under cyclic loads, none of the studies considered the rate of permanent deformation of the material to evaluate track performance. Therefore, this study considered the rate of permanent strains and the shakedown mechanism to further evaluate the performance of RIBS. This will certainly enhance the confidence of external stakeholders and encourage them to implement the outcomes of this project in real tracks.

There are numerous constitutive models (Ueng and Chen, 2000; Indraratna and Salim, 2002; Lee et al., 1999; Youwai and Bergado, 2003; Qi et al., 2018) which discuss the stress-strain behaviour of ballast itself and rubber aggregates in sand/soil/road base/capping material, but there is a distinct lack of research, particularly related to

mixing rubber aggregates with ballast material. Therefore, a constitutive model has been developed to demonstrate the potential impact of ballast with rubber through numerical simulations in order to give industry and academia a better understanding of this material under different loading conditions and with differing rubber content.

It is identified that the industry collaboration plays a vital role implementing R & D outcomes in real tracks. Therefore, a trial track is completed with rubber mixed ballast and conventional ballast aiming performance evaluation, knowledge sharing and identifying limitations.

1.3 Objectives and Scope

This study aims to promote the concept of using rubber granules from waste tyres as elastic aggregates blended with traditional ballast particles to enhance the performance of rail tracks, i.e., a Rubber Intermixed Ballast System (RIBS). The main objective is to investigate the mechanical and compressibility characteristics of RIBS under monotonic and cyclic loads and to determine the optimal rubber content needed in the proposed RIBS through a comprehensive design criterion.

The main objectives of this study are summarised below:

1. Investigate the range of sizes of rubber granules that can be used to optimise the performance of RIBS by identifying the possible drawbacks and advantages from the findings available in the literature. The proposed new range of rubber granules will be evaluated and recognised through the experimental outcomes.

2. Conduct a series of large-scale static triaxial tests to investigate the geotechnical properties (i.e., friction angle, dilation angle, shear strength), stress-strain and degradation response of mixtures of ballast and rubber granules, i.e., Rubber Intermixed Ballast System (RIBS) with different rubber contents (0–15% by weight) at effective confining pressures of 10, 30 and 60 kPa.

3. Evaluating the RIBS under cyclic loading to examine the influence of rubber on the initial compaction characteristics, material resiliency, damping characteristics, energy absorption, and shakedown behaviour.

4. Propose an optimal rubber content ($R_b\%$) for a RIBS mixture by evaluating the RIBS with different $R_b\%$ based on the geotechnical properties, that will ensure a better performance than the conventional ballast.

5. Developing a constitutive model to study the stress-strain behaviour of RIBS while incorporating the effect of rubber.

6. Provide a complete practical design and construction example to encourage stakeholders with a broader perspective of research by incorporating RIBS material and its properties into track design and construction aspects. Moreover, limitations of RIBS in real-time applications are discussed.

1.4 Thesis Outline

This PhD thesis is organised into nine chapters, as briefly outline as follows.

This current Chapter 1 (Introduction) has already provided the background to the salient aspects of this research on the use of recycled rubber particles mixed with rail ballast in

rail track substructure, elucidated a statement of originality and research motivation, and defined the scope of research in relation to the key objectives.

The outline of the remaining thesis chapters is succinctly described below.

Chapter 2 is a review of relevant literature: (i) an overview of the current state of research on the behaviour of ballast, (ii) background of waste tyres and a discussion of using elastomeric materials in track substructure, (iii) the properties of ballast-granular rubber mixtures considered in previous studies, and a critical review, (iv) a description of widely used energy-based constitutive models for ballast under both monotonic and cyclic loads.

Chapter 3 explains the material preparation and laboratory test plan. It describes the selection of particle sizes for rubber granules derived from waste tyres by optimising the benefits and limitations. It also describes the target particle size distribution, laboratory test plan, including large-scale monotonic and cyclic triaxial tests, specimen preparation, description of the test apparatus, test methods, and the basic geotechnical properties of the samples.

Chapter 4 presents the results of the monotonic drained triaxial tests. Further to that, findings such as variations of the deviator stress ratio, friction angle, initial tangent modulus, variations of secant modulus, modulus degradation, shear stress-shear strain, strain energy density, ballast breakage, and the dilatancy behaviour under changing rubber content and changing confining pressures, are discussed in detail and compared with pure ballast.

Chapter 5 focuses on evaluating the characteristics of RIBS subjected to cyclic loads by conducting large-scale triaxial tests for changing rubber contents (0-15%) under confining pressures (30-60 kPa) and a loading frequency of 20 Hz following a monotonic

conditioning phase. The discussion includes an assessment of RIBS in terms of total deformation (axial strain and volumetric strain), rate of permanent deformation, shakedown mechanism, the resilient modulus, damping ratio and energy absorption compared to pure ballast. Finally, the influence of the rubber content and particle degradation is assessed by quantifying the breakage of ballast particles.

Chapter 6 presents an assessment of the optimal rubber content based on the performance of RIBS with different percentages of rubber (0-15%) under monotonic and cyclic loads. In this chapter, a design criterion is introduced to assess the optimal rubber content in a RIBS mixture while considering the effective friction angle, dilatancy angle and ballast breakage, as well as the energy absorption and modulus degradation at the peak deviator stress ratio. The rubber content determined is further evaluated under cyclic loads for the resilient modulus and track longevity (based on the amount of accumulated permanent deformation at the corresponding number of cycles).

Chapter 7 describes a simple constitutive model to study the stress-strain behaviour of RIBS while incorporating the effect of rubber in a modified, conventional Mohr–Coulomb yield criterion. Typical stress–strain behaviour is approximated by the hyperbolic stress–strain curve (Duncan and Chang 1970) in order to obtain the required parameters in addition to the conventional triaxial tests conducted for RIBS. General constitutive relationships are computed incorporating model parameters and validated with test results from the current study and an independent study.

Chapter 8 includes the design and construction example of a 20 m long section of track with RIBS material that contains the optimum rubber content (10% by total weight) as a field trial and a 20 m long section of conventional track as a reference for the RIBS track.

In addition to the track design calculations and construction stages, it also discusses considerations and limitations of RIBS in real-time applications. The original intention was not only to build the track but also monitor the track for a considerable peiod and include field data analysis in to this chapter. Unfortunately, due to COVID-19 restrictions implemented in NSW, Australia constructions were terminated for a substantial period of time and that resulted in delaying field data collection.

Chapter 9 summarises and synthesises the main conclusions of this research, and also provides recommendations for future studies in the same discipline.

CHAPTER TWO

2 LITERATURE REVIEW

2.1 Introduction

Numerous attempts have been made to understand the behaviour of rail ballast with resilient material inserted into the ballast. In this chapter the current state of research into the behaviour of ballast, including the use of tyre derived rubber granules in track substructure, is reviewed.

This chapter has five sections as follows:

- End-of-life tyres (ELT): including the generation and recovery of waste tyres
- Ballast: describes the formation of ballast, factors effecting the ballast behaviour, ballast behaviour under monotonic loading and the ballast behaviour under cyclic loading
- The use of tyre derived rubber granules in track substructure: presents the current state of research on the use of rubber crumbs as a capping material and tyre derived aggregates in the ballast layer

- Constitutive modelling: describes the current constitutive models developed for the stress-strain behaviour of ballast based on plastic deformation, and discusses constitutive models developed for other granular materials with rubber such as sand-rubber mixtures and rubber crumbs in capping material under monotonic and cyclic loads.

- Field tests for ballast with tyre derived aggregates: presents the current state of research on field trials where ballast mixed with rubber granules is used in track substructures.

2.2 End-of-Life Tyres (ELT)

Globally, more than 30 million tons (metric) of tyres reach the end of their life every year, but more than 40% have an undetermined end use or are not recovered, so they eventually end up in stockpiles or dumping sites (Deloitte, 2019). Moreover, while the volume of ELT increases with the increasing number of vehicles in use, the sustainable and cost-effective recovery routes are expanding slowly, and therefore the environmental, social, and economic hazards associated with the disposal and management of waste tyres also increase. Furthermore, the spontaneous fires that occasionally occur in contaminated stockpiles under extreme temperatures release toxic gases (Sidhu et al., 2006; Gulfnews 2021), and improperly discarded tyres on landfills are ideal breeding grounds for mosquitoes and other rodents. Thus, the recycling and reuse of rubber waste is essential, thus in the form of rubber aggregates in ballast matrix can contribute to the widespread use of waste rubber in other civil engineering applications.

2.2.1 Scrap Tyre Products

Granulation is a well-established and straightforward process whereby tyre-derived-aggregates (TDA) are already used in numerous recycling technologies such as energy recovery, cement kilns, outdoor play areas, and rubberised asphalt pavements. Moreover, there are no significant or scientifically justified risks associated with the use of rubber granules made from ELT (ETRMA 2016).

Scrap tyre derivatives come in three categories based on the size and basic shredding process of these materials (Siddique and Naik 2004). Shredded/chipped tyres are larger particles that typically contain steel wires produced in the primary shredding process. The shreds derived from primary shredding can vary from 100-460 mm and tyre chips derived from primary and secondary shredding range from 13-76mm. Ground rubber manufactured through magnetic separation and screening is typically between 0.15-19 mm. The smallest size subjected to milling is generally known as crumb rubber, which ranges from 0.075-4.75 mm.

The specific gravity of rubber aggregates (G_R) with the steel wires removed, as reported in different studies, are tabulated in Table 2.1.

Table 2.1 The specific gravity of tyre derived aggregates

Reference	Specific Gravity (G_R)
Edil and Bosscher (1994)	1.15
Feng and Sutterer (2000)	1.11
Kaneko et al. (2013)	1.15
Youwai and Bergado (2003)	1.15
Ghazavi and Sakhi (2005)	1.18
Arroyo, M. et al., (2007)	1.1
Kim and Santamarina (2008)	1.14
Hazarika et al., (2010)	1.15
Mashiri et al., (2015)	1.12
Indraratna et al., (2018)	1.15

2.3 Ballast

Ballast is a track element consisting of coarse angular aggregates whose primary purpose is to ensure the stability of rail superstructure. Ballast also acts as a load bearing platform for the rail track and provides sufficient permeability for drainage. The shear strength, irreversible permanent deformation (settlement), resiliency, and ballast degradation are some of the other important mechanical properties of ballast (Indraratna et al., 2011). Ballast usually consists of rhyolite, dolomite, gneiss, granite, basalt, limestone, and blast furnace slag (Lackenby et al., 2007). Ballast thickness can vary between 150-300mm, depending on the traffic and/or ground conditions (ARTC 2012). Ballast has important properties such as degradation, fouling, resiliency, and hydraulic conductivity, etc., all of which are quantified by various indexes; those developed mainly for rockfill materials and other applications of rock aggerates will be discussed later in this chapter.

2.3.1 Factors affecting ballast behaviour

Indraratna and Salim (2005) identified the following factors that govern the mechanical response of ballast:

1. Individual particle characteristics such as size, shape, surface roughness, the strength of the parent rock, and resistance to attrition and weathering.
2. Characteristics of a granular assembly such as particle size distribution, void ratio (density), and the degree of saturation
3. Loading characteristics such as confining pressure, pre-pressures, the current state of stress, the number of load cycles, and the amplitude and loading frequency.
4. Particle degradation
5. Wetting and drying cycles deteriorate physical and mechanical properties of rock material

All these factors directly influence track stability, resiliency, track degradation, and deformation, and hence, track longevity. In Australia, ballast material mostly complies with AS 2758.7(2015), ARTC A1 Specification for Ballast, and RIC Standard TS 3402/ARTC Standard TPS 04 Specification for the Supply of Aggregate for Ballast. The particle size distribution of ballast aggregates, when determined in accordance with AS 2758.7(2015), must conform to the requirements set out in Table 2.2.

Table 2.2 Ballast grading requirements AS 2758.7(2015)

Sieve size (mm)	Nominal size (mm) 60 Graded % passing by mass
63.0	100
53.0	85-100
37.5	50-70
26.5	20-35
19	10-20
13.2	2-10
9.5	0-5
4.75	0-2
1.18	-
0.075	-

Durability is another important factor of ballast material because it is needed to maintain the ballast gradation required for better functioning. The durability of the ballast layer directly effects the frequency of track maintenance (recycling or replacing the ballast layer), long lasting ballast material reduces the track maintenance cycles and that saves money. Different countries follow different specifications for evaluating the durability of the ballast layer mainly due to the ballast specifications adopted. In Australia, according to AS 2758.7(2015) the durability assessment of ballast shall be satisfied by one of the following test methods.

Set 1: Aggregate Crushing Value < 25 % and Wet Attrition Value <6%

Set 2: Aggregate Crushing Value < 25 % and Los Angeles Abrasion Value < 25

2.3.2 Ballast fouling

Ballast fouling is caused by the accumulation of fine particles in the voids of the ballast matrix. Over time ballast deteriorates due to particle splitting, angular corner breakage,

and grinding or wearing away from the surface, all of which lead to ballast fouling. Moreover, ballast can be contaminated with fine particles due to sleeper wear, infiltration from subgrade and underlying granular layers, and surface infiltration by coal fouling which may result in unacceptable track deformation. The lack of void spaces due to ballast fouling restricts effective drainage within the track substructure, which results in poor track geometry.

The Fouling Index, *FI* is a widely used method proposed by Selig and Waters (1994) to measure the degree of fouling. The equation for *FI* is

$$FI = P_4 + P_{200} \tag{2.1}$$

where P_4= percentage passing 4.75 mm (No. 4) sieve, and P_{200} = percentage passing 0.075 mm (No. 200) sieve. As shown in Table 2.3, Selig and Waters (1994) classified the degree of fouling based on the *FI* value obtained from Equation 2.1.

Table 2.3 Fouling classification (Selig and Waters, 1994)

Fouling Classification	**Fouling Index, *FI***
Clean	$FI<1$
Moderately clean	$1< FI<10$
Moderately fouled	$10< FI<20$
Fouled	$20 < FI<40$
Highly Fouled	$FI\geq 40$

The criterion for fresh ballast is that fouling material should not exceed 2% by total weight; it has been identified that fouling may not be significant if the amount of fouling material is less than 10% (Selig 1984).

A more sensitive fouling index, Void contaminant Index *(VCI)* introduced by (Tennakoon 2012) incorporated the specific gravity of the fouling material. Here the fouling material can be separated using a 9.5mm sieve. Equation 2.2 can be used to calculate this new parameter VCI where $V_{f\prime}$ and V_{vb} are the actual volume of fouling material and the total volume of voids respectively.

$$VCI = \frac{V_{f\prime}}{V_{vb}} \times 100 \tag{2.2}$$

Equation 2.2 can be rearranged like Equation 2.3, by using the specific gravity (G), void ratio (e), and dry mass (M) parameters. Here the subscripts b and f represent clean ballast and fouling material.

$$VCI = \frac{(1 + e_f)}{e_B} \times \frac{G_B}{G_f} \times \frac{M_b}{M_f} \times 100 \tag{2.3}$$

2.4 Behaviour of Granular/Ballast Material under Monotonic Loading

Numerous studies have considered the behaviour of ballast material under monotonic loading by carrying out triaxial shearing tests at various confining pressures, σ_3' (Indraratna et al., 1998; Anderson and Fair 2008; Qian et al., 2013; Trinh et al., 2012; Salim, 2004; Sun, 2015). Marachi (1969) explained the boundary effect during their tests for granular materials on triaxial space when the ratio of the diameter of the test specimen to the largest particle size is not less than 6. Researchers also tested ballast by adopting one of the following options; i) using large-scale triaxial apparatus, or ii) tests on scaled-down aggregates to avoid the boundary effects; in terms of reliability, large scare testing is preferred (Indraratna et al., 1998).

A very common observation from past studies shows that with an increased σ_3', specimens undergo larger compressions while delaying and limiting dilation. The axial strain at failure, the peak deviator stress increases and the particle degradation quantified up to the failure state increases due to increased deviator stress, and the volumetric change because of the increased interparticle contacts. The effective friction angle of granular material is mainly influenced by particle size, gradation, surface texture, and angularity (Holtz and Gibbs 1956; Marschi et al., 1972). The apparent friction angle φ_{fb} corresponds to the friction angle which do not account dilatancy and the peak friction angle (φ_p) corresponds to the maximum principal stress ratio (p'/q) which decreases with the increased σ_3', as shown in Figure 2.1 (Indraratna et al., 1998).

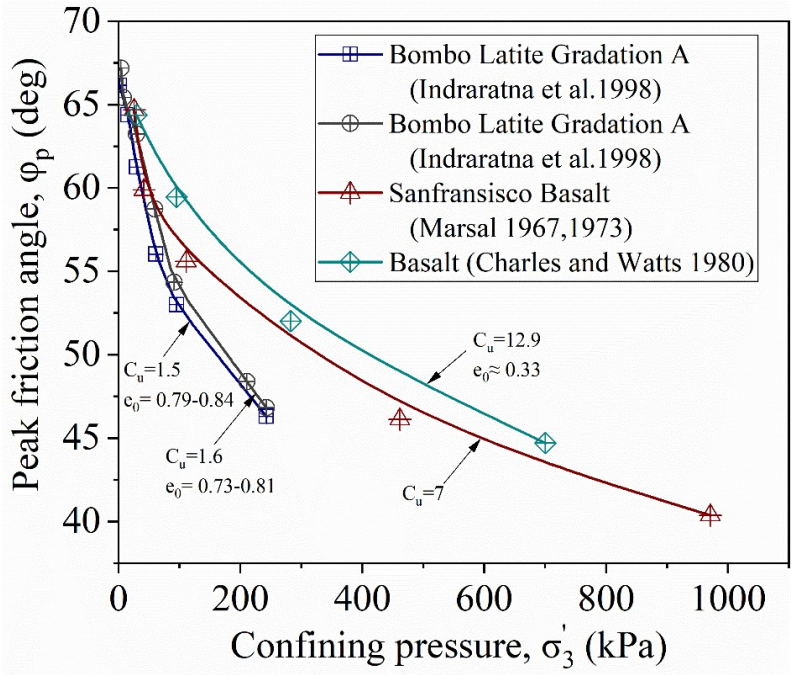

Figure 2.1 The influence of confining pressure on the angle of internal friction (adopted from Indraratna et al., (1998)).

Considerable particle breakage has taken place under monotonic shearing tests on granular media, starting with local crushing at interparticle contacts and then particle splitting under increased deviator stress (Indraratna et al., 1998). It is imperative to study

ballast breakage as a quantitative analysis because grain breakage causes ballast fouling which then leads to track settlement and lateral deformation. Around 76% of ballast fouling is due to physical ballast breakdown, whereas ballast tamping during maintenance can cause almost 20 percent of the total damage done to the ballast (Aursudkij, 2007).

The way ballast breakage is regulated has been studied extensively by observing the effects of the confining pressure, frequency, and deviator stress which are independent of the type of rock material. Different breakage indices can be found in the literature regarding ballast breakage based on changes in the particle gradation of ballast before and after loading. Marsal's breakage index, B_g (Marsal, 1967) is the summation of the difference in retained percentage on each sieve before and after the test. Marsal's Breakage Index $B_g = \sum(\Delta W_k > 0)$

$$\Delta W_k = W_{ki} - W_{kf} \tag{2.4}$$

Where W_{ki} is the percentage retained on sieve size k before the test, and W_{kf} is the percentage retained on sieve size k after the test.

The new method (Indraratna et al., 2005) uses the term 'BBI' to refer to the ballast breakage index, it depends on the particle size distribution curve before and after the test. The definition of the BBI is shown in Figure 2.2. Ballast Breakage Index or BBI is a significant modification of the relative breakage index (Hardin, 1985). BBI is specifically formulated for the relatively narrow hence uniform range of railway ballast (typically 10-55 mm, with a corresponding uniformity coefficient < 2; Indraratna et al., 2011), for which the horizontal scale for grain sizes can be conveniently represented using an arithmetic scale. In this approach, the value of BBI is conveniently quantified by the area ratio subtended by the shift in the ballast gradation curve at a given time considering an

arbitrary lower limit for fine gravel, i.e., > 2.36 mm sieve (Figure 2.2). In contrast, Hardin's approach considers a very broad particle size distribution, thereby adopting a logarithmic horizontal scale for the grain sizes, for which the lower bound is taken as the 74-micron sieve capturing coarse silt to fine sand. In this respect, Hardin's method is not practical for most real-life conditions of ballast degradation; this is because, under typical heavy haul loading and routine track maintenance conditions, the degraded ballast aggregates still fall within the gravel range, as realistically incorporated in the BBI approach.

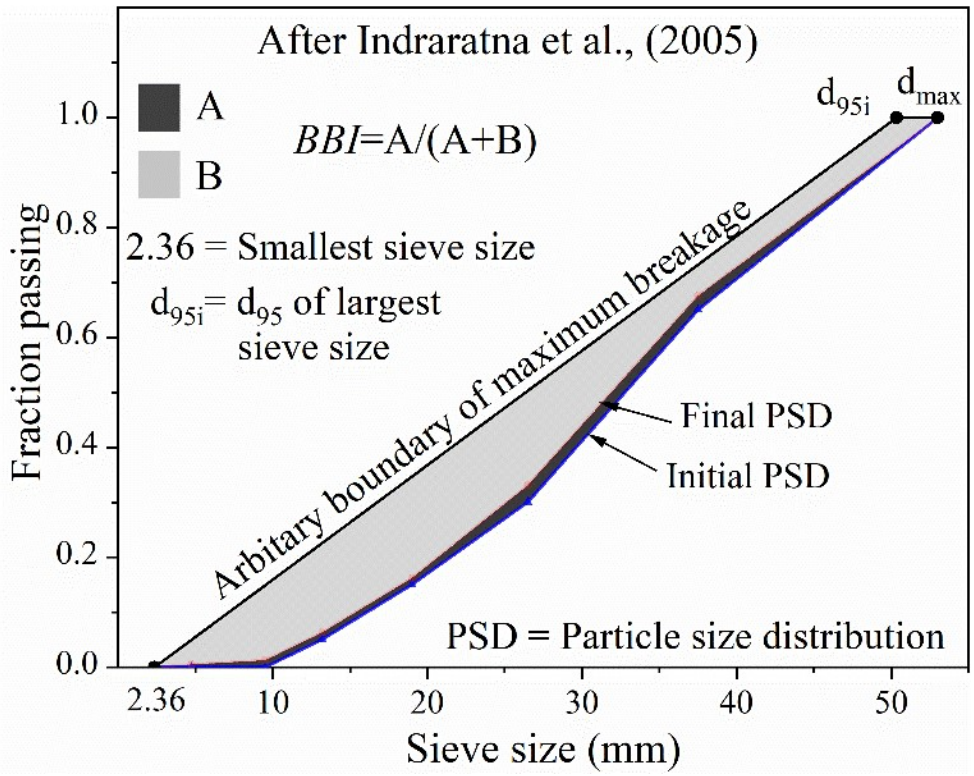

Figure 2.2 Ballast Breakage Index (Indraratna et al., 2005)

The equation for the Ballast Breakage Index, $BBI = A/(A + B)$ where A is the shift in the particle size distribution curve after the test and B is the area between the arbitrary boundary of maximum breakage and the final particle size distribution curve. The effect of particle breakage, dilatancy, and confining pressure on the friction angle of latite basalt

was investigated by Indraratna and Salim (2002). It is shown in Figure 2.3, where φ_p is the peak friction angle, φ_{fb} is the apparent friction angle that includes the effect of particle breakage but excludes dilatancy, and φ_f is the basic friction angle evaluated at zero dilatancy and zero particle breakage.

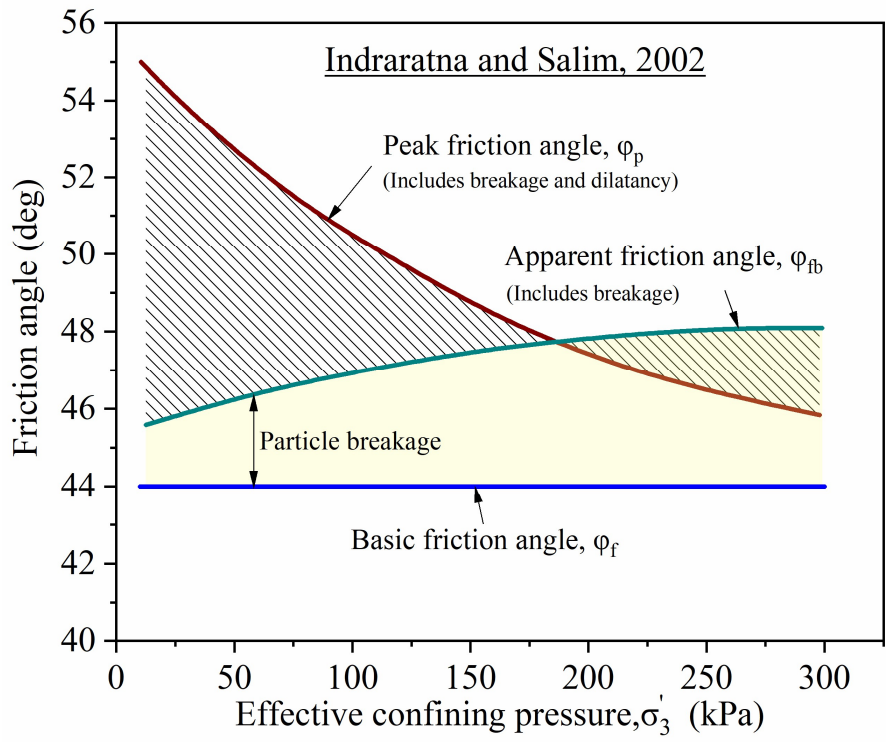

Figure 2.3 The effect of particle breakage, dilatancy and confining pressure on the friction angle of latite basalt, as investigated by Indraratna and Salim (2002).

Several reports have shown that the confining pressure and particle breakage have a relationship with the shear strength of granular material. Most investigators consider the shear strength of granular soils by the internal friction angle and dilatancy (Varadarajan et al., 2003; Marsal, 1967; Indraratna et al., 1998), but a strong conclusion cannot be made for the influence of the coefficient of uniformity and the initial void ratio, and the maximum particle size for the strength of the granular assembly.

2.5 Behaviour of Granular/Ballast Material under Cyclic Loading

Tracks are generally subjected to repeated cyclic/dynamic loading induced by the passage of trains, and hence the dynamic properties of ballast change constantly with the changing plastic particle rearrangement. Researchers such as (Raymond and Williams, 1978; Diyaljee, 1987; Selig and Waters, 1994; Indraratna and Ionescu, 2000; Indraratna et al., 2006; Lackenby, 2006) investigated the dynamic properties of ballast by conducting various laboratory tests using triaxial apparatus or box (ballast box/direct shear) testing.

Sun et al., (2016) conducted cyclic triaxial tests on 300 mm diameter samples and tested them under changing confining pressures representing maximum cyclic load q_{cyc} of 230 kPa, this equals 25 t axial loads respectively. They observed nonlinear permanent axial deformations ε_a as the number of cycles increased (Figure 2.4). The permanent strains (axial strain ε_a and volumetric strain ε_v) were generally greater during the initial cycles but then the strains decreased and then became stable. This observation agrees with previous studies (Shenton, 1985; Diyaljee, 1987; Ionescu et al., 1998; Lackenby et al., 2007; Suiker, 2002). The empirical models developed by various authors to determine the accumulated permanent axial strain after any number of cycles are summarised in Table 2.4. Most of the existing models found in literature were developed to predict permanent deformation, they are mainly based on the deformation incurred after the first load cycle $\varepsilon_{a,1}$, and the number of load cycles *N*.

Table 2.4 Empirical models developed to determine the permanent axial strain after any number of cycles

Reference	Model	Empirical constants
$\varepsilon_a = \varepsilon_{a,1}(1 + logN)$	Shenton (1978)	
$\varepsilon_a = \varepsilon_{a,1}(1 + c_1 logN)$	Raymond et al., (1978)	c_1
$\varepsilon_a = b_1 N^{b_2}$	Sweere (1990)	b_1 , b_2
$\varepsilon_a = \varepsilon_{a,1} N^z$	Chrismer and Selig (1993)	z
$\varepsilon_a = \alpha + \beta logN)$	Indraratna and Salim (2003)	α, β
$\varepsilon_a = \varepsilon_{a,1}(1 + alnN + 0.5blnN^2)$	Indraratna and Nimbalkar (2013)	a, b

Werkmeister et al., (2005) reported a new shakedown mechanism to study material failure under repeated loads, while Sun et al., (2016) then extended the idea of a shakedown mechanism for railway ballast material. There are three ranges in the plots for the permanent axial strain rate against the number of cycles, namely, Plastic shakedown (Range I), Plastic shakedown and Ratcheting (Range II), and Plastic collapse (Range III); these ranges are used to characterise the failure mechanism. Range I stands for progressively decreasing rate of plastic axial strain which eventually stabilises and leads to an asymptotic value in response to cyclic loading, thus achieving a state of 'shakedown'. In the plastic shakedown and ratcheting (Range II) range the material experiences an initial shakedown, but as loading continues the permanent strains increase until they eventually fail due to ratcheting. Range III describes the specimen failure that occurs in the form of plastic collapse within a small number of load cycles. Sun et al. (2016) tested pure ballast under a confining pressure of 30 kPa, where $q_{cyc,max}$ equals 230 kPa at different frequencies and is characterised into shakedown ranges, as shown in Figure 2.5.

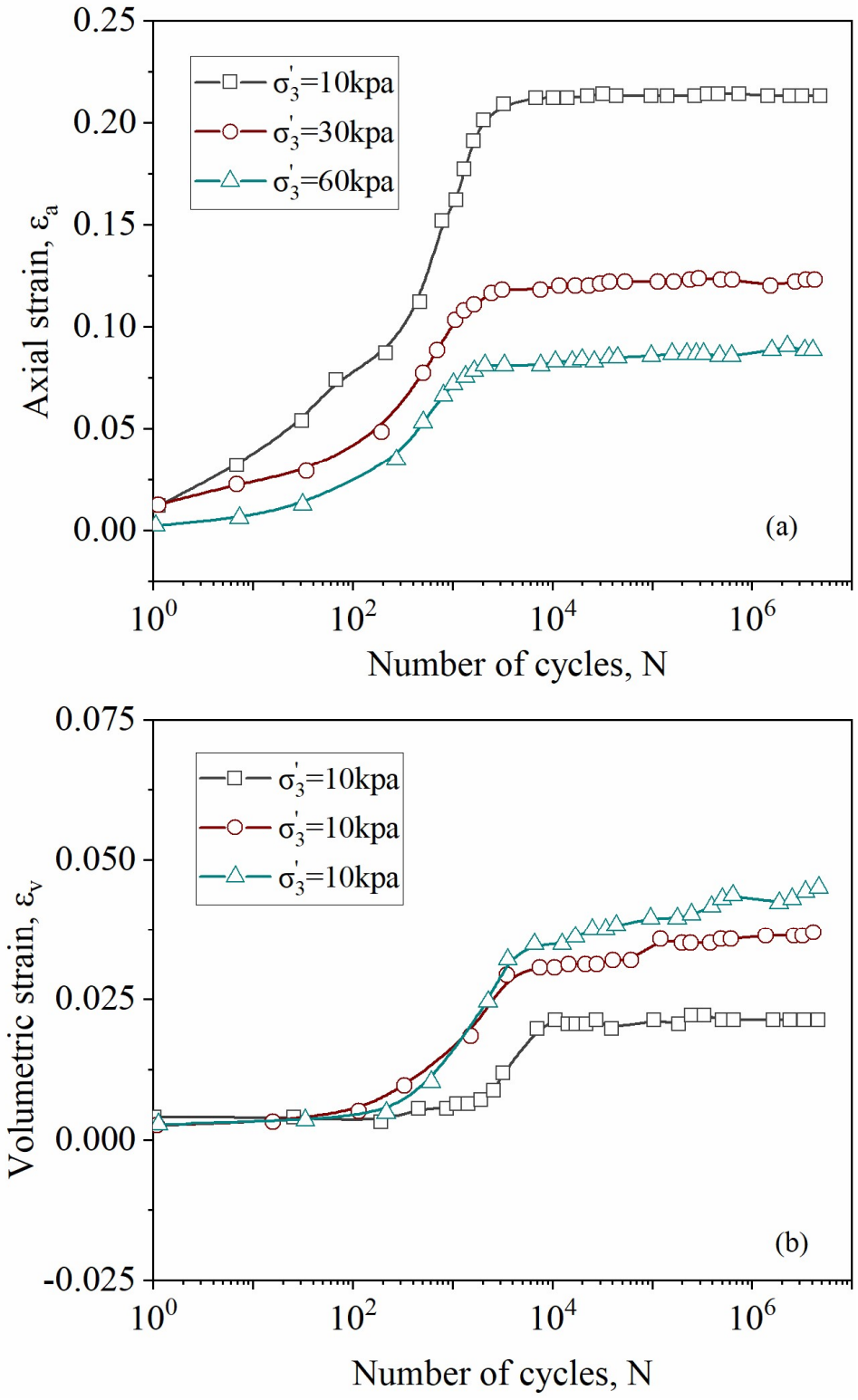

Figure 2.4 Strain response under cyclic loading (adopted from Sun et al., 2016)

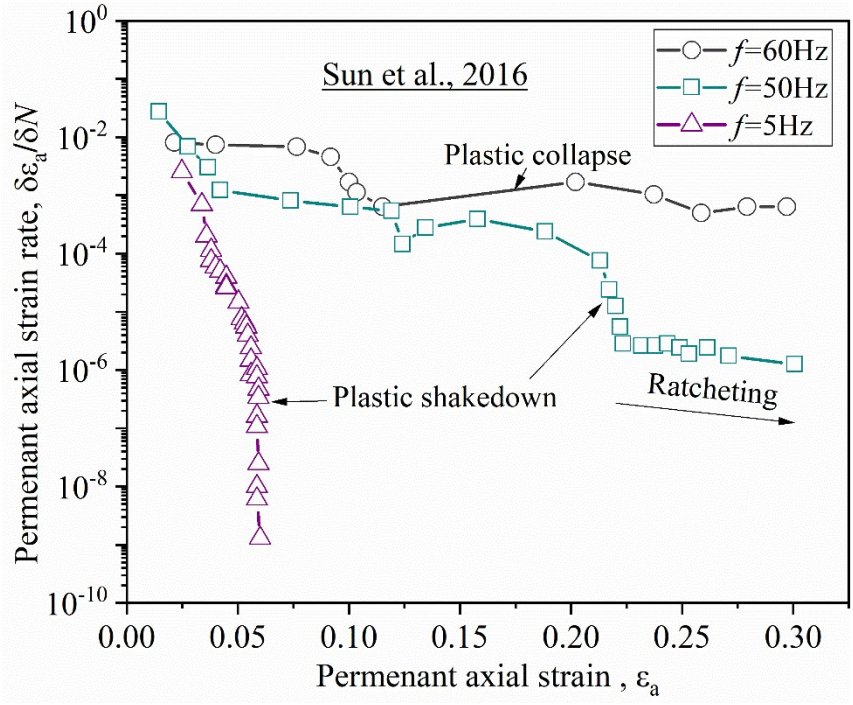

Figure 2.5 An example of the shakedown mechanism (adopted from Sun et al., 2016)

The resilient modulus M_R is an important parameter in track design; it is defined as the ratio of applied cyclic stress (Δq_{cyc}) to the recoverable strain (ε_{rec}); this definition can be found in Figure 2.6.

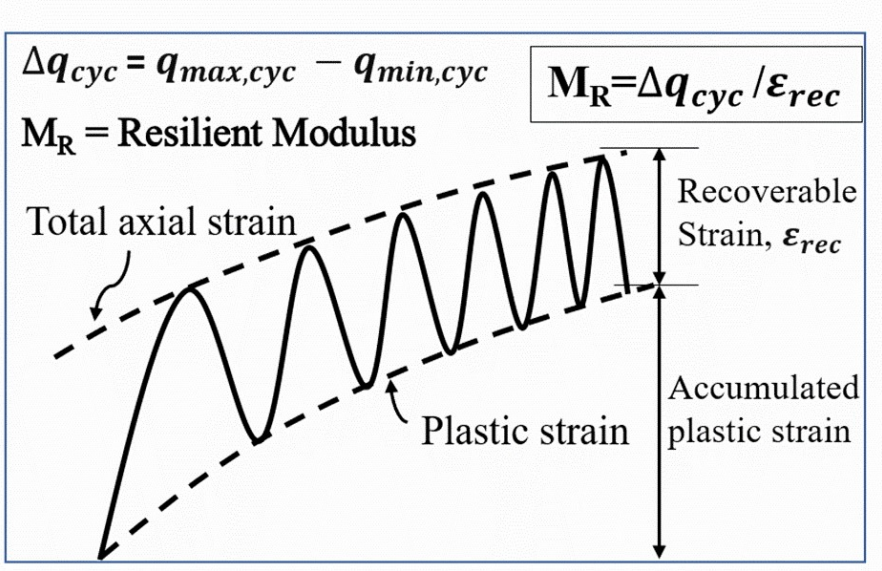

Figure 2.6 Definition of the resilient modulus, M_R

It is well known that the M_R of unbounded granular material depends on factors such as the confining pressure, bulk stress, density, particle size distribution, moisture content, loading history, loading frequency, and the number of load cycles, etc., (Allen, 1973; Lekarp et al., 2000; Aursudkij et al., 2009). It was not until 2009 that researchers considered the influence of particle breakage on M_R worthy of scholarly attention. Indraratna et al., (2009) found that an increase in particle breakage will increase the interparticle contact area, and hence an increase in M_R.

2.6 Use of Elastic Tyre Aggregates in Railway Substructure

In recent years, researchers have been investigating a number of approaches to utilise aggregates derived from tyres in railway substructures in order to identify and evaluate sustainable and innovative solutions while reducing track degradation and enhancing performance. Different approaches such as using shredded or crumbed rubber for road subgrade, as an alternative solution for leachate collection and stones in landfills (Ahmed, 1991; Park et al., 1993), as an energy-absorbing material in bituminous concrete, and as a lightweight material for embankment fill (Jones, 2001; Youwai and Bergado, 2003) have already been reported. Indraratna et al., (2017) showed that waste mixtures such as steel furnace slag and coal wash with 10% rubber crumbs added, can perform as a subballast material with high enough energy absorbing capacity, an adequate damping ratio, an acceptable magnitude of resilient modulus while maintaining significantly reduced particle breakage.

Besides the prevailing methods of utilising rubber intrusions as a resilient material in railways to reduce track degradation, control train-induced vibration and increase track stability, only a few writers have been able to draw on any systematic research into the

use of granular rubber in a granular matrix of ballast. The use of elastomeric particles bounded with polymer matrix resin to reduce ballast degradation and associated track maintenance has already been studied (Carrascal et al., 2010; Ho et al., 2013; Costanzo et al. 2016; Kennedy et al., 2013; Fontserè et al., 2016). However, the one common drawback of these methods is the initial construction costs; therefore, the life cycle cost and long-term benefits for each alternative approach must be quantified. In addition, there have been forming discussions about using rubber aggregates in ballast without any binder (Sol-Sanchez et al., 2015; Esmaeili et al., 2016; Fathali et al., 2016; Esmaeili et al., 2018).

In recent years, researchers have investigated a variety of approaches to mix rubber granules with conventional ballast material, but those conclusions published on the optimum mixing criteria of rubber granules are not consistent. Many of these studies (Sol-sanchez et al., 2015; Fathali et al., 2016; Esmaeili et al., 2016, 2018; Song et al., 2019; Gong et al 2019) attempted to evaluate the impact of rubber granules in ballast based on total settlement, ballast breakage, stiffness, and dissipated energy. Some of them (Fathali et al., 2016; Esmaeili et al., 2018) carried out uniaxial cyclic compression tests using ballast box apparatus, while others (Song et al., 2019; Gong et al., 2019) carried out direct shear tests for cyclic loads by adding different percentages of rubber granules. Gong et al., (2019) performed discrete element modelling of the work by Song et al., (2019) to evaluate ballast breakage during direct shear tests for cyclic loads. Most of these studies considered the particle size distribution of rubber granules as the same as the standard ballast gradation, followed by various national standards, and there are no previous studies that used the availing Australian standards.

Some researchers (Sol-Sanchez et al., 2015) suggested adding rubber granules that are much smaller than the sizes of ballast particles (8–22.4 mm), but this may not be a better option because the ultimate particle size distribution of the ballast and rubber mixture deviates from the complying standard. The particle size distributions of rubber and ballast particles used by Sol-Sanchez et al., (2015) study is shown in Figure 2.7. Moreover, the loading frequency of 4 Hz was used in this study, but it is not comparable to the high speed trains towards which industry is moving. Figure 2.8 provides the settlement and energy dissipation obtained from a ballast box test from the same study for conventional and modified ballast with different percentages of rubber crumbs R_b%. However, the explanation given to quantify the association between settlement and the percentage is arguable because the settlements were insignificant (1-3 mm) compared to the depth of the ballast layer.

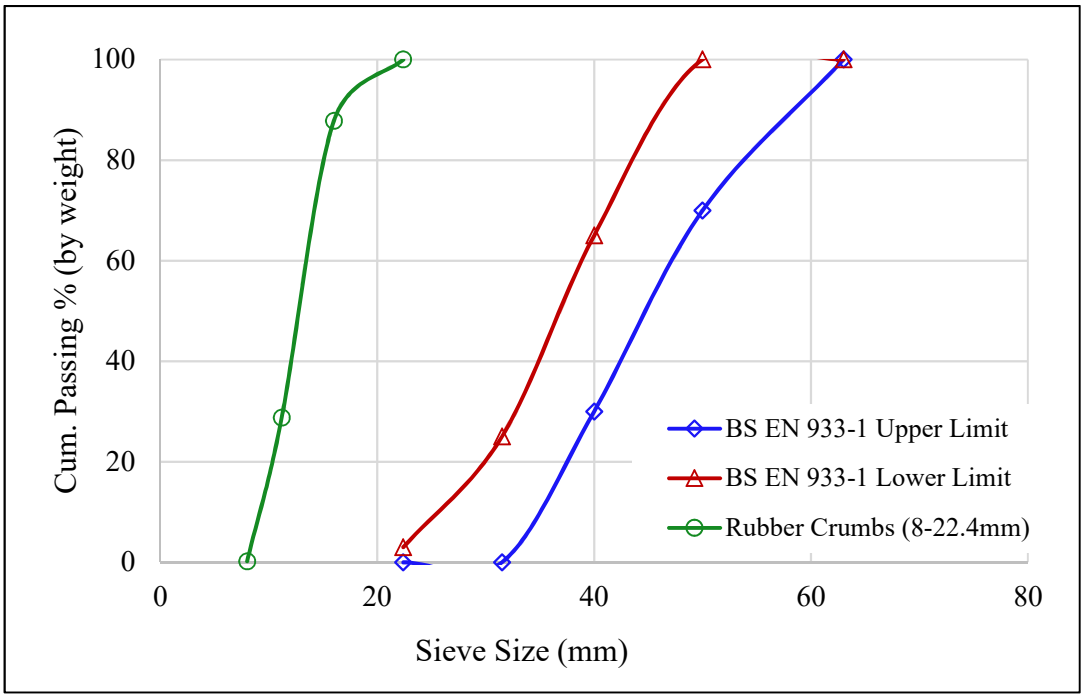

Figure 2.7 Particle size distribution of ballast mixed with rubber that was used in the study by Sol-Sanchez et al., (2015)

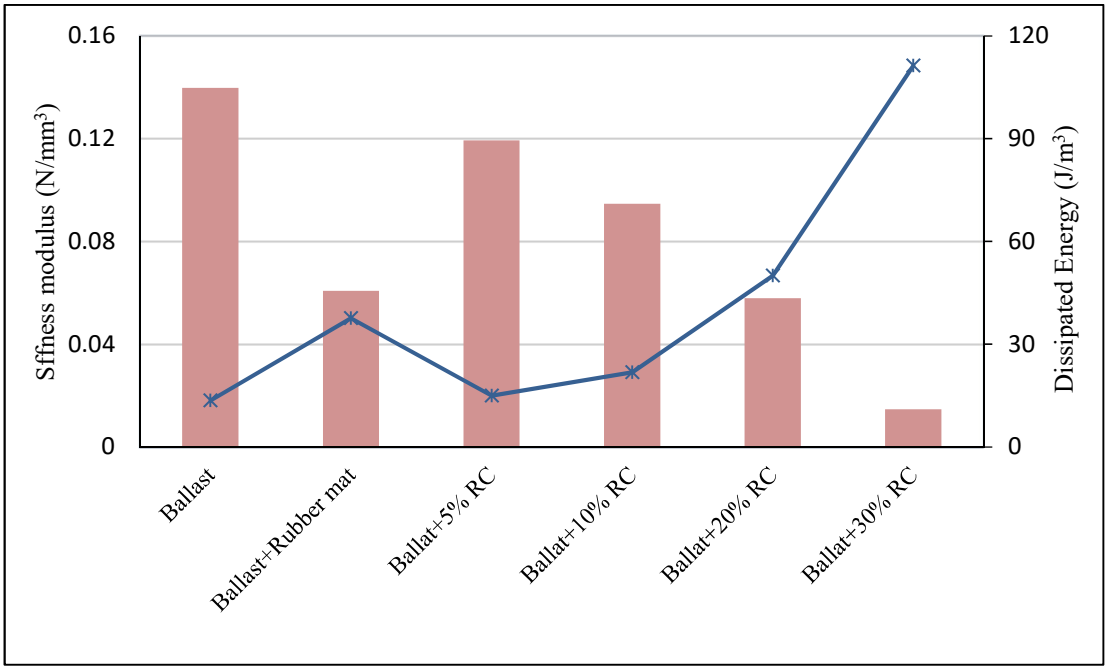

Figure 2.8 Settlements and energy dissipation capacity (adopted from Sol-Sanchez et al., 2015)

An experimental study on the dynamic properties of railway ballast mixed with tyre derived aggregate-TDA (Esmaeili et al., 2016), revealed there was a significant reduction in overall stiffness that was associated with an increase in the damping ratio as the amount of TDA increased up to 22%. (e.g. 22% of TDA in the ballast mixture reduced the stiffness by more than 90% and increased the damping ratio by more than 60%) (Figure 2.9). These experiments were carried out using a modal shaker test, they show that 10% (by volume) of tyre-derived aggregates can be taken as an optimum percentage for practical use when the particle size distribution of TDA was the same as the standard ballast gradation, followed by AREMA NO.4. In the same article, they explained how the ignorable water absorption of TDA ensured its efficiency during the freeze and thaw cycles that occur on tracks that operate in all seasons. A follow-up study by the same authors (Esmaeili et al., 2018) found that 10% by volume of TDA could reduce the

stiffness of pure ballast to one-fourth. This confirms that the overall behaviour of ballast and rubber mixtures is directly influenced by the amount of rubber particles.

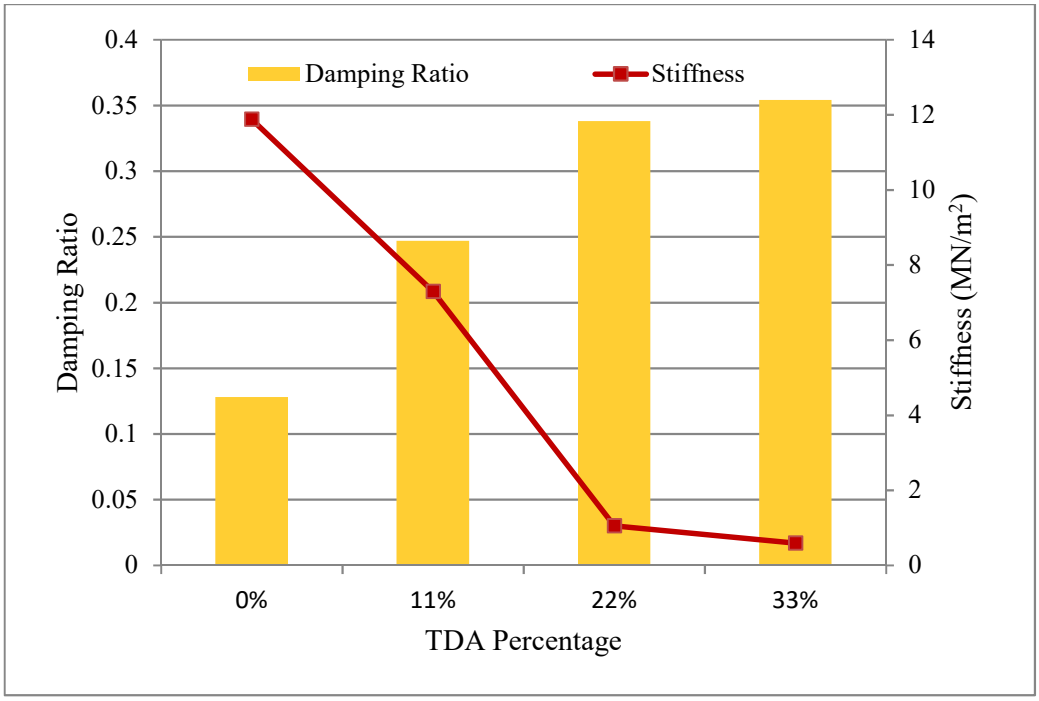

Figure 2.9 Stiffness modulus and damping ratio with diverse % of TDA (data source Esmaeili et al., 2016)

In 2016, Fathali et al. published a paper (Fathali et al., 2016) in which they further described the influence of tyre derived aggregate in ballast when they used a ballast box to carry out laboratory experiments on physical and mechanical properties and durability. This study was an expansion of a previous study (Esmaeili et al., 2016) where the authors stated that the optimal percentage (R_b%) of rubber inclusion suitable for practical usage is around 10% by weight. However, this argument is inconsistant because 10% by volume and 10% by weight are two different amounts of rubber. Moreover, the loading was limited to sinusoidal loading at a frequency of 3 Hz but it is now understood that the speed of the train (frequency) plays an important role in particle breakage and wear. Therefore, the performance for loads at higher frequencies may be different, and that has

not as yet been studied. Figure 2.10 shows a comparison of settlements from similar ballast box tests at stresses of 300 kPa where the depth of ballast used by Sol-Sanchez et al., (2015) is 300mm and 400mm by Fathali et al., (2016). In both of these studies, the settlements had decreased with R_b=10% but for R_b>10%, the settlement increased in comparison to pure ballast.

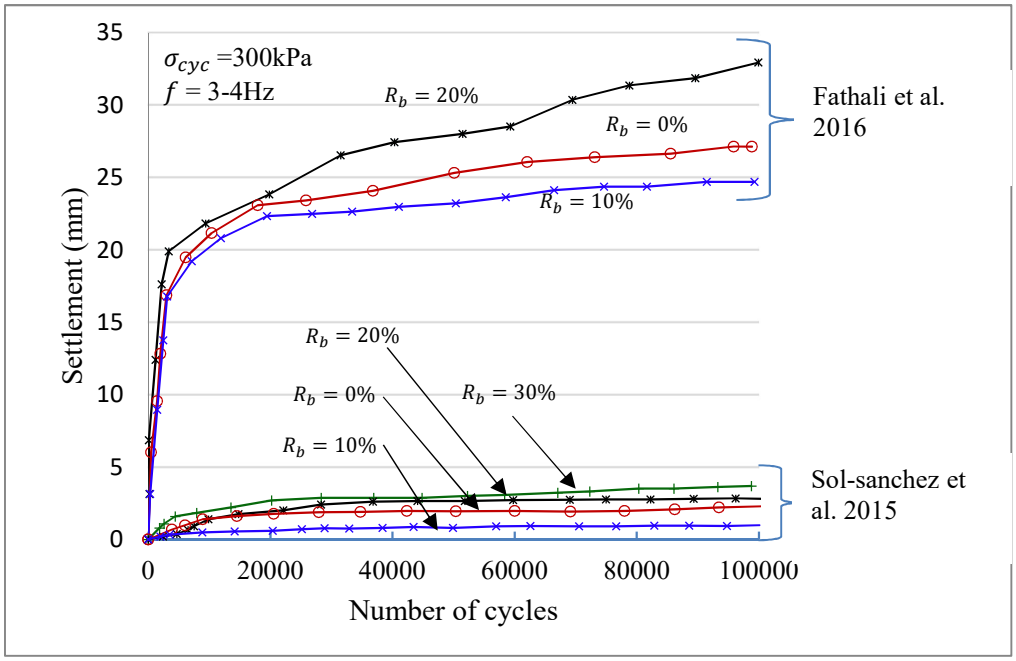

Figure 2.10 Settlement of ballast with different R_b% under cyclic loading (after Fathali et al., 2016 and Sol-Sanchez et al., 2015)

The authors also showed rubber crumbs mixed with ballast and rubber granules the same size as the ballast could reduce ballast degradation under cyclic loads. Fathali et al., (2016) noted that this reduction is significant when the ballast particle size is ≥ 38 mm (66 % reduction when $R_b = 10\%$), as shown in Figure 2.11.

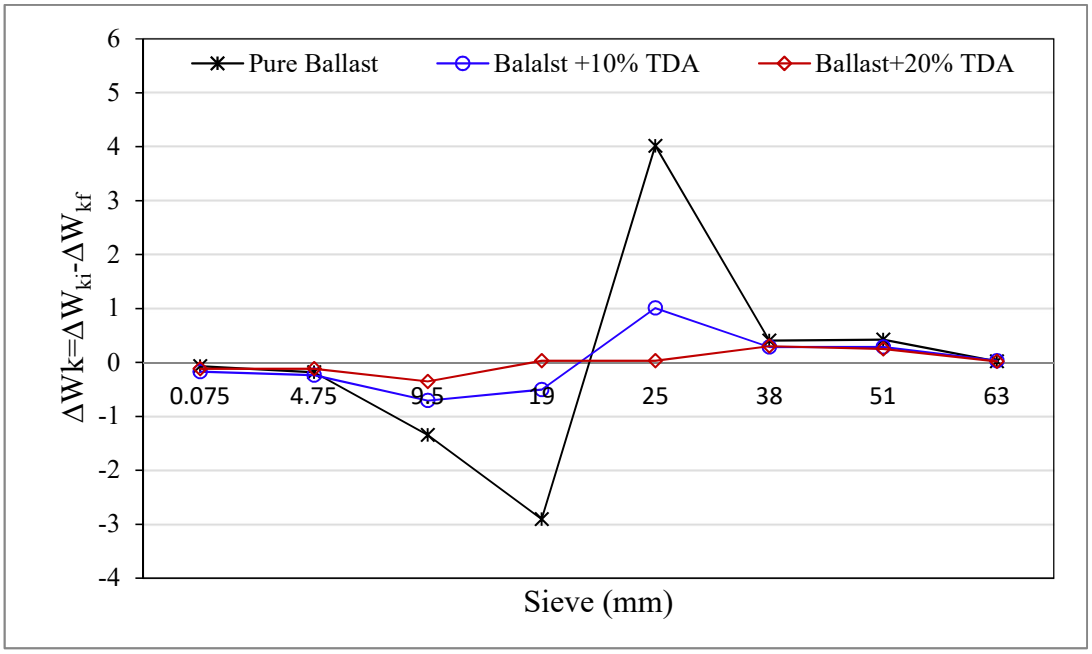

Figure 2.11 Comparison of particle breakage for ballast with different R_b% (adopted from Fathali et al., 2016)

For an optimum rubber content, Sol-sanchez et al., (2015) and Esmaeili et al., (2016) suggested that 10% of rubber granules by volume could reduce ballast degradation and increase the energy dissipation capacity of the ballast layer while keeping the reduction in stiffness at an acceptable level. Fathali et al., (2016) proposed 10% by weight as the suitable value of rubber granules based on the combined effects of the physical and mechanical properties, while Gong et al., (2019) and Guo et al., (2019) agreed with the same recommendation of 10% by weight while considering the tendency towards breakage. According to Song et al., (2019), $R_b = 5\%$ of rubber crumbs by volume is far more suitable for keeping the mechanical and damping properties required for the ballast. Collectively, all these experiments confirmed that mixing more than 20% of rubber granules by weight with ballast causes a significant decrease in stiffness and an inappropriate increase in settlement. Thus, more than 20% of rubber granules by weight is technically not recommended.

Moreover, Koohmishi and Azarhoosh (2020) conducted tests for hydraulic conductivity of ballast and crumb rubber mixtures by changing the crumb rubber size (2-25mm) and the percentage of rubber in the mix (0-30% by volume). They concluded that adding crumb rubber would reduce the hydraulic conductivity, but rubber-ballast mixtures could still satisfy the required permeability even under very high rubber contents (ballast with 30% of fine-grained crumb rubber).

However, the idea of mixing rubber and ballast as a replacement of conventional ballast layer can be justified reasonably in the following different views.

1. Rubber granules mixed with ballast can be expected as the similar approach of using USP and Under Ballast Mats (UBM) which certainly absorb excessive energy, and thus mitigate anticipated damage to the track superstructure.
2. Rubber granules mixed with ballast can be used in transition zones where rigid foundations meet soft subgrade; this will ensure smooth passage of trains over bridges and the approaches to tunnels.
3. Ballast tamping is the most frequent method used to compact ballast under sleepers and restore the settlement of the substructure. However, it is identified that the penetration of vibrating tines leads to ballast breakage (Paderno, 2010). Ballast mixed with rubber tends towards softer particle interaction during tamping; this may control the ballast from wearing and breaking to a certain extent.
4. Rubber granules increase the damping property of ballast and dissipate more energy from the track; they also enhance track performance by controlling vibration and particle breakage. Difficulties arise, as the stiffness is reduced however, a consistent study is needed to optimize the pros and cons.

5. There is also a need to assess material permeability and the possibility of rubber particles being drained away because they are not as heavy as ballast.

A summary of previous studies by laboratory testing and numerical investigations for ballast with rubber granules are listed in Table 2.5.

Table 2.5 Summary of previous studies for ballast-rubber mixtures under cyclic loads

Reference	Ballast Grading	Rubber size	Rubber content	Apparatus/Tests	Principle conclusions
Sol-Sanchez et al., (2015)	BS EN 13450:2013	8-22.4 mm	0-30% by volume	200x460x300 Ballast box	R_b =10% rubber was defined as the optimum
Fathali et al., (2016)	AREMA Group 4:2014	19 -51 mm (Similar to ballast)	0-30% by weight	290x700x400 Ballast box	An optimal value of 10% is proposed Reduction of particle breakage and settlement
Esmaeili et al., (2016)	AREMA Group 4:2014	19-51 mm (Similar to ballast)	0-33% by weight	Model shaker test	Around 10% of R_b is proposed by moderating stiffness and increased damping property
Esmaeili et al., (2018)	AREMA Group 4:2014	19-63.5 mm (Similar to ballast)	0-10% by volume	Dynamic impact field test	R_b =10% can decrease the stiffness of ballast by one fourth
Esmaeili et al., (2017)	AREMA Group 4:2014 and sand (sand fouled Ballast	19-51 mm (Similar to ballast)	0-15% by weight	700x300x450 Ballast box	Considering settlement, ballast breakage, and the damping ratio, $R_b = 5\%$ suggested with sand fouling material
Song et al., (2019)	AREMA Group 4:2014	19-63.5 mm	0-15% by volume	500x500x350 Direct shear	$R_b = 5\%$ is recommended
Gong et al., (2019)	AREMA Group 4:2014	19-63.5 mm	0-10% by volume	Discrete element modelling	R_b =10% significantly reduces ballast breakage
Guo et al., (2019)	30-35 and 40-45 mm	3-5 mm, 10-15 mm and 20-25mm	0-30% by weight	The LAA tests Laser scanning	When $R_b > 10\%$, it does not reduce ballast degradation significantly
Koohmishi and Azarhoosh (2021)	AREMA Group 3:2010 AREMA Group 25:2010	4.75-9.5 mm and 12.5-25 mm	0-30% by volume	Impact load tests	Optimum rubber content, R_b =10%

2.7 Constitutive Modelling

Other than the empirical models discussed earlier, there are a number of other nonlinear plasticity models such as critical state models, bounding surface plasticity models, and energy-based constitutive models in the literature that can be used to determine plastic deformation of ballast. Most of these methods were initially developed for clay, sand, and other granular materials, but they can be applied for ballast material.

Roscoe et al., (1958) developed the Cam-clay model to define the critical state concept, the state where clay continuously yields at a constant volume under constant effective stresses. The stress paths of specimens subjected to drained or undrained triaxial compression tests reach the stable state boundary surface (SSBS) that spans the normal consolidation curve and the critical state line. Schofield and Wroth (1968) then presented the "Granta-gravel" model for sand as the characteristics of loose and dense sand that are similar to consolidated clay, where failure occurs on the surface of the state boundary surface. Dense sand dilates during shearing loose sand contracts initially and then begins to dilate; this means that particles do not necessarily move in the direction of applied stress. Jefferies (1993) identified the inability to explain the obvious dilatancy behavior of sand in the Granta-gravel model, so he assumed an associated flow rule (normality) and infinity of the isotropic compression line (NCL) in his Nor-Sand model. Numerous models (Lade, 1977; Pender, 1978; Nova and Hueckel, 1981) with modifications of isotropic hardening models (Cam-clay model) were later proposed, but they still cannot adequately describe the bahaviour of soil, especially under cyclic loads. As a result, researchers proposed other plasticity models such as the kinematic hardening model (Mroz, 1966; Iwan, 1967)

and the bounding surface plasticity model (Dafalias and Popov, 1975; Dafalias, 1982) that allow for plastic deformation within the state boundary surface.

In the case of railway ballast, volume contraction due to internal attrition, abrasion, and splitting (i.e., degradation) under monotonic and cyclic loads complicates the stress-plastic dilatancy relationship. From the various elastoplastic constitutive stress-strain models available in the literature, only a few models consider grain breakage and change of internal energy due to the change in volume during shear deformation and also under cyclic loads. Studies by Lee and Seed (1967) and Miura and Sukeo (1979) considered the ratio between the increment of surface area and the increment of plastic work to quantify the consumption of energy attributed to particle breakage, but they did not investigate the constitutive stress-dilatancy relationship. Ueng and Chen (2000) developed an energy-based constitutive model that included the effects of particle breakage correlating increased surface area and frictional sliding during shearing. In Ueng and Chen (2000) study, Rowe's well known minimum energy stress ratio principle (Rowe, 1962) was used to develop the stress-dilatancy relationship of sand under triaxial loading. By considering particle breakage, (Ueng and Chen, 2000) modified Rowe's equation as shown in Equation 2.5.

$$\frac{\sigma_1'}{\sigma_3'} = \left(1 + \frac{d\varepsilon_v}{d\varepsilon_1}\right) tan^2\left(45° + \frac{\varphi_u}{2}\right) + \frac{dE_B}{\sigma_3' d\varepsilon_1}(1 + sin\varphi_u) \tag{2.5}$$

Here the term dE_B represents the energy consumed for particle breakage when $dE_B = k\ dS_v$. Indraratna and Salim (2002) adopted Marsal's breakage index (B_g) in the modified equation. The relationship between the rate of energy consumed and the rate of particle breakage was obtained from Figure 2.12, it is represented by a power function, as shown in Equation 2.6.

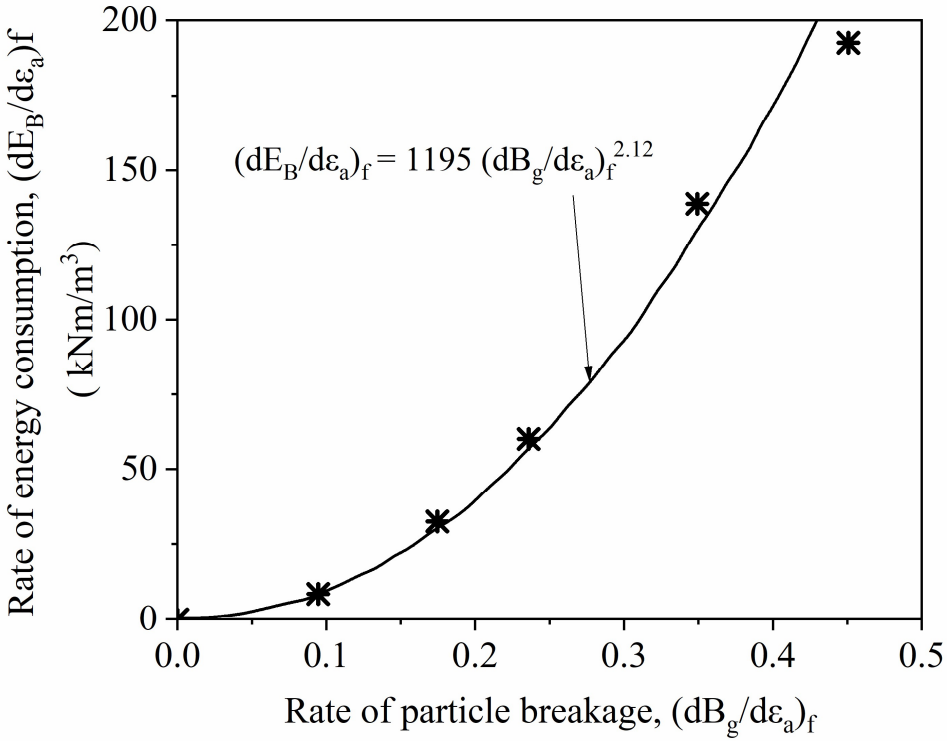

Figure 2.12 Rate of energy consumption against the rate of particle breakage (Adopted from Indraratna and Salim (2002)

$$\left(\frac{dE_B}{\sigma_3' d\varepsilon_1}\right)_f = a\left[\left(\frac{dB_g}{d\varepsilon_1}\right)_f\right]^b \tag{2.6}$$

In the above equations φ_u is the angle of friction between the particles of soil; it can vary from φ to φ_{cv} where the angle of friction is at the maximum relative density and constant volume (loose packing), respectively.

Later in 2004, Salim and Indraratna extended this model to a new constitutive (incremental) stress–strain-degradation model using the critical state concept and the theory of plasticity with a kinematic tyre yield locus (Salim and Indraratna, 2004). The proposed basic equation for the ratio between the increment of plastic volumetric strain and the increment of plastic distortional strain is given in Equation 2.7.

$$\frac{\delta\varepsilon_v^p}{\delta\varepsilon_s^p} = \frac{9(M-\eta)}{9+3M-2\eta^* M} + \frac{\beta\delta B_g}{p\delta\varepsilon_s^p}\left(\frac{9-3M}{9+3M-2\eta^* M}\right)\left(\frac{6+4M}{6+M}\right) \quad (2.7)$$

Where p is the effective mean stress, the stress ratio, and the critical stress ratio, and $\eta^* = \eta(p/p_{cs})$. Here p_{cs} is the value of p by the critical state line at the current void ratio.

Constitutive models have been developed for mixtures of sand and rubber (Lee et al., 1999; Youwai and Bergado, 2003; Qi et al., 2018). However, they may not be directly applicable for mixtures of rubber and larger rock aggregates such as ballast because as shearing progresses, mixtures of rubber and ballast show strain hardening behaviour instead of the strain softening that occur with mixtures of rubber and sand.

2.8 Field Testing for Mixtures of Ballast and Granular Rubber

There are a few field studies in the literature that were carried out to evaluate mixtures of ballast and tyre derived aggregate. In one study (Fathali et al., 2019), the effect of rubber granules on ground-borne vibrations were evaluated by recording the vibrations using electronic seismometers. Load excitations were applied onto tracks by running a passenger train and freight train (16 t and 20 t) at 80 km/h and 120 km/h respectively. The vibration responses were measured 2.5 m away from the rail and data showed a 59% and 55% reduction in vibration for the passenger train and freight train due to the inclusion of 10% of rubber in the ballast layer.

The other study by Esmaeili et al., (2018) tested the effect of the TDA on the stiffness and damping of ballast and rubber mixtures by applying an impact force on the rail with a hammer. This study shows that adding 10% of TDA reduced the stiffness by one fourth and increased the damping ratio by more than 50%, compared to pure ballast.

However, none of these previous field studies on ballast mixed with rubber evaluated the deformation and degradation of the ballast layer due to the inclusion of rubber.

2.9 Chapter Summary

In recent years, researchers have been investigating a variety of approaches to utilise waste tyre products in railways due to their energy absorbing and damping properties, i.e., their ability to reduce noise and vibration. While it is well known that ballast deteriorates under train loading and accumulates fine particles due to abrasion and the breakage of angular corners and sharp edges. Therefore, many attempts have been made to understand the behaviour of rail ballast inserted with resilient material. The recent discussions on the use of rubber aggregates derived from waste tyres inserted into the ballast matrix can contribute to the widespread use of waste rubber in civil engineering applications. Some previous studies attempted to evaluate the impact of adding rubber granules to ballast, but all the experimental and numerical studies found in literature so far are limited to the dynamic properties of railway ballast. Previous studies were mainly carried out with ballast box apparatus or direct shear apparatus, hence there is no indication of the influence of confining pressures on the tested samples. These previous studies revealed that the inclusion of tyre aggregates into a ballast assembly increases its capacity to absorb energy, increases its damping properties, and reduces ballast breakage. However, the conclusions regarding the deformations of ballast mixed with rubber are confusing because some studies indicated that rubber reduces ballast deformation, while others found opposite results. However, the records show that ballast loses its strength and settlement is difficult if there is more than 20% rubber. Moreover, previous studies did not offer a consistent and convincing explanation of the optimum amount or size of

rubber particles. Detail about the behaviour of ballast and rubber mixtures under monotonic loads, including the effect of rubber on the resilient modulus also needs a thorough investigation.

Despite the numerous mathematical/constitutive models in literature for granular materials and mixtures of rubber and sand, they are mainly based on critical state theory, and the frictional state and energy, there is a distinct lack of models for rubber and ballast mixtures. In addition, attention should be drawn to practical applications and limitations of using mixture of rubber granules and ballast in real tracks.

CHAPTER THREE

3 MATERIALS AND TESTING PROGRAMME

3.1 Introduction

This chapter explains the material preparation and laboratory test plan, including the sizes of rubber granules derived from waste tyres that would optimise the benefits and drawbacks.

3.2 The Sizes of Rubber Granules

The addition of rubber reduces the shear strength and internal friction of ballast and increases its total settlement (Song et al., 2019). The reduction in strength is primarily attributed to the elastic modulus of rubber granules which is much lower than rock aggregates. In previous studies with mixtures of ballast and rubber, the particle size distribution of rubber granules generally followed the same shape of ballast gradations for the compatibility of intermixing (Esmaeili et al., 2016; Fathali et al., 2016; Gong et al., 2019). Some researchers (Sol-Sanchez et al., 2015) suggested using rubber granules that are much smaller than the ballast particles (8–22.4 mm), but this may not be a practical option because smaller rubber particles can lead to ballast fouling (void filling)

and segregation rather than improving the energy-absorbing capability of a well-interlocked granular assembly.

The internal friction of ballast material governs the stability of the track. Previous studies (Indraratna et al., 2011; Salim, 2004) revealed that the effective friction angle (φ_{ef}) of fresh ballast varies from 46° to 69° as the effective confining pressure increases from 10 to 300 kPa. However, it can be challenging to obtain RIBS mixtures without reducing their shear strength in comparison to intact rock aggregates. For instance, Song et al. (2019) showed that a mixture of ballast and rubber with the same gradation $(R_b = 10\%)$ significantly reduces the internal friction angle of ballast (by 24%). Therefore, selecting rubber granules in a particular size range is essential, but the ultimate particle size distribution of a granular assembly (a mixture of ballast and rubber particles) should satisfy the required gradation as per the incorporated ballast specification.

3.2.1 Particles prone to breakage

According to past experimental studies (Indraratna et al., 1998, Indraratna and Salim, 2002) on ballast commonly used in NSW, Australia (latite basalt), larger grains of ballast (>19 mm) are more susceptible to breakage than smaller particles. In this current study, large-scale triaxial tests were carried out on pure ballast (latite basalt) under monotonic and cyclic loads. Marsal's breakage index (B_g) is an index to quantify the particle breakage expressed as a percentage. B_g is the difference in percentage of the weight of particles retained in the sieve before and after the test, i.e., $B_g = \Delta W_k = W_{ki} - W_{kf}$, where W_{ki} represents the percentage retained in a sieve size k before the test, and W_{kf} is the percentage retained in the same sieve size after the test. Figure 3.1 shows the particle

breakage index from the preliminary tests carried out in this study using the latest Australian standards (AS2758.7, 2015). It was note that particles >19 mm were subjected to higher particle breakage than the smaller particles.

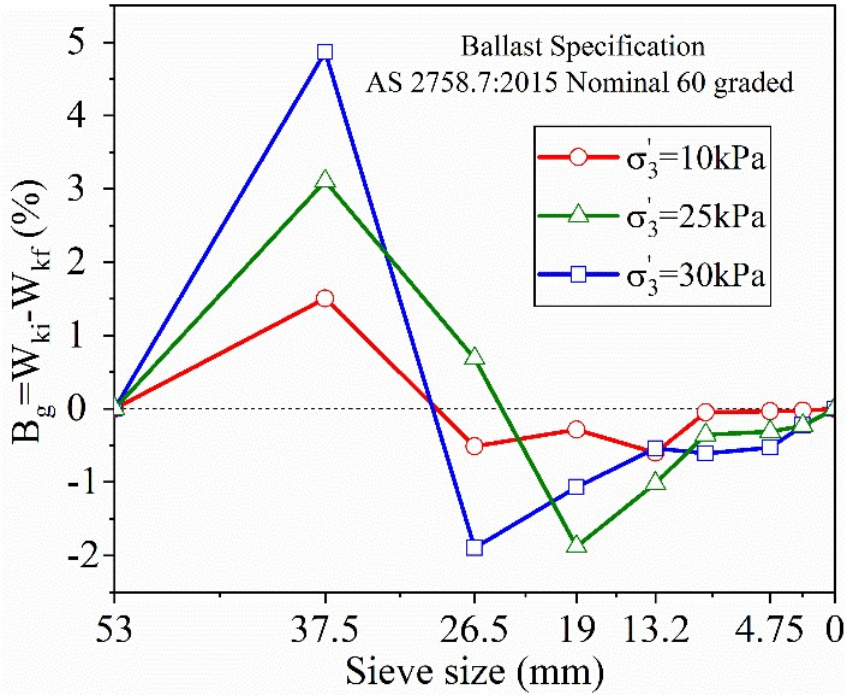

Figure 3.1 Marsal's breakage index, ($B_g = \sum \Delta W_k > 0$) for pure ballast (latite basalt)

Table 3.1 shows how the different types of ballast associated with various specifications responded to particle breakage, including those in this study. Previous studies revealed similar trend, as identified from the tests carried out in this study although the complying standards are different.

Table 3.1 Particle sizes most likely to break

Study	Tests conducted	Specification	Particles prone to break
Indraratna et al., (1998)	Large-scale triaxial tests under monotonic loading	Railway Services Authority (1983) upper limit lower limit	25–63 mm 19–63 mm
Indraratna and Salim (2002)	Large-scale triaxial tests under monotonic loading	Rail Infrastructure Corporation (TS 3402, 2001)	25–45 mm
Fathali et al., (2016)	Ballast box test under cyclic loading	Iran Ballast Specifications (IMRT 2005)	23–38 mm
Current study	Large-scale triaxial tests under monotonic loading	AS 2758.7:2015 Nominal 60 graded	19-53 mm

The interesting fact about the data in Table 3.1 is that under static and cyclic loads, larger particles (>19mm) are more susceptible to breakage than smaller particles because larger particles form the skeleton of compacted ballast and consequently taking most of the applied stresses (Indraratna et al., 1998). Previous results (Lee et al., 2007) have shown that when the rubber particles are comparatively smaller and the volume percentage of rubber is < 20%, there is only a secondary effect on the stiffness; this is because the larger particles consist of natural rock aggregates form the load bearing skeleton. On the other hand, if rubber particles are comparatively larger, the inclusion of 10-20% of rubber by volume leads to arching in a vertical direction and increases the lateral confinement (Kim and Santamarina, 2008). This means the relative size of rubber in relation to the rock aggregates controls the load transfer mechanism and changes the macroscale behaviour. Perez et al., (2016) explains that the magnitude of deviator stress is influenced by the amount of rubber and the size of rubber granules because their sizes contribute to various types of contacts, i.e., rock to rubber, rock to rock, and rubber to rubber contacts. Besides, Khoshoei Mehran et al., (2021) also carried out some experiments with steel slag

aggregates and tyre-derived aggregates and found that the specimens with larger rubber aggregates (20–60 mm) were not as stiff as the samples with smaller rubber aggregates (10–20 mm). Nevertheless, it is important to have larger and stiffer rock particles in a ballast matrix in order to transfer loads safely into the layers below, without compromising the stiffness of the ballast layer.

3.2.2 Shape of rubber particles

It can be visually observed that the larger particles derived from scrapped tyres are too planar and flaky due to the thickness of the tyre and the shredding process, thus may not be appropriate for a typical rail ballast mix. Figure 3.2 shows the particle shape of various sizes of rubber granules derived from the normal shredding process. The elongated nature of the larger particles (>19 mm) is different from the usual angular shape of ballast, so they cannot interlock properly. However, particles between 9.5 and 19 mm have the similar angular shape of rock aggregates used in conventional ballast layers. Furthermore, rubber particles that less than 9.5 mm can cause ballast fouling without adding any favourable effects to RIBS. As discussed in section 2.3.2, external particles other than ballast which are less than 9.5 mm in size are considered to be a fouling material (Tennakoon, 2012).

Rubber granules without wires are better in use as a ballast material because the steel wires can lead to the risk of fire from the railway electrification system. Although wires can be removed from scrap tyres, there is still the possibility of having bits of broken steel inside larger rubber granules. Moreover, ballast should meet the necessary electrical resistance requirements for the satisfactory operation of signalling track circuits, and therefore pieces of steel should not be presented within the top ballast layer.

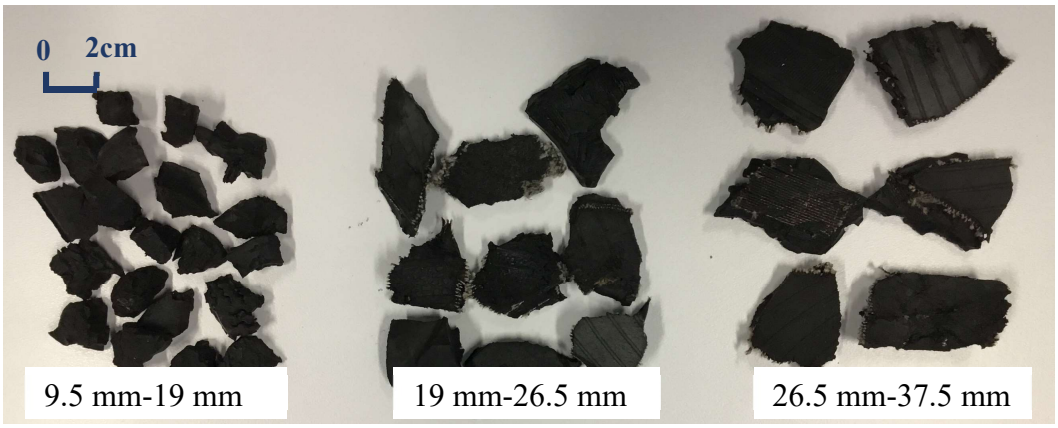

Figure 3.2 Different size rubber granules

After combining the factors mentioned above, the optimum sizes for rubber granules have been evaluated as shown in Figure 3.3.

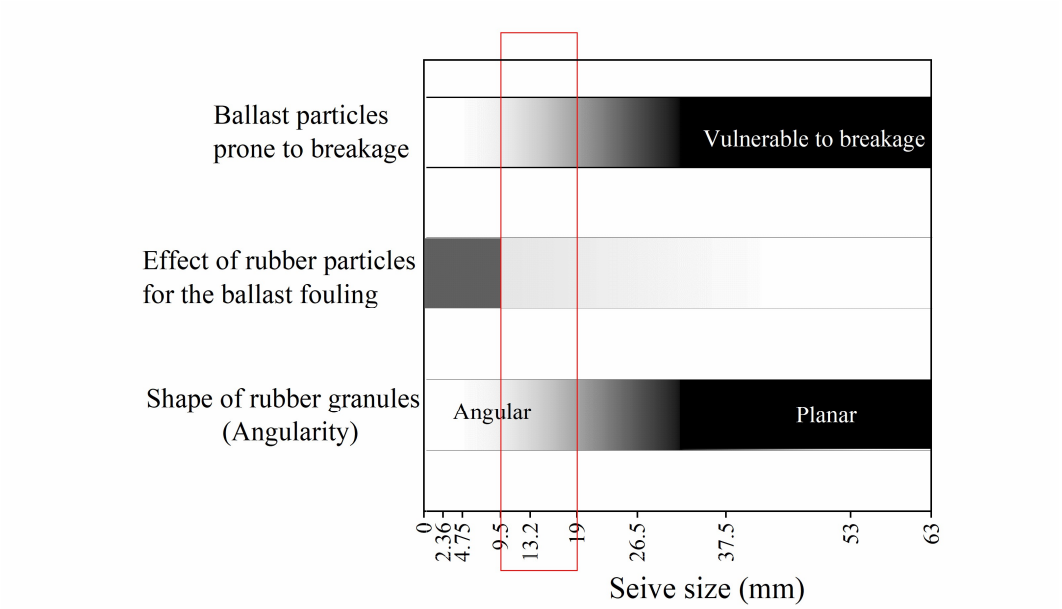

Figure 3.3 Evaluation of best particle size for rubber granules

To ensure that specimens of RIBS would experience less ballast breakage and better particle interlocking, while preventing fouling, rubber granules from 9.5 to 19 mm were used in this current study in lieu of the same size fraction of natural ballast aggregates.

3.2.3 Criteria for assessing durability

Various authorities worldwide have developed and adopted a variety of methods for assessing the durability of railway ballast, most of which consists of rock aggregates. In many countries the climate and track conditions vary, so it is important to have appropriate criteria for assessing ballast durability. In Australia, ballast mostly complies with the durability specified in AS 2758.7(2015); these criteria are assessed by two main groups of requirements, as indicated below.

Set 1: Aggregate Crushing Value (AC) < 25 % and Wet Attrition Value (WA) <6%

Set 2: Aggregate Crushing Value (AC) < 25 % and Los Angeles Abrasion (LAA) < 25

The aggregate crushing value (AC) shall be determined according to AS 1141.21 for the fraction of material passing 26.5 mm and retained by 19 mm. The wet attrition value (WA) shall be determined according to AS 1141.27 for the fraction of material passing 53 mm and retained by 37.5 mm. The Los Angeles abrasion (LAA) value shall be determined for material categorised into grading F (particle size between 26.5-53.0 mm) and G (particle size between 19.0-37.5 mm) as per AS 1141.23:2021. Since the proposed rubber granules range between 9.5-19 mm, it can be confirmed that the AC,WA, and LAA values will not be changed from conventional ballast material that is followed by the specification (AS2758.7, 2015).

3.3 Test Materials and Laboratory Test Plan

Fresh ballast for this study was obtained from Bombo Quarry (New South Wales, Australia), it consisted of latite basalt, which is widely used for railway tracks in the local region. Lattie (Volcanic) basalt is a crushed igneous rock aggregate and one of the

primary sources of railway ballast used in New South Wales tracks. Latite Basalt contains minerals such as feldspar, plagioclase and augite and the characteristics of latite basalt from Bombo quarry can be found elsewhere (Indraratna et al., 1998) Rubber granules were obtained from tyres scrapped by the standard shredding process. The properties of the ballast material used in this study are summarised in the following Table 3.2.

Table 3.2 Characteristics of Latite Basalt (after Indraratna et al., (1998))

Parameter	Results	Recommendation
Strength		
Crushing Strength	130 MPa	-
Point load index	5.39 MPa	-
Aggregate Shape		
Flakiness	25 %	< 30 %
Misshapen Particles	20 %	< 30 %
Durability		
Aggregate Crushing Value	12 %	< 25 %
Loss Angeles Abrasion Value	15 %	< 25 %

The specific gravities of the ballast and rubber granules were 2.8 and 1.15, respectively. The specific gravity of rubber (G_R =1.15) used in this study is based on Qi et al., (2018) test results, noting that it came from the same supplier. Qi et al., (2018) provided details of the specific gravity testing of rubber after being soaked in distilled water for (≥7 days) to ensure saturation and prevent floating. Moreover, G_R =1.15 agrees with previous studies (Table 2.1), where the specific gravity of similar rubber materials was in the range of 1.1-1.18.

The target particle size distribution (PSD) curve of RIBS with different percentages of rubber granules (0-15%), along with the details such as the maximum (D_{max}) and

minimum (D_{min}) particle sizes, the coefficient of uniformity (C_u), the coefficient of gradation (C_c), and the particle size distribution of rubber granules, are shown in Figure 3.4. The RIBS gradation is appropriate for use as a railway ballast according to the nominal 60 graded specifications specified by the latest Australian Standard (AS 2758.7:2015).

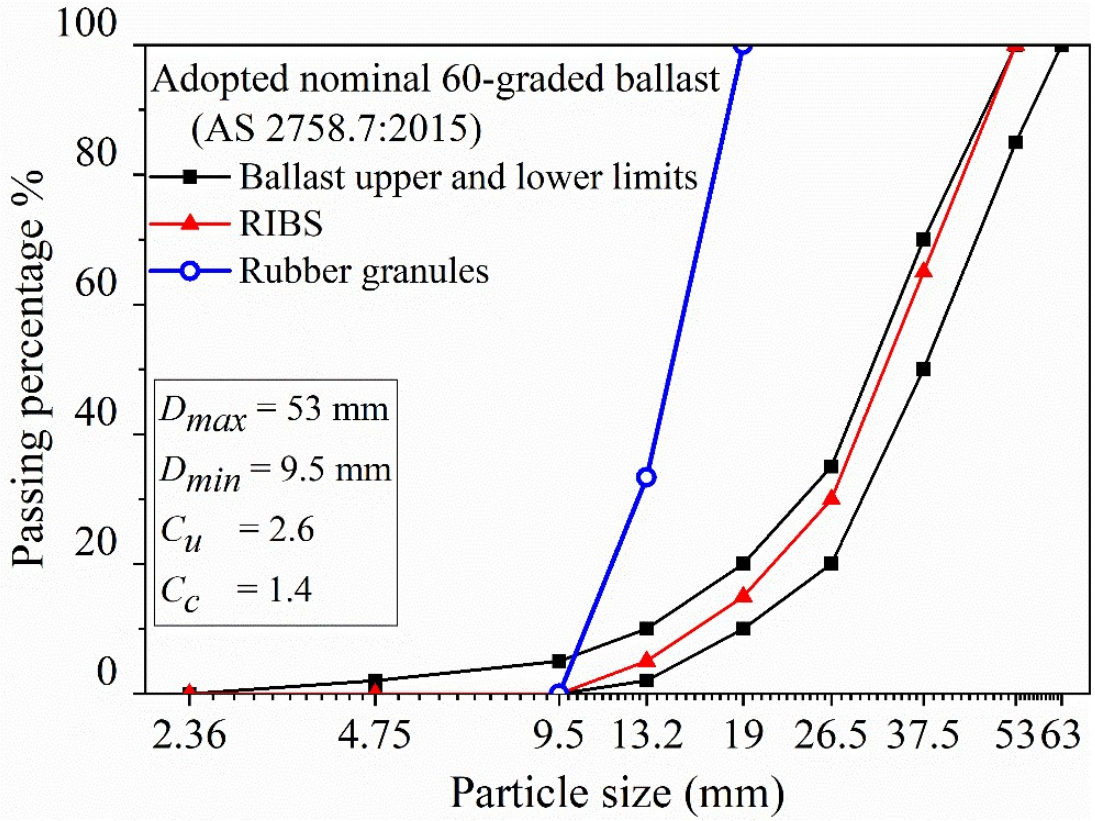

Figure 3.4 Particle size distribution of RIBS and rubber granules

Fresh ballast was sieved using a vibrating shaker with appropriate sieves that followed the specification. The sieved material was then washed and dried in the laboratory to obtain clean ballast in different size ranges. Figure 3.5 (a-d) shows the preparation of clean ballast for the laboratory experiments.

Figure 3.5 Ballast material preparation (a) vibrating shaker, (b) washing, (c) drying, and (d) prepared ballast

The freshly prepared ballast was then mixed with a certain amount of rubber granules (0-15 % by total weight) to achieve the target PSD. This step was carried out by pre-calculating the mass of each particle range as per the standard. The rubber granules used for this study were 100% recycled material supplied by Tyrecycle Australia. The amount of rubber in the testing samples was limited to 15% by weight because mixing more than 20% of rubber granules is not recommended. The reason is that ballast with more than 20 % rubber significantly compromises the stiffness and causes an inappropriate increase in settlement (Fathali et al., 2016; Sol-Sanchez et al., 2015; Esmaeili et al., 2016).

Figure 3.6 (a-b) shows the fresh ballast and rubber granules before mixing, and Figure 3.6 (c) shows the Rubber Intermixed Ballast Stratum (RIBS) with the amount of rubber, $R_b = 5\%$.

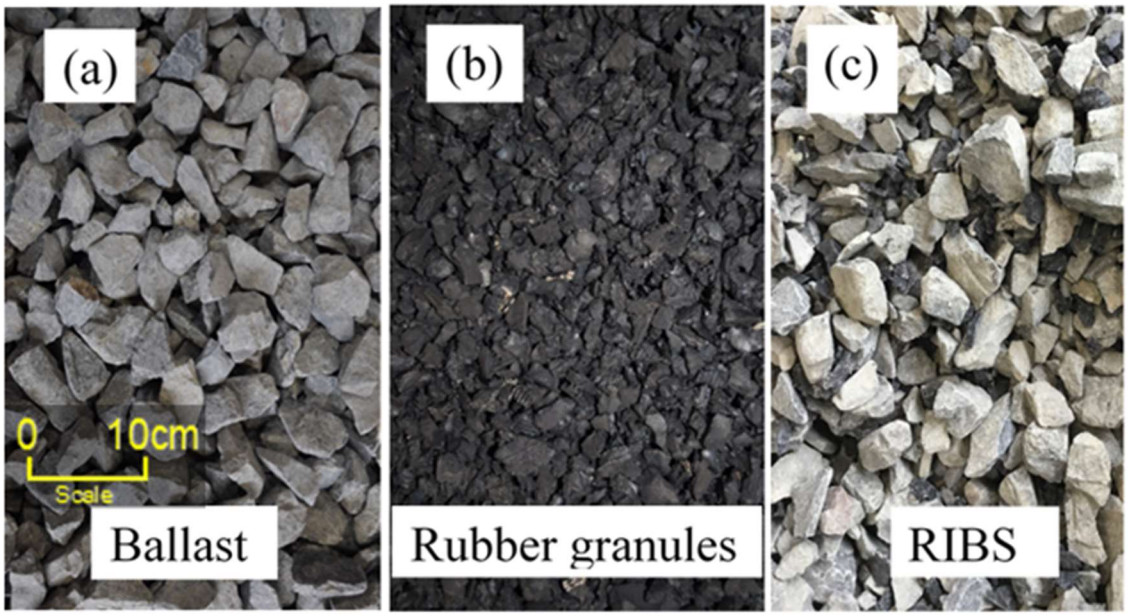

Figure 3.6 Ballast mixed with rubber, (a) conventional Ballast, (b) rubber granules, and (c) RIBS with R_b=5%.

As Figure 3.7 shows, the experimental program for this research study was divided into two categories: (a) monotonic triaxial tests, and (b) cyclic triaxial tests. It is worth mentioning that no previous studies have examined ballast mixed with rubber under a triaxial space or under different confining pressures.

During the monotonic loading test series, the target isotropic effective confining pressures (i.e. σ'_3 = 10, 30 and 60 kPa) were selected representing actual field conditions for conventional tracks (Suiker, 2002). It is found that under the confining pressure of 10 kPa, RIBS with increased rubber (R_b ≥10%) demonstrated reduced peak deviator stress (q_{peak}) compared to the maximum cyclic stress ($q_{cyc,max}$) of 25 t axle load train. Therefore, confining pressures 30 - 60 kPa were considered for cyclic loading tests. Triaxial tests under cyclic loading focused on assessing the effect of cyclic loading on RIBS in terms of the degradation and deformation behaviour, together with the damping properties.

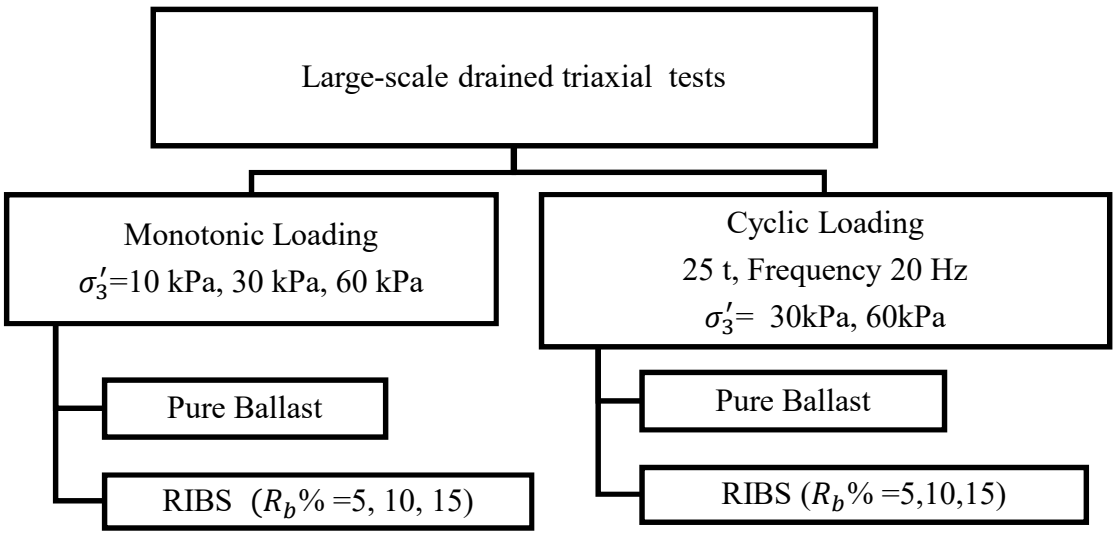

Figure 3.7 Laboratory testing program

3.4 Sample Preparation and Test Setup

Testing larger granular materials such as railway ballast and rockfill materials using conventional triaxial test apparatus is likely to provide false or confusing results because of the influence of the boundary on larger particles. Marschi et al., (1972) suggested that a ratio of specimen diameter to maximum particle dimension of 6 is needed to obtain reliable results. Therefore, the maximum particle size of the ballast was limited to 53 mm to ensure that the diameter of the test specimen (300 mm) to the largest particle size is not less than 6, to avoid the boundary effect during triaxial testing.

The large-scale triaxial apparatus consisted of a main chamber, a pressure control unit, a volume change, a measuring device, a loading actuator, and a data logger, all of which were controlled by the fully automated servo-control unit. This apparatus enables a specimen to undergo triaxial loading under a constant effective confining pressure. Confining pressure is applied to the test specimen by air and water. The influence on cell

pressure due to the change in volume of the specimen during loading is adjusted by the compressed air in the pressure control chamber. A vertical load is applied via a hydraulic pump connected to the loading frame and was measured by a pressure transducer. Two transducers measured the cell and pore water pressures. Axial deformation and the movement of the co-axial piston of the volumetric measurement device were measured by two linear variable differential transducers (LVDT). Figure 3.8 presents the schematic diagram of the large-scale triaxial apparatus, and a more detailed description of the test apparatus can be found in (Indraratna et al., 1998).

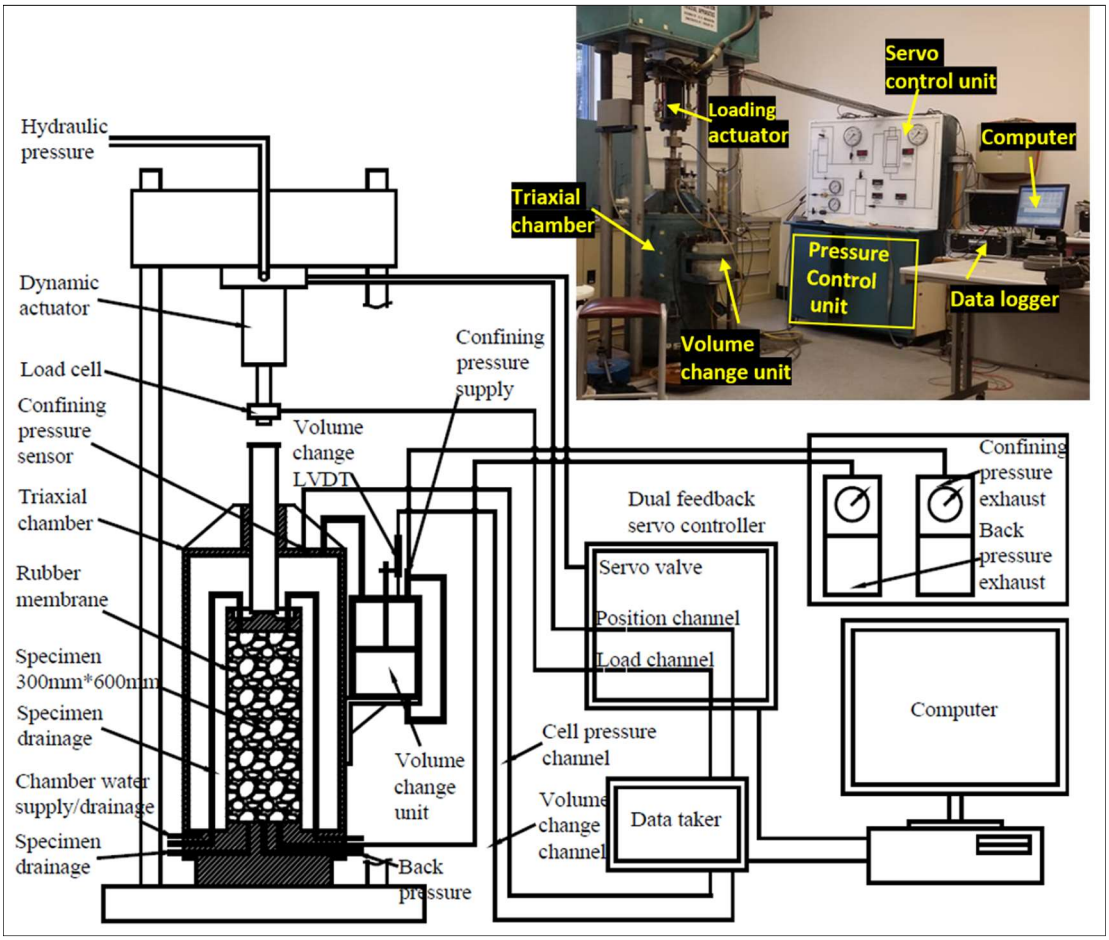

Figure 3.8 Schematic illustration of the large-scale triaxial testing system (modified after Sun, 2015)

Tests were carried out on specimens 300 mm in diameter and 600 mm high. The amount of material for each specimen was determined by calculating the mass of each particle range while keeping the same initial void ratio of 0.824, the same as the pure ballast for every specimen. To obtain a uniform mixture of RIBS with a given amount of rubber (R_b), ballast particles and dry rubber particles were mixed in a cement mixer at a very slow rotating speed (to avoid particle breakage). Figures 3.9 (a-g) show the steps of specimen preparation and testing setup. The precalculated amount of material was divided into four portions and compacted with a rubber padded vibrating plate inside the membrane in 150 mm thick layers, to ensure minimum particle breakage while preparing the test specimens. Two split moulds supported the 7 mm thick membrane while preparing the specimen (Figures. 3.9 a-e). Figures 3.9 (f-g) show the outer cell chamber that houses the specimen, the vertical loading unit, and the servo controller.

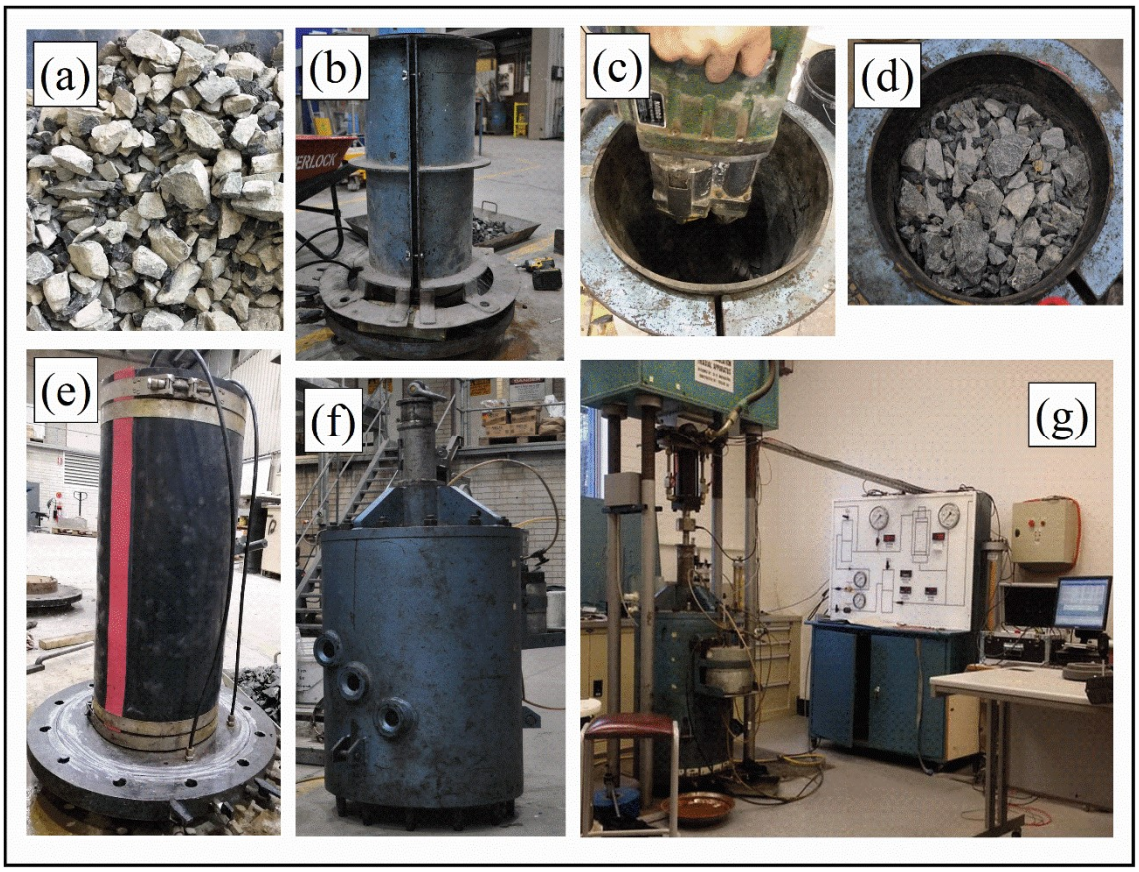

Figure 3.9 Sample preparation and test setup: (a) prepared RIBS material (R_b=5%), (b) 7mm membrane supported by two split moulds, (c) compacting the layers with a vibrating plate, (d) last layer of RIBS (R_b=5%), (e) prepared sample, (f) a sample is placed inside the outer cell chamber, and (g) setup of the large scale triaxial apparatus.

Before testing, each specimen was saturated under a back pressure of 10 kPa until a Skempton's B value of 0.97/0.98 was achieved. Target isotropic effective confining pressures (i.e., σ'_3 =10, 30 and 60 kPa) were selected to represent the actual field conditions for conventional tracks (Suiker, 2002). The specific gravity of RIBS (G_s) with different R_b% was calculated using the Equation,

$$G_s = \frac{1}{\left(\frac{(1 - R_b\%)}{G_B}\right) + \frac{R_b\%}{G_R}} \tag{3.1}$$

where $G_B = 2.8$ and $G_R = 1.15$ are the specific gravity of ballast and rubber, respectively.

The densities and specific gravities of RIBS after compaction are given in Table 3.3. The initial relative density (D_r) is decreasing with the increased rubber content as the rubber replaces a fraction of rock particles (same size range) which has higher specific gravity compared to rubber. The density calculations and the amount (mass) of ballast and rubber granules used for each test specimen are given in Appendix A.

Table 3.3 Basic properties of RIBS

R_b (%) in the RIBS mixture	Initial specific gravity (G_s)	Density (kg/m^3)	Initial relative density, D_r %
0	2.8	1535	1.00
5	2.61	1432	0.93
10	2.45	1342	0.87
15	2.3	1263	0.82

3.5 Monotonic Shearing

Monotonic shearing tests were planned to study the geotechnical characteristics such as shear strength parameters (friction angle), dilation angle, peak deviator stress, and initial tangent modulus of RIBS and then compare them with the pure ballast. Also, monotonic shearing represents the static loads on the track where the trains are stopped at stations and moving at very low speeds.

Monotonic loading triaxial tests were conducted as per ASTM D7181 (ASTM, 2020) under drained conditions. The monotonic triaxial program is given in Table 3.4.

Table 3.4 Monotonic loading triaxial program

Test	Rubber content R_b (%)	Confining pressure, σ_3' (kPa)
1	0	10
2	5	10
3	10	10
4	15	10
5	0	30
6	5	30
7	10	30
8	15	30
9	0	60
10	5	60
11	10	60
12	10	60

After setting up the fully saturated specimen, the corresponding confining pressure was gradually applied. Each specimen was subjected to an axial strain between 20–25% until the samples either failed or reached the maximum axial strain limit of the apparatus. The shearing rate was 1.5 mm/min, which was gradual enough to prevent the build- up of any excess pore pressures, and maintain a drained condition. The stress measurements were corrected for the membrane effect as per ASTM D7181-20. After completing each test, the specimens were then sieved to determine the extent of ballast breakage.

3.6 Cyclic Loading

After setting up the apparatus, confining pressures ($\sigma_3' = 30$ and 60 kPa) were applied to the specimens and the pore water pressure was monitored throughout the tests to ensure

effective drainage during cyclic loading. The program of drained cyclic loading triaxial tests under drained condition is given in Table 3.5.

Table 3.5 Cyclic loading triaxial program

Test	Rubber content R_b (%)	Confining pressure (σ'_3) kPa
1	0	10
2	5	10
3	10	10
4	15	10
5	0	30
6	5	30
7	10	30
8	15	30

The loading frequency *(f)* was 20 Hz resembling train speed (V) of about 150 km/h (Hussaini et al., 2015). All the tests were conducted up to 400,000 cycles or until the vertical deformation reached the limit of the equipment (@ 25% axial strain). Before and after the tests, the particles were sieved to quantify ballast breakage according to the ballast breakage index (BBI). More details, including the loading procedure will be discussed in Chapter 5.

3.7 Chapter Summary

This chapter proposed that the size of rubber granules should be between 9.5 mm to 19.5 mm to replace ballast of the same size, and with a similar angularity according to the nominal 60-graded specifications of the current Australian Standard for ballast (AS2758.7, 2015). This chapter also described the materials, particle size distribution, and laboratory test plan used to investigate the impact of using rubber granules in a ballast

assembly as an alternative ballast material. The tests were carried out under monotonic and cyclic loads in a large-scale cylindrical triaxial apparatus with different amounts of rubber (0–15% by weight) and at effective confining pressures of 10, 30, and 60 kPa. The features of the test apparatus, specimen preparation, and basic properties of the ballast and rubber mixtures tested in this study, and the testing procedures, are also included in this chapter.

CHAPTER FOUR

4 BEHAVIOUR OF RIBS MIXTURES UNDER MONOTONIC LOADING

4.1 Introduction

The main aim of this chapter is to understand the behaviour of Rubber Intermixed Ballast System (RIBS) under monotonic loading. The following sections present the results of a series of drained triaxial tests planned in Chapter 3. The effect of rubber (R_b) under different confining pressures (σ_3' =10-60 kPa) on stress-strain behaviour, modulus degradation, friction angle, dilatancy, stress-ratio, particle breakage and strain energy of RIBS mixtures were examined and evaluated by comparing the results with conventional ballast material.

4.2 Stress-Strain Response

As mentioned in section 3.5, each specimen was strained at a rate of 1.5 mm/min until they failed or reached the 20-25% of axial strain limit. The stress measurements were corrected for the membrane effect as per ASTM D7181-20 [2].

In this study the conventional triaxial stress parameters: p' (mean effective stress) and q (deviator stress) were calculated from $p' = \frac{\sigma_1' + 2\sigma_3'}{3}$ and $q = \sigma_1' - \sigma_3'$, where σ_1' and σ_3' are principal effective compressive stresses. The volumetric strain (ε_v) can be determined from ($\varepsilon_a + 2\varepsilon_r$) where ε_a and ε_r are the axial and radial strain, respectively. Typical stress-strain curves for RIBS mixtures with different R_b (i.e., 0%, 5%, 10% and 15%) at different effective confining pressures (i.e., σ'_3 =10, 30 and 60 kPa) are shown in Figure 4.1.

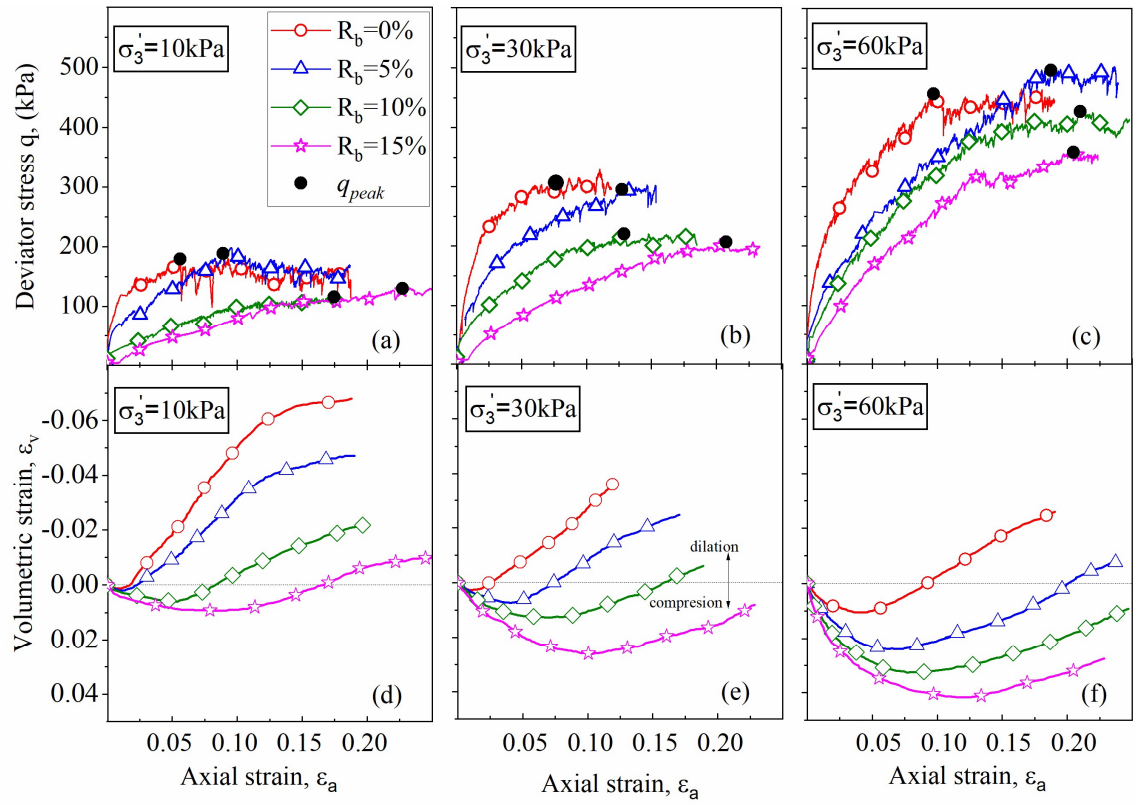

Figure 4.1 Effect of the rubber on: (a-c) deviator stress-axial strain curves; (d-f) volumetric-axial strain curves

Note that the deviator stress of all the specimens increases with the axial strain until they reach the peak deviator stress, and there is no pronounced strain-softening except for pure ballast and for the ballast with 5% rubber at $\sigma'_3 = 10$ kPa. This complements the observations made earlier by Indraratna et al., (2015) and Lackenby et al., (2007), because

failure of ballast is generally accompanied by bulging towards the centre of the specimen, rather than a distinct shear plane across the specimen. The computed peak deviator stress ratio (η_{peak}) is denoted by a dark solid circle on each plot. Note that the peak deviator stress (q_{peak}) increases as the effective confining pressure increases, whereas under the same effective confining pressure, q_{peak} decreases with an increasing R_b when the amount of rubber is >5%. However, when R_b=5%, the RIBS mixtures have a relatively similar q_{peak} to pure ballast, but when the amount of rubber increases the RIBS mixtures exhibit a rubber-like behaviour (Figure 4.1(a-c)) as they reach their peak stress at relatively higher axial strains, thus transforming the RIBS mixture from a brittle to a ductile state. Moreover, the volumetric strain of RIBS with R_b >5% barely stabilised by the end of the test, probably because the rubber particles continued to deform until the end of the test, thus preventing the volumetric strain to attain a constant value, i.e. a critical state.

Unlike the light tamping while preparing the test specimen, increased deviator stress and larger effective confining pressure compress the rubber particles in the RIBS mixtures and make notable changes in the compressive behaviour of the mix compared to pure ballast specimens (Figure 4.1(d-e)). The rubber grains in a compressed state trigger effective particle interlocking (i.e., it reduces the volume of voids) to make the material denser than its initial state. It can be due to the volume change of rubber or change of the shape of the rubber particles at the compressed state. Similar to the way in which an increased effective confining pressure would suppress volume expansion, an increased density reduced the volume compression, followed by dilation of the dense granular assembly as shearing progressed.

As shown in Figure. 4.1(d-e), pure ballast and RIBS with 5% rubber (σ'_3<30 kPa) show only limited initial volumetric contraction in contrast to overall dilation, whereas test

specimens of RIBS with R_b>5% undergo significant initial compression before any dilation. RIBS with increased R_b at larger effective confining pressures demonstrate larger compressions (e.g. 4% for RIBS with 15% rubber at effective confining pressure, $\sigma'_3 = 60$ kPa); this may cause relatively large initial settlements in the ballast layer. A closer inspection of Figure 4.1(a-c) shows that some abruptly fluctuating undulations in the otherwise relatively smooth stress-strain curves represent ballast breakage or the attrition of rough and angular surfaces of coarse particles during shearing (slipping). It is noted that these erratic undulations become insignificant as the percentage of rubber increases, which indicates reduced ballast breakage within the granular assembly. This may be attributed to an increase in the contact surface area between ballast and rubber (i.e., a better interlock) which resist slipping and alleviates to some extent the high stress concentrations at particle contacts.

4.3 Dilatancy Behaviour

Figure 4.2 shows the variation of deviator stress ratio (η= q/p') with the increasing axial strain (ε_a) for the fresh ballast and RIBS material. It is clear that pure ballast exhibits a higher peak stress ratio compared to RIBS, especially at low confining pressures (i.e., $\sigma'_3 = 10\ kPa$). It also reveals that the increment of deviator stress ratio was delayed by adding rubber and that this is predominant at increased confining pressures. At low confining pressures ($\sigma'_3 \leq 30\ kPa$) and with lower rubber contents ($R_b \leq 5\%$) the peak stress ratio of the RIBS gradually decreases as shearing progresses. At increased confining pressures ($\sigma'_3 > 30\ kPa$) and with increased rubber ($R_b > 5\%$), however, the deviator stress ratio of RIBS reaches a stable value at higher axial strains. In terms of stress ratio, an increase in confining pressure does not make a significant effect on RIBS

($R_b > 5\%$) compared to the pure ballast primarily due to the absence of dilatancy. This is clearly reflected by the plots for dilatancy $d = d\varepsilon_v/d\varepsilon_a$ versus stress ratio shown in Figure 4.3 and further explained below.

Figure 4.3 (a-c) shows that the peak stress ratio decreases as the confining pressure increases for conventional ballast and RIBS with ($R_b = 5\%$). However, when $R_b > 5\%$, the change in the confining pressure shows an insignificant effect on the peak stress ratio and dilatancy of RIBS.

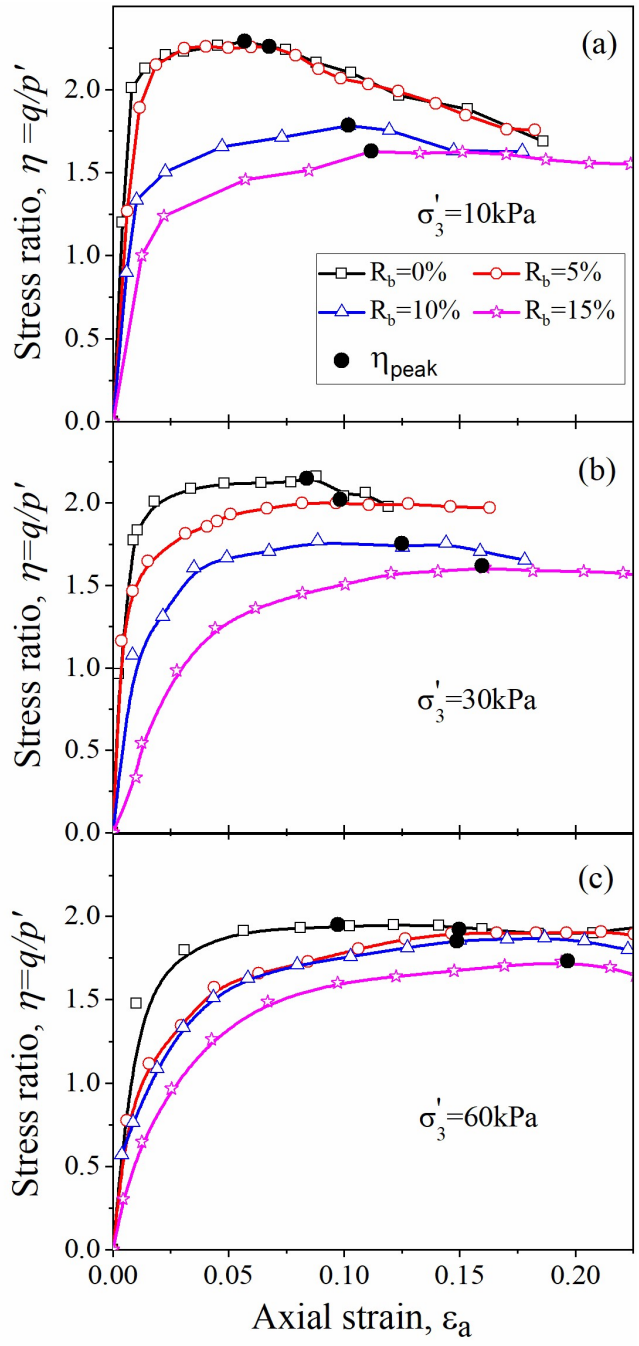

Figure 4.2 Variation of deviatoric stress ratio with axial strain

The reason for this can be attributed to the induced rubber contracting during the initial shearing stage (up to $d\varepsilon_v/d\varepsilon_a$=0 for the first time) which then influences the stress-dilatancy behaviour more than the change in effective confining pressures (10–60 kPa). Having a broadly similar stress-dilation behaviour with changing effective confining pressures is an advantage for RIBS mixtures (R_b>5%) in terms of controlling the lateral

misalignments along the track from a practical perspective. However, while an increase in the amount of rubber decreases the peak stress ratio, this difference is not as significant under higher effective confining pressures (e.g. 60 kPa). It is observed that the maximum dilatancy generally decreases with the increased rubber content, and the effect of confining pressure on dilatancy is insignificant when (R_b>10%) (Figure 4.3 d).

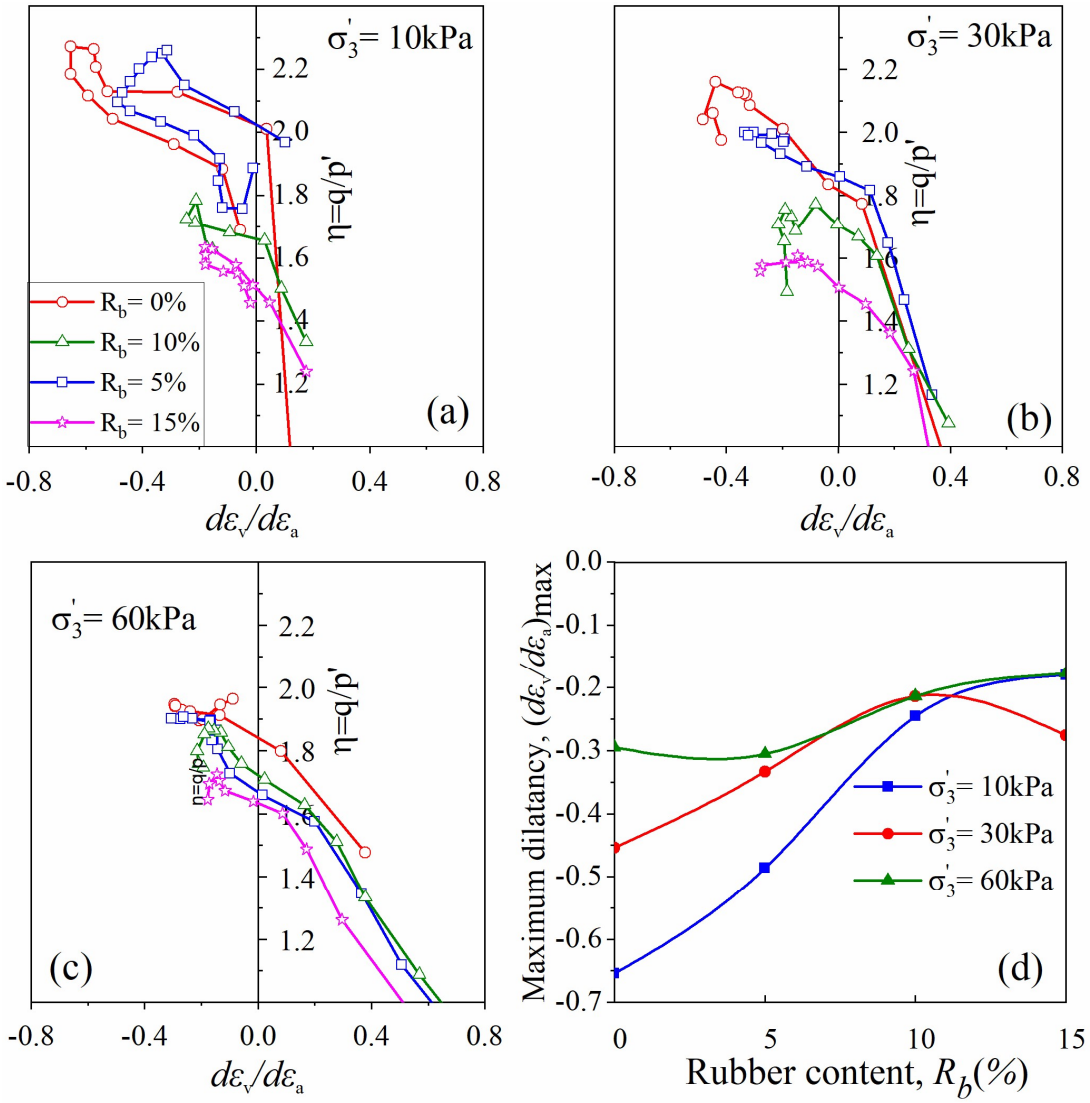

Figure 4.3 (a–c) Dilation-stress ratio responses of RIBS under different effective confining pressures: (a) 10 kPa, (b) 30 kPa and (c) 60 kPa; (d) maximum dilatancy with rubber content

4.4 Modulus Degradation

The stress-strain plots in Figure 4.1 (a-c) follows the typical stress-strain behaviour for loose sand. This typical stress-strain behaviour was approximated by the nonlinear hyperbolic stress-strain curve (Duncan and Chang, 1970) as shown in Figure 4.4 and is given by the following equation.

$$q = \frac{\varepsilon_a}{a + b\varepsilon_a} \tag{4.1}$$

where a and b are model parameters determined by curve fitting the experimental data ($R^2 > 0.98$).

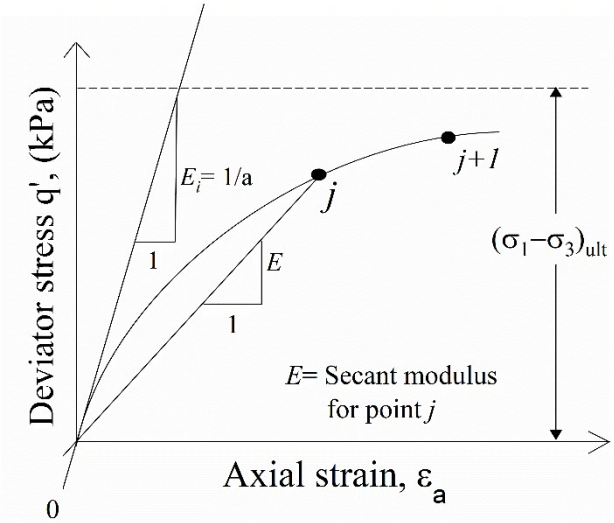

Figure 4.4 Hyperbolic approximation (after Duncan and Chang (1970))

In Figure 4.4, based on the hyperbolic fit, $1/a$ is the initial tangent modulus E_i and $1/b$ is the ultimate principal stress difference. The secant modulus of soil (E), is defined as the ratio between the differences in deviator stress to the corresponding axial strain, where $E = \Delta q/\Delta\varepsilon_a$. Modulus degradation at a point is determined by the ratio, E/E_i: The initial tangent modulus E_i, represents the short-term static modulus of elasticity, which is required to calculate the initial elastic track settlements. Figure 4.5 presents initial tangent

modulus versus rubber content graphs for different confining pressures. It is also a good indicator of the ductility of the materials because a lower E_i means higher ductility. In Figure 4.5 there is a clear trend of decreasing E_i with the introduction of rubber into the mixture, thus indicating reduced stiffness and increased ductility. Under the same confining pressure when (R_b=5%), the reduction of E_i is around 60% compared to pure ballast. Any further increase in the amount of rubber in the RIBS tends to have a lesser influence on further reducing the value of E_i. It is also clear that for the specimens with the same rubber content, an increase in the effective confining pressure increases the value of E_i.

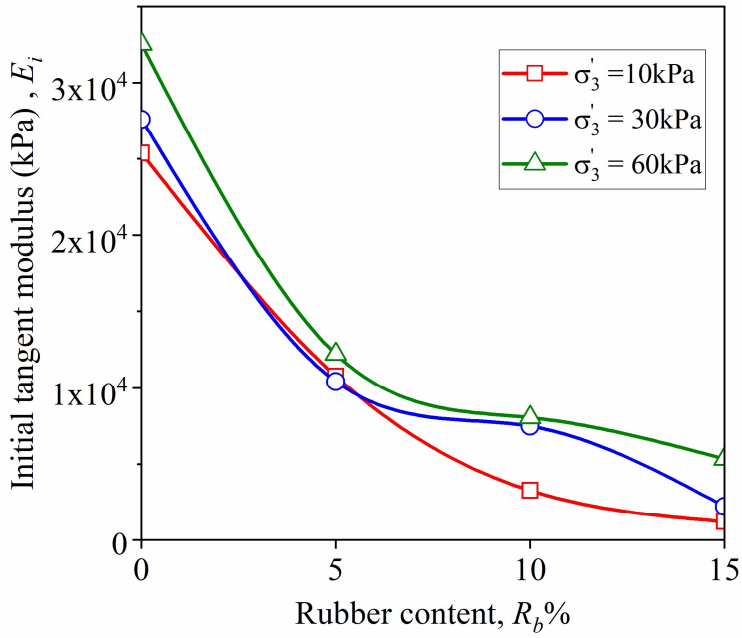

Figure 4.5 Initial tangent modulus, E_i

Figure 4.6 a shows the plots for modulus degradation against the axial stain under the confining pressure of 60 kPa. The modulus degradation E/E_i rapidly decreases and attains stability in pure ballast, but an increase in the amount of rubber in the RIBS mixtures slows down the rate of modulus degradation. Therefore, for the RIBS samples with increased rubber (R_b>10%), the modulus degradation is notable, even at the large

axial strains (ε_a>0.15). The reason for this gradual decrease in the rate of modulus degradation (shape of modulus degradation curve) can be attributed to the increased particle interlocking due to the deformation of rubber granules. The modulus degradation at η_{peak} is also shown in Figure 4.6 a, where η_{peak} is the peak stress ratio obtained by determining the maximum stress ratio (η) based on $\eta - \varepsilon_a$ plots (Figure 4.2).

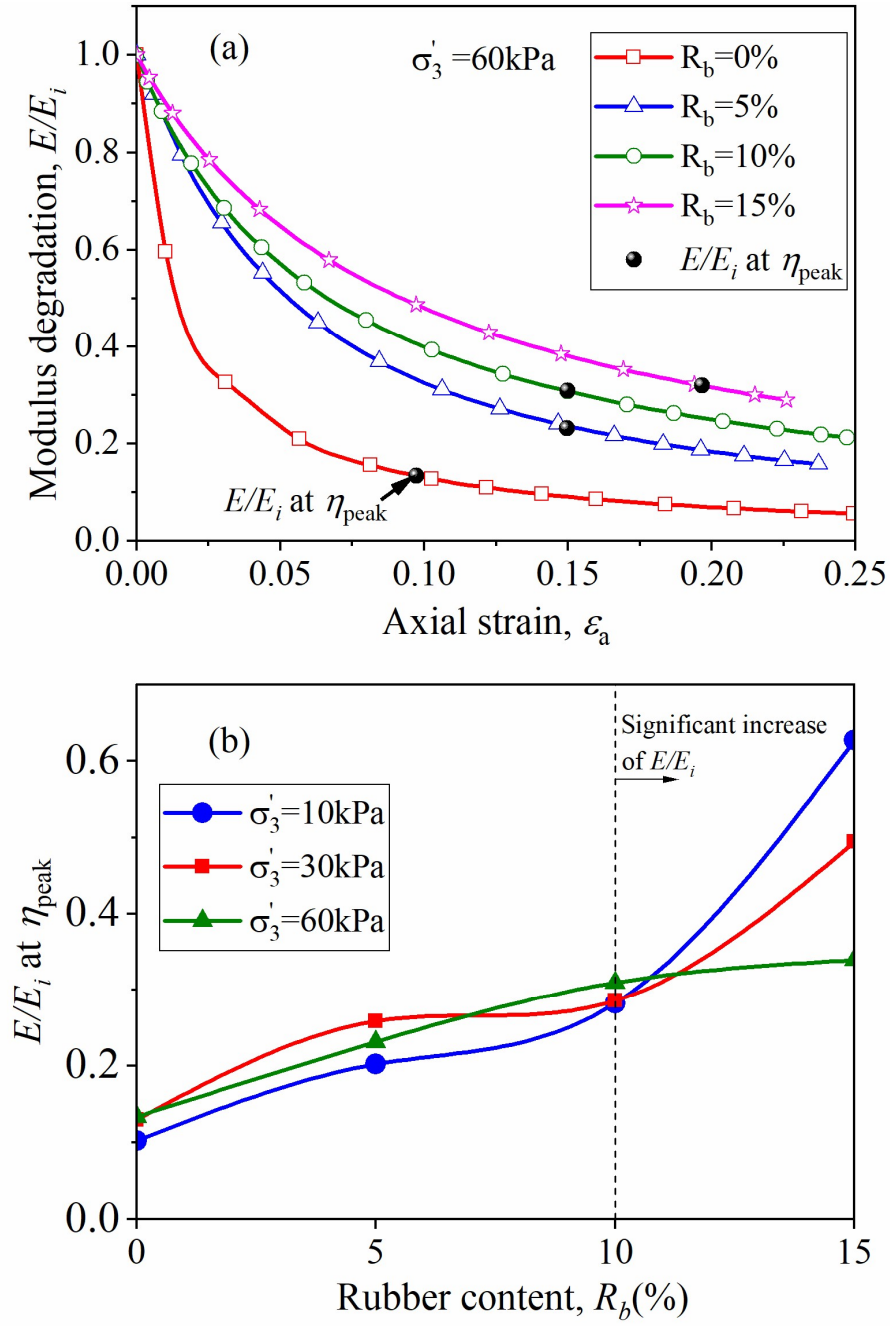

Figure 4.6 (a) Secant modulus degradation of pure ballast and RIBS (σ_3' = 60 kPa); (b) secant modulus degradation of RIBS at η_{peak} against the rubber content

RIBS materials with increased rubber can undergo significant axial deformation before failure compared to pure ballast. In other words, the reduced rate of modulus degradation increases the failure strain, i.e. increased ductility. For instance, at σ_3' = 60 kPa the axial strain at peak stress ratio (where E/E_i starts stabilising) increases from 0.09 to 0.2 when R_b increases from 0 to 15%. Therefore, due to the increased ductility, the value of E/E_i

at peak stress ratio increases with the increased rubber content (Figure. 4.6 b). However, when R_b increases to 15% there is a sharp increase in E/E_i . Note that when R_b>10%, the influence of confining pressure on the E/E_i becomes pronounced, and E/E_ireduces as σ_3' increases.

4.5 Friction Angle and Dilation Angle

The internal friction of ballast material governs the stability of the track. Previous studies (Indraratna et al., 2011; Salim, 2004) revealed that the effective friction angle (φ_{ef}) of fresh ballast varies from 46° to 69° as the effective confining pressure increases from 10 to 300 kPa. However, it can be a challenging task to obtain a RIBS mixture without reducing its shear strength attributed to the lower strength of rubber compared to intact rock aggregates, hence the importance of ensuring the ideal or optimum rubber content in the mix. For instance, Song et al., (2019) showed that a mixture of ballast and rubber with the same gradation (R_b=10%) significantly reduces the internal friction angle of ballast (by 24%). The effective friction angle of RIBS mixtures in this study was calculated using the peak deviator stresses, and tabulated in Table 4.1.

Table 4.1 Effective friction angle of pure ballast and RIBS

R_b (%) in the RIBS mixture	**Effective friction angle, φ_{ef}**
0	48.8
5	48.4
10	47.7
15	46

Note that increasing R_b from 0 to 15% led to a minor change in the effective friction angle for RIBS mixtures from 48.8° to 46.0°. This indicates that replacing the typical size range

of ballast between 9.5 and 19.5 mm with up to 15% of rubber granules may have only marginally compromised a reduction in the overall shear strength. In addition to the effective friction angle, the mobilised friction angle of all the specimens at the peak stress ratio $\varphi_p$was also determined and plotted against the percentage of rubber (Figure 4.7 a). The mobilised friction angle at the peak stress ratio incorporates the effect of breakage and dilatancy of the sample thus corresponding to the stresses at peak stress ratio, whereas the effective friction angle (φ_{ef}) does not (Indraratna and Salim, 2002). It can be seen that the difference between the φ_p and the φ_{ef} decreases as the amount of rubber increases; this represents reduced dilation and breakage.

The relationship between the effective friction angle at a certain confining pressure and the rubber content can be correlated by a linear function for the range of rubber contents considered in this study (i.e. 0-15%). As shown in Figure 4.7 (a) the equation for the effective friction angle of the mixtures used in the study can be written as;

$$\varphi_{ef} = -0.182 \times R_b(\%) + 49 \tag{4.2}$$

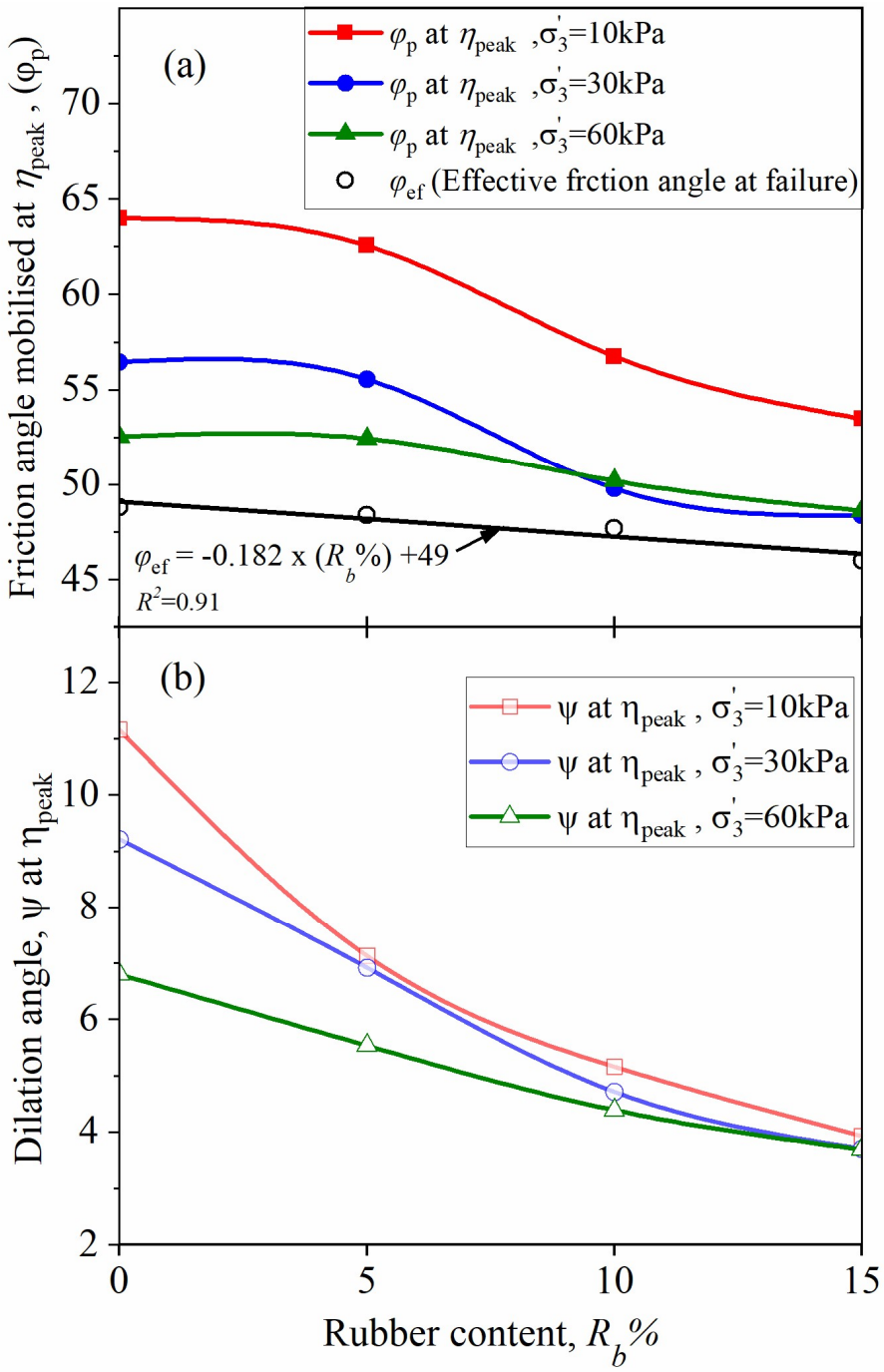

Figure 4.7 Effect of the rubber on (a) effective friction angle (φ_{ef}), friction angle at η_{peak} (φ_p) (b) dilation angle ψ at η_{peak}

In the previous studies (Salim and Indraratna, 2004; Xu and Song, 2009; Indraratna et al., 1998), increased grain breakage has been identified as the reason for the reduced φ_p of ballast/rock fill materials at larger confining pressures. Thus they observed non-liner strength envelops associated with dilatant behaviour. The Experimental results for RIBS

show that the confining pressure and rubber content, R_b significantly affect φ_p but the particle breakage is negligible in RIBS compared to the conventional ballast material. The reason is that the compression of RIBS assembly is increasing with the increase of R_b at increased confining pressures. Therefore the relationship for variation of φ_p of RIBS with R_b and σ_3' can be determined by plotting measured φ_p values against R_b under different confining pressures (Figures 4.8 and 4.9).

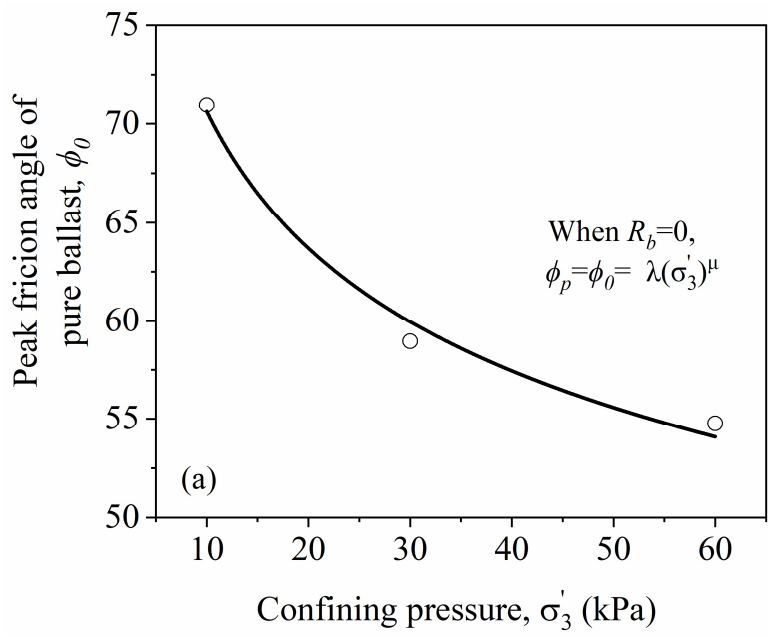

Figure 4.8 Effect of confining pressure (σ_3') on φ_p of pure ballast (R_b=0)

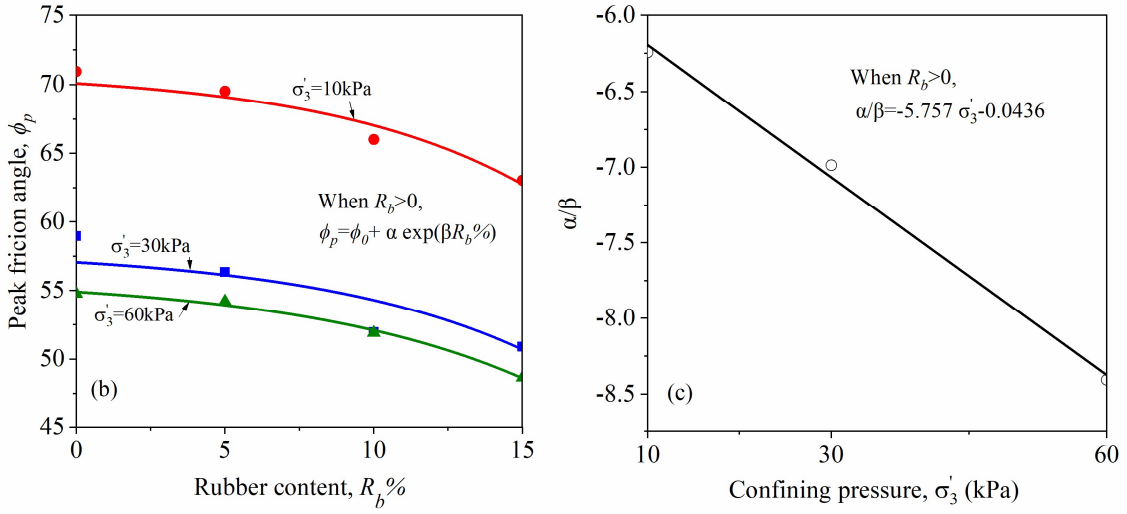

Figure 4.9 (a) Effect of rubber content (R_b) on φ_p of RIBS (R_b >0) (b) Relationship of α/β with confining pressure, σ_3' ($R_b > 0$)

For the approximate confining stress range applicable for railways tracks ($\sigma_3' < 60kPa$) the variation of φ_p with σ_3' and R_b is described by the following exponential equation:

If $R_b = 0$ (for pure ballast),

$$\varphi_p = \varphi_0 = \lambda(\sigma_3')^{\mu} \tag{4.3}$$

If $R_b > 0$ (for RIBS),

Referring to Figures 4.8 and 4.9, φ_p and α/β can be written as;

$$\varphi_p = \varphi_0 + \alpha \exp\ (\beta\ R_b\%) \tag{4.4}$$

$$\alpha/\beta = (-5.757\ (\sigma_3')) - 0.0436)\beta \tag{4.5}$$

By substituting α in the equation 4.4;

$$\varphi_p = \varphi_0 + (-5.757\ (\sigma_3')) - 0.0436)\beta \exp(\beta\ R_b\%) \tag{4.6}$$

where φ_0 is the peak friction angle of ballast at corresponding confining pressure and λ, μ , α and β are empirical coefficients.

Figure 4.10 compares the φ_p of pure ballast (latite basalt) and RIBS from the current study with a previous study by Indraratna et al., (1998). Note here that the results from the current study agree with the results from the previous study by decreasing the peak friction angle with the increased confining pressures. However, the values of the peak fiction angle from the study by Indraratna et al. (1998) are higher than those from the current study due to two different particle gradation.

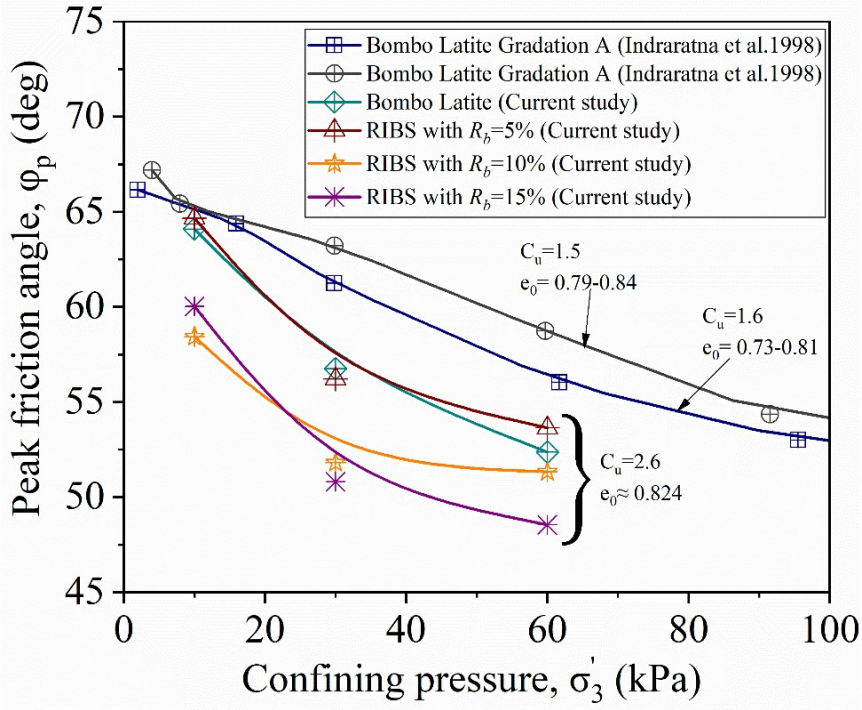

Figure 4.10 Comparison of peak friction angle, φ_p from the current study with a previous study by Indraratna et al., (1998).

The dilation angle (ψ) is calculated using the equation $\sin\psi = -\frac{d\varepsilon_v/d\varepsilon_a}{2-d\varepsilon_v/d\varepsilon_a}$, where $d\varepsilon_v$ is the increment of volumetric strain, and $d\varepsilon_a$ is the increment of axial strain. As also shown in Figure 4.7 (b), the dilation angle at peak deviator stress ratio (ψ at η_{peak}) decreases as the amount of rubber increases and when (R_b >5%), ψ of RIBS is less than that of conventional ballast; ψ decreases as the confining pressure increases, and the effect of confining pressure is suppressed by the increased rubber content. This is also

in agreement with the plots for dilatancy $d = d\varepsilon_v/d\varepsilon_a$ versus stress ratio shown in Figure 4.3.

4.6 Ballast Breakage

Ballast breakage is one of the key factors that cause track degradation. In this study, the particle breakage of RIBS mixtures has been quantified using the ballast breakage index (BBI) (Indraratna et al., 2005) and the classical particle breakage index (B_g) (Marsal, 1967). The definition of BBI and the B_g was discussed in the section 2.4. B_g is expressed as a percentage. BBI is a parameter that can be conveniently used to examine the overall particle breakage of the RIBS, while Marsal's breakage index B_g can demonstrate the sizes of ballast particles that are more prone to breakage and how the addition of rubber can control breakage for each particle size range. It has been found that if the $BBI < 0.1$, breakage can then be considered negligible (Indraratna and Ngo, 2018). Figure 4.11 shows the BBI of RIBS mixtures varying with R_b. A considerable amount of breakage (BBI = 0.15–0.23) is found for pure ballast specimens under σ_3' = 10, 30 and 60 kPa; this agrees with previous studies by Indraratna and Salim (2005) and Indraratna et al. (2015b). The investigations of BBI in RIBS mixtures demonstrate negligible ballast breakage ($BBI < 0.1$) after adding 5% or more of rubber. Therefore, these insignificant BBI values for RIBS cannot be compared to each other concerning R_b. The change in B_g with the percentage of rubber in each RIBS mixture under an effective confining pressure of 10 and 30 kPa are shown in Figure 4.12.

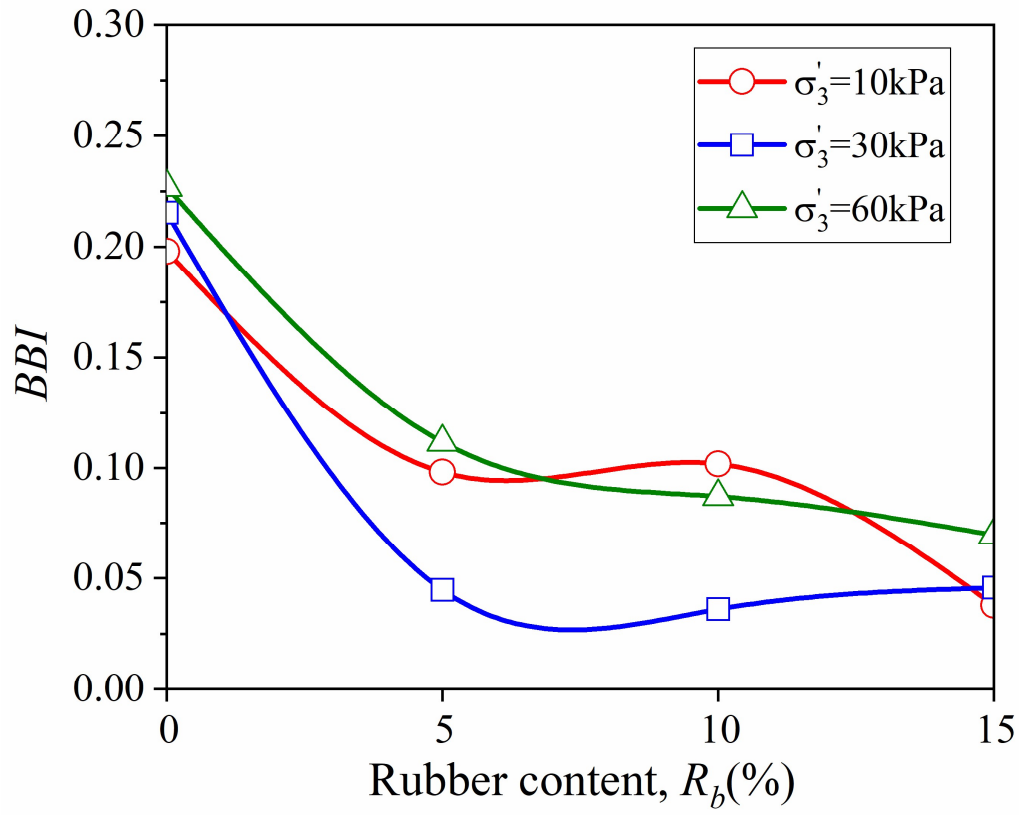

Figure 4.11 Influence of R_b on ballast breakage index (BBI)

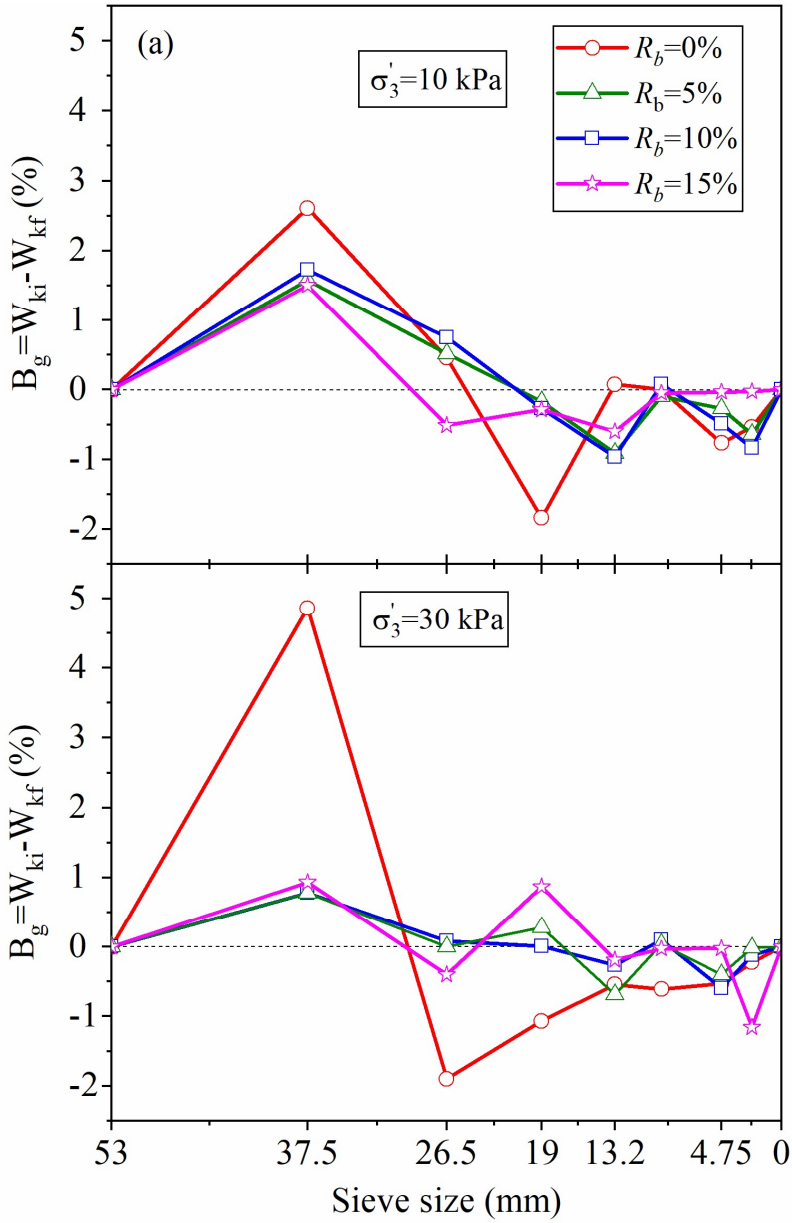

Figure 4.12 Influence of R_b on Marsal's breakage index, $B_g = \sum(\Delta W_k > 0)$

It can be clearly seen that the reduction in breakage was significant in the larger ballast particles (>38 mm) in all the specimens with rubber (irrespective of R_b) compared with pure ballast. Under the confining pressure of 30kPa, the reduction was observed as more than 70%. A small increase in the amount of rubber enhances the internal stress distribution with an increased damping effect, and this significantly reduces the degradation of the larger particles. In this study, it is observed visually after the sieve analysis for pure ballast, that corner breakage of highly angular particles contributed more

to ballast degradation than splitting (i.e. across the body of the particles). The other possible reason for reduced ballast breakage in RIBS is the reduced angular corner breakage due to the increased contact areas between the ballast and rubber within the blended matrix (Figure 4.13). These observations seem to support the idea of replacing ballast with rubber granules in the size range of 9.5–19 mm rather than larger sizes (>19 mm), not only to preserve the strength of the material but also to reduce ballast breakage.

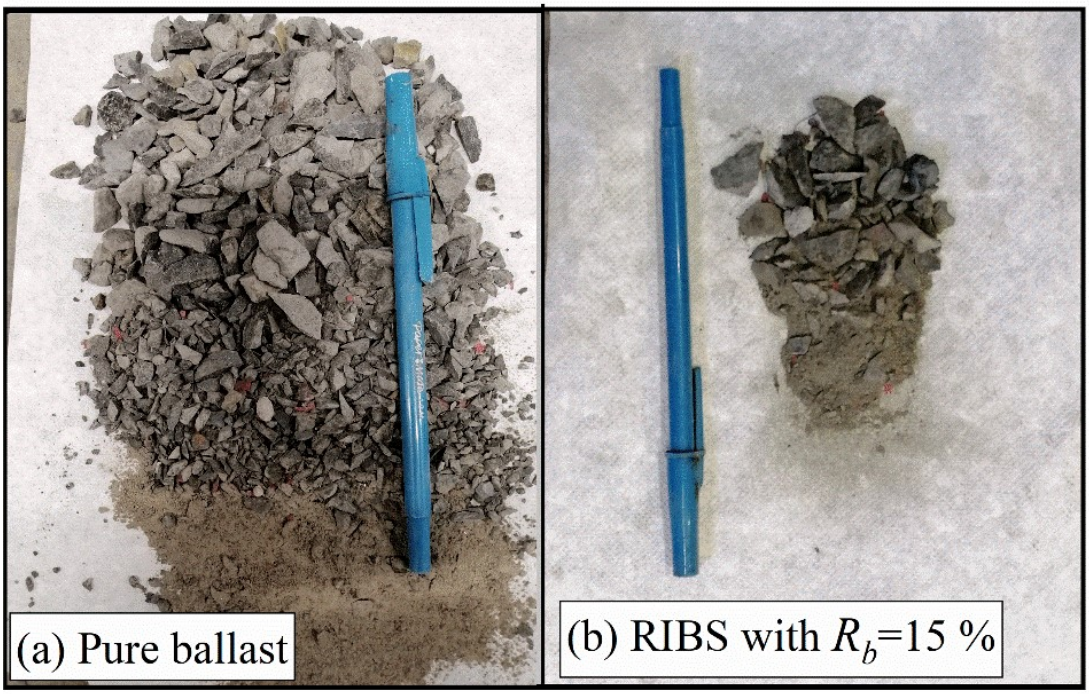

Figure 4.13 Particles passed through 4.75 mm sieve (after the shearing test at $\sigma_3' = 30\ kPa$)

4.7 Energy Absorption

4.7.1 Strain energy density

To evaluate the energy absorption capacity of the RIBS mixture, the strain energy density (E_d) is used herein:

$$E_d = \int_0^{\gamma_f} \tau d\gamma \tag{4.5}$$

where γ_f is the shear strain up to the peak shear stress and τ is the shear stress; here $\tau = q/2$ and the shear strain is $\gamma = 3\varepsilon_q/2$. Here ε_q is the deviator strain where $\varepsilon_q = \varepsilon_a - \varepsilon_v/3$.

Figure 4.14 shows the shear stress–strain plots for RIBS under effective confining pressure of 10 kPa. In Figure 4.14a, the points at which the shear stresses become stable (approaching a constant value) are taken as the peak shear stress point. It can be seen that the shaded area under the shear stress–strain curve up to the peak shear stress point increases as more rubber is added, meaning E_d increases under $\sigma_3' = 10\ kPa$. To better evaluate the energy absorbing capacity of RIBS by adding rubber, a dimensionless ratio representing the normalised strain energy density $\hat{E}_d$ is proposed, namely the amount of absorbed energy density with respect to pure ballast. $\hat{E}_d$ is calculated for all specimens and is shown in Figure 4.14 (b). Note that the inclusion of rubber increases $\hat{E}_d$ indicating the energy absorption capacity of RIBS increases, which is because more energy is consumed during the contraction of highly compressible mixtures. The increase is more pronounced under low confining pressures (e.g. $\sigma_3' = 10$–30 kPa). This is more favourable as the ballast layer in the field is normally subjected to only a very low confining pressure 10–30 kPa (Indraratna et al., 2015). This is a justifiable reason for adding rubber to ballast materials the increased energy absorbing capacity of the ballast layer not only decreases ballast breakage internally, it also reduces the amount of energy transferring to other substructure layers (e.g. subballast and subgrade), hence reducing damage to overall track elements (Qi et al., 2020).

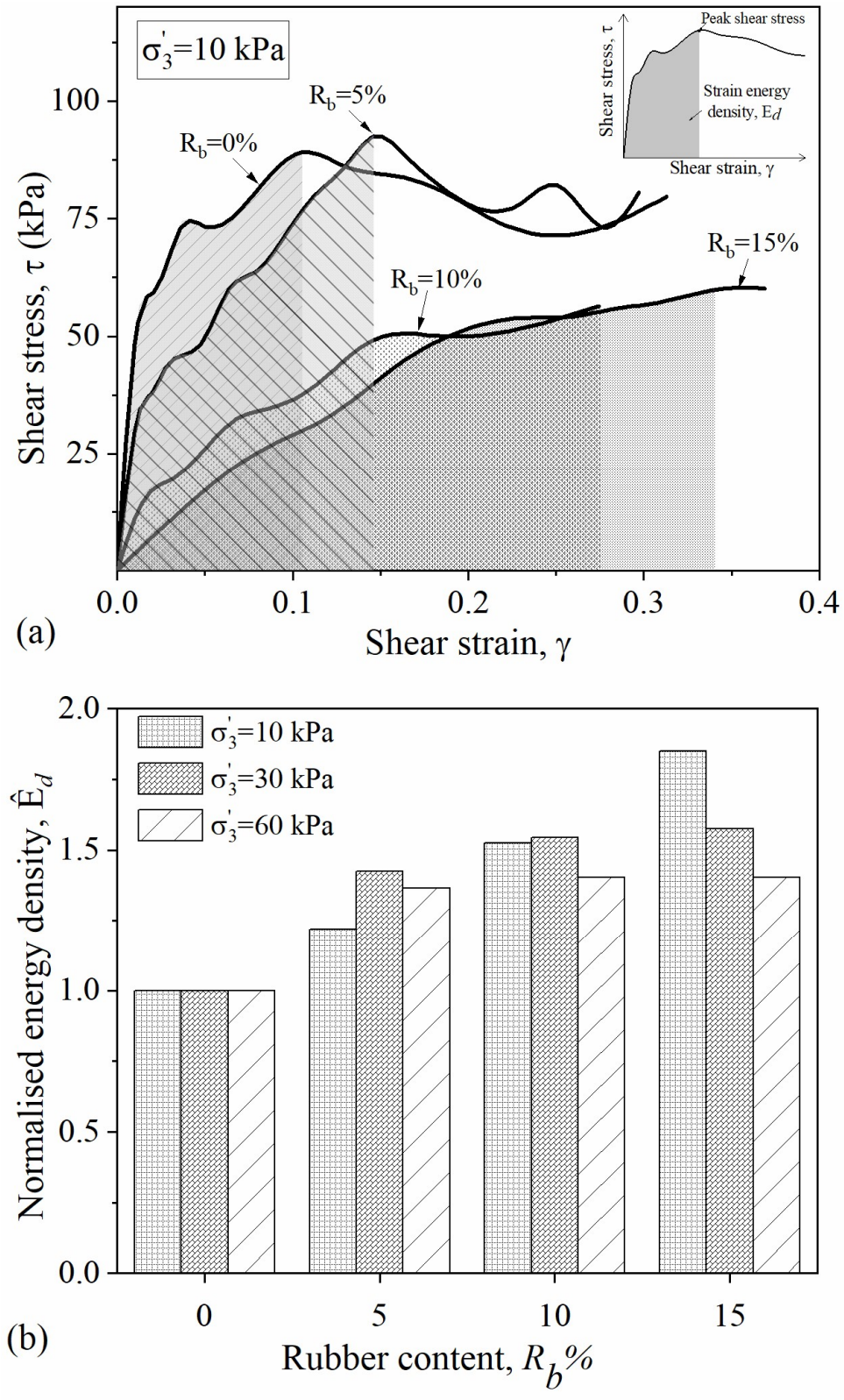

Figure 4.14 (a) Shear strain versus shear stress σ_3'= 10 kPa, and (b) normalised strain energy densities variation against the rubber content.

4.7.2 Effect of replaced rubber and distortional energy

As mentioned in the previous section, adding rubber changes the energy absorption capacity and the deformation of the materials. Suppose the change moves $\eta - \varepsilon_q$ curves from 1 to 2, as shown in Figure 4.15. The shaded area between curve 1 and curve 2 can be defined as the incremental distortional energy (ΔU) and it can be written as in Equation 4.6.

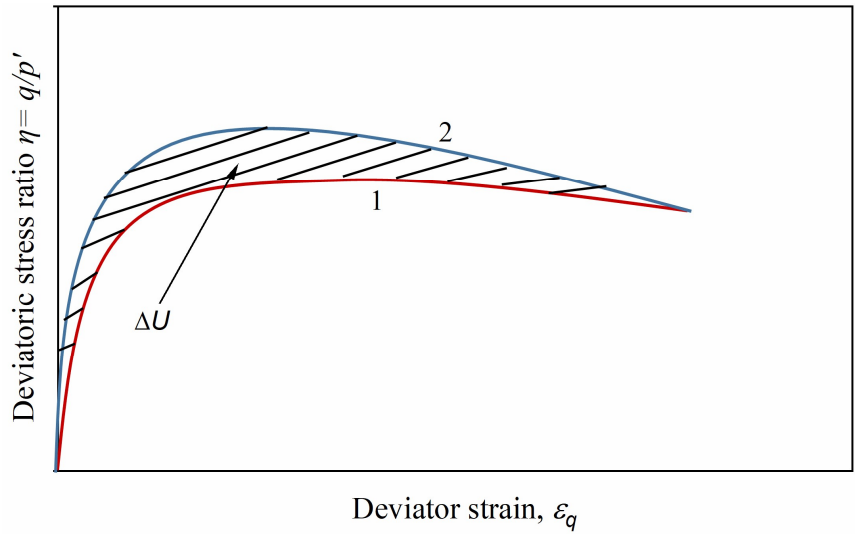

Figure 4.15 Incremental distortional energy (ΔU)

$$\Delta U = \int_0^{\infty} (\eta_2 - \eta_1) d\varepsilon_q \tag{4.6}$$

If $\Delta \rightarrow 0$, The differential incremental distortional energy can be written as,

$$du = \eta_2 d\varepsilon_q - \eta_1 d\varepsilon_q \tag{4.7}$$

$$\Delta U = \int_{\varepsilon_q=0}^{\varepsilon_q=\varepsilon_q^*} du = \int_{\varepsilon_q=0}^{\varepsilon_q=\varepsilon_q^*} \eta_2 \, d\varepsilon_q - \int_{\varepsilon_q=0}^{\varepsilon_q=\varepsilon_q^*} \eta_1 \, d\varepsilon_q \tag{4.8}$$

Suppose curve 1 represents the RIBS material ($R_b > 0$) and curve 2 represents pure ballast ($R_b > 0$). The difference in energy calculated from curve 2 and curve 1 represents the energy absorbed by the mixture by replacing some ballast particles between 9.5 -19 mm with the same size rubber particles. Figure 4.16 shows plots for $\int \eta d\varepsilon_q$ against ε_q for pure ballast and RIBS material. Along each curve the distortional energy (U) at a given deviator strain (ε_q^*) can be found. All the plots can be empirically correlated in the form of Equation 4.9, where α' and β' are functions of R_b.

$$U = \alpha' \left(\varepsilon_q\right)^{\beta'} \tag{4.9}$$

Note that the curves rotate clockwise as $R_b\%$ increases, this indicates that α' and β' are parameters associated with $R_b\%$ replaced with the same size ballast particles (Figure 4.16). As expected, Figure 4.17 shows that α' and β' are in a linear relationship with $R_b\%$.

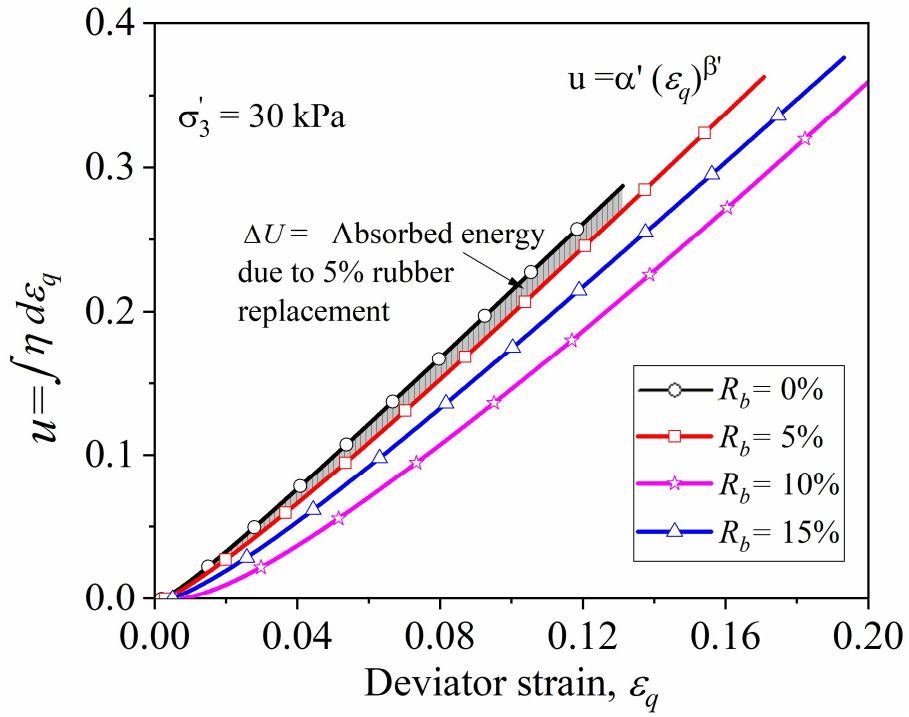

Figure 4.16 Distortional energy (U) due to $R_b\%$ replaced with the same size of ballast particles at a given deviator strain (ε_q^*)

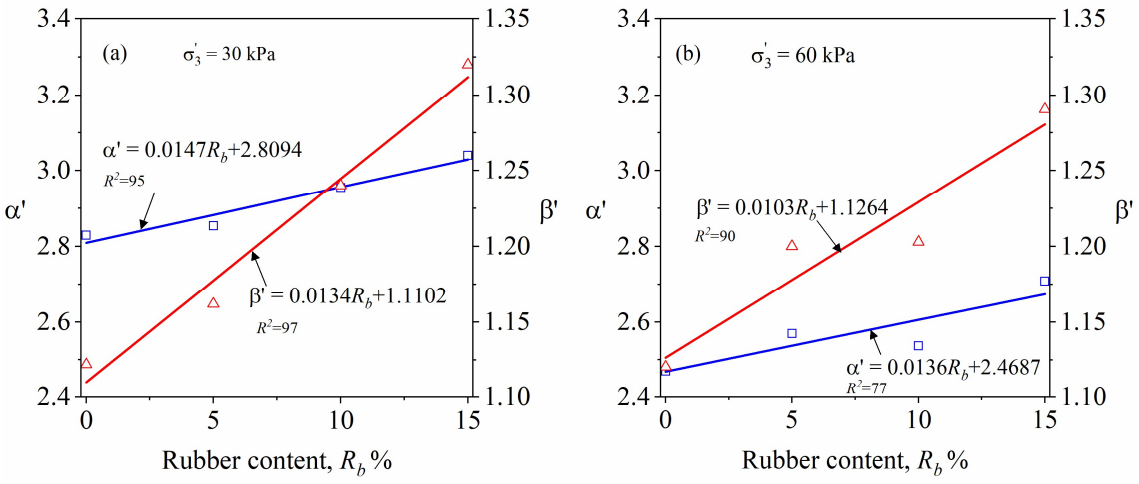

Figure 4.17 The relationship of α' and β' in terms of $R_b\%$ for the specimens tested at (a) $\sigma_3' = 30\ kPa$ and (b) $\sigma_3' = 60\ kPa$

4.8 Critical State Behaviour

Specimens were axially strained up to 20-25% and terminated as they reached the maximum axial strain limit of the apparatus. Unfortunately, only a few specimens reached their critical state because the specimens with increased rubber contents required larger strains to reach their critical state. This has been confirmed by previous studies on rubber and granular materials mixtures (Mashiri et al., 2015; Youwai and Bergado, 2003; Qi et al., 2018). The stress-strain data shows that there is a trend towards reasonably constant stresses with the increased strains (Figure 4.1), which have been assumed to be the critical state. Thus, the data is extrapolated according to the methods suggested by Carrera et al., (2011) to obtain the critical stress ratio, M_c.

Method 1 Extrapolating the stress ratio–dilatancy graph until the end of the curve intersects the zero dilatancy axis, as shown in Figure 4.18.

Method 2 Estimation of the critical state stress ratio by employing stress ratio, volumetric strain, and axial strain Figure 4.19.

By following these two methods, the representative critical stress ratio is identified in the current study.

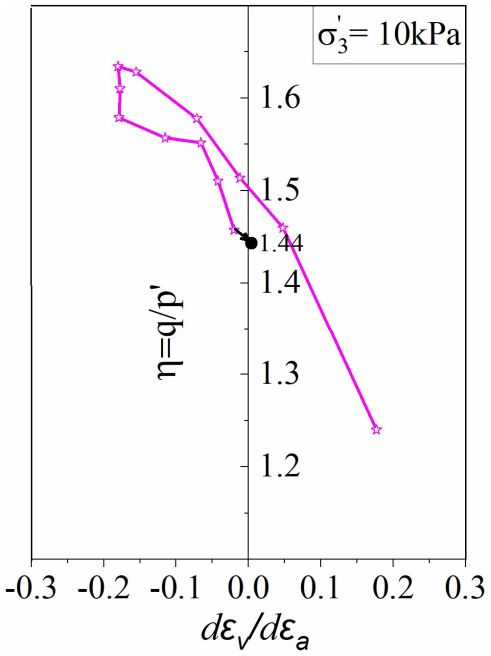

Figure 4.18 Estimation of the critical state stress ratio employing the stress ratio and dilatancy

As the specimens reach the critical stress ratio, deformation occurs under constant stress and constant volume. Therefore, at the critical state $d\varepsilon_v/d\varepsilon_a$ can be considered as zero due to the no change in volume. As shown in Figure 4.8, the critical stress ratio is determined by extrapolating the curve until it intersects $d\varepsilon_v/d\varepsilon_a = 0$. The stress ratio at the intersection is taken as the critical stress ratio ($M_c = 1.44$) and it is verified by the Method 2 approximation shown in Figure 4.19.

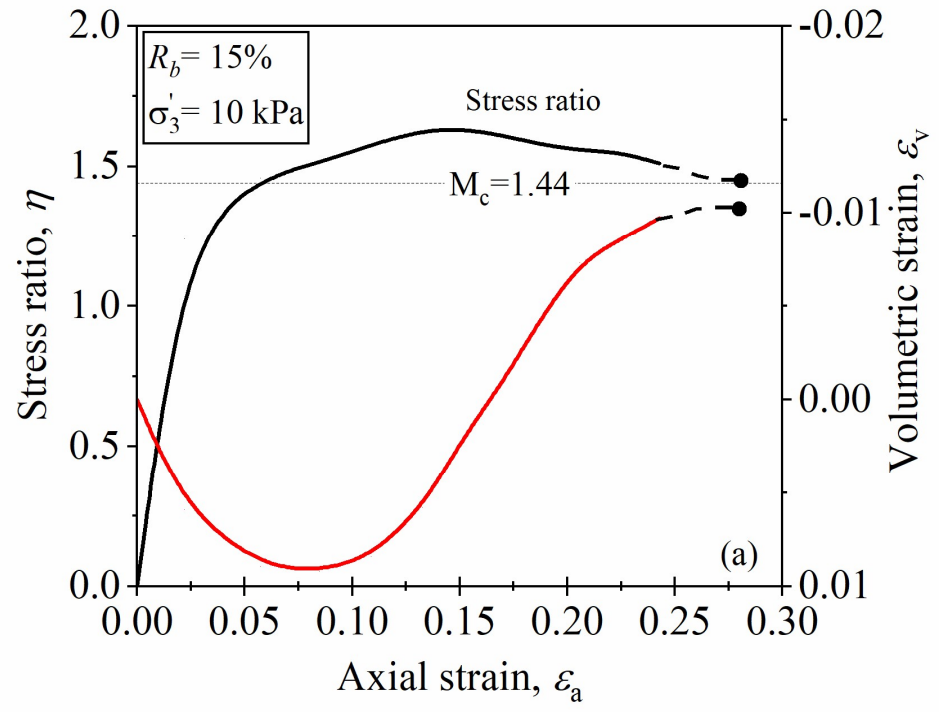

Figure 4.19 Estimation of the critical state stress ratio employing the stress ratio and volumetric strain

As shown in Figure 4.19, $\eta - \varepsilon_a$ and $\varepsilon_v - \varepsilon_a$ curves are also extrapolated until the constant η and εv are obtained. From both methods M_c =1.44 has been determined.

Variation of the critical stress ratio, (M_c) with the rubber content $(R_b\%)$ and confining pressure (σ_3') are shown in Figure 4.20. It is noted that the $R_b < 5\%$ doesn't make a considerable impact on the critical stress ratio under any of the considered confining pressures. But when $R_b > 5\%$, M_c is decreasing following the same pattern at confining pressures 10, 30 and 60 kPa.

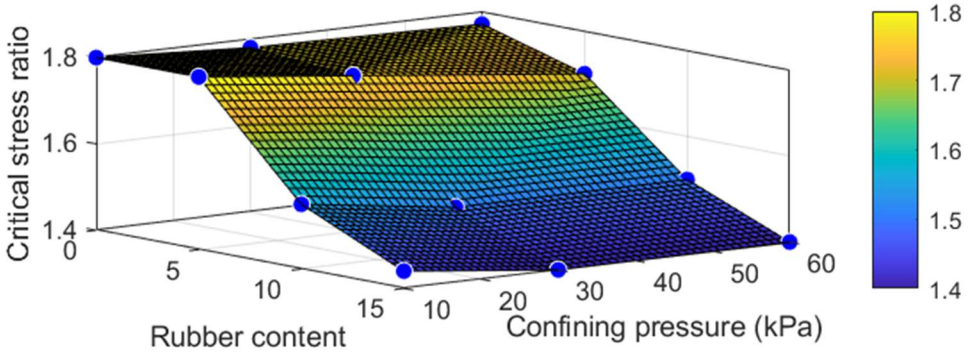

Figure 4.20 3D surface plot of the critical stress ratio, M_c

It is also clear that the increase in R_b decreases M_c , but changing the confining pressure between 10-60 kPa has almost no influence on pure ballast and RIBS mixtures.

4.9 Chapter Summary

This chapter focuses on evaluating the characteristics of RIBS subjected to monotonic loads by conducting large-scale triaxial tests for a range of rubber contents (0-15%) under different confining pressures (10-60 kPa). Overall, the current test results revealed that the inclusion of rubber increased the axial strain, the compressive volumetric strain, and the energy-absorbing capacity while decreasing the dilation and ballast breakage. The inclusion of rubber offered a significant reduction in ballast breakage, with a significant reduction in breakage of coarser ballast particles (38 mm) in all the RIBS mixtures. The critical stress state of RIBS is also discussed in this chapter and a relationship was obtained to quantify the energy absorbed during the shearing process due to the replacement of a fraction of ballast with rubber.

CHAPTER FIVE

5 BEHAVIOUR OF RIBS MIXTURES UNDER CYCLIC LOADING

5.1 Introduction

It is well known that the cyclic loads induced by trains cause ballast degradation that leads to the irrecoverable deformation of the track. It is now well established from a variety of studies that rubber inclusions such as rail pads, under sleeper pads, under ballast mats, and capping/ballast material modified with rubber aggregates helps to reduce ballast degradation (Remennikov et al., 2006; Jayasuriya et al., 2019; Navaratnarajah et al., 2018; Qi and Indraratna, 2021; Tawk et al., 2021). Some recent past studies carried out under cyclic loads (e.g. Fathali et al., 2016; Song et al., 2019; Esmaeili et al., 2018; Sol-Sanchez et al., 2015) concentrated on the role that rubber granules derived from tyres placed in the ballast layer to reduce train induced surface vibrations and also control deformation and breakage by improving damping and resiliency. However, while even a small increase in confining pressure (σ'_3=30-60 kPa) has a significant impact on the permanent deformation of ballast under cyclic loads (Thakur et al., 2013), previous studies on ballast mixed with rubber aggregates did not consider the changes in the confining pressures.

This chapter focuses on evaluating the characteristics of RIBS subjected to cyclic loads by carrying out large-scale triaxial tests for changing rubber contents (0-15%) under confining pressures (30-60 kPa) and a loading frequency of 20 Hz following a monotonic conditioning phase. This study, therefore, focused on assessing the effect of cyclic loading on RIBS in terms of the degradation and deformation behaviour, together with the damping properties.

5.2 Loading Procedure

The maximum and minimum cyclic deviator stresses ($q_{cyc,max}$ and $q_{cyc,min}$) considered as a sinusoidal wave were 230 kPa and 45 kPa respectively (Figure 5.1). This is equivalent to a 25 tonne axle load and in-situ stresses on an unloaded track (Lackenby et al., 2007). These equivalent pressures were from the field measurements gathered by Indraratna et al., (2010) for coal trains with an axle load of 25 t (Figure 5.1).

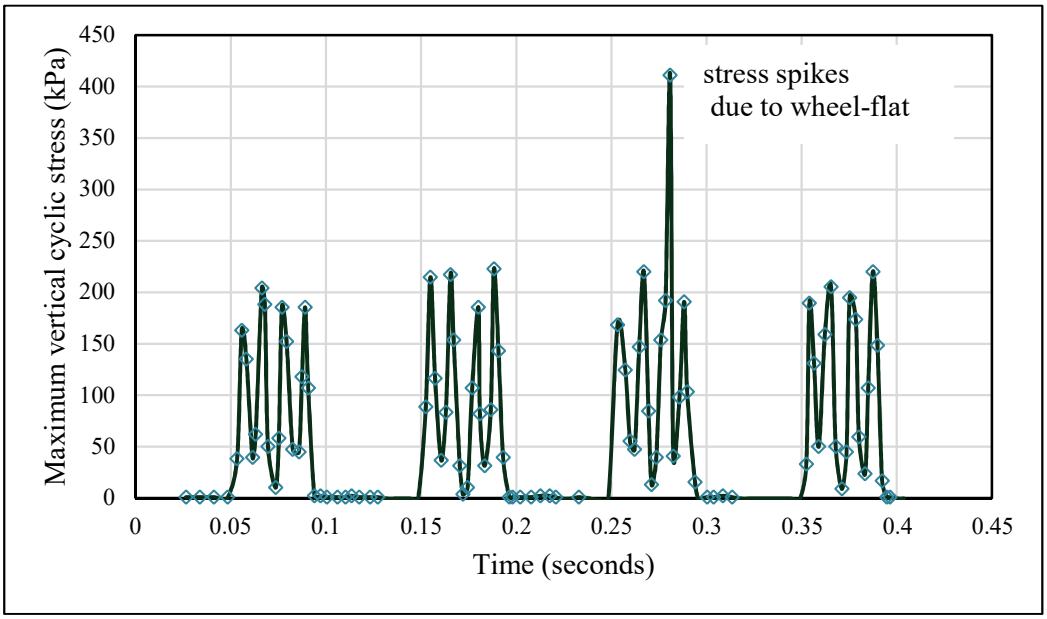

Figure 5.1 Vertical cyclic stresses, q_{cyc} transmitted to the ballast layer underneath the rail by 25 t axle load coal train with wagons (adopted from Indraratna et al., 2010)

The loading frequency of a train is expressed as f = V/L, where V is the train speed and L is the characteristic length. Since a typical freight wagon often has multiple axles (e.g., four axles), the distance between the axles is much smaller than the distance between the bogies. Therefore, considering an axle distance of 2.02 m, the loading frequency *(f)* was 20 Hz resembling a train speed (V) of about 150 km/h.

After setting up the apparatus, confining pressures ($\sigma_3' = 30$ and 60 kPa) were applied to the specimens and the pore water pressure was monitored continually to ensure effective drainage during cyclic loading. As notable initial settlement with increased rubber under static loading could be observed, at the outset of testing, a conditioning phase was introduced, where up to the maximum cyclic stress magnitude was applied monotonically to the test specimens before applying the cyclic loads at a frequency of 20 Hz. In addition to that, it minimises the effect of improper contact between the top and bottom ends of the specimen with the sample cap and base plate. This phenomenon is also comparable with newly built tracks where trains run at slower speeds at the beginning to ensure the track settles properly and reduce the chance of buckling. Details of the loading procedure are shown in Figure 5.2.

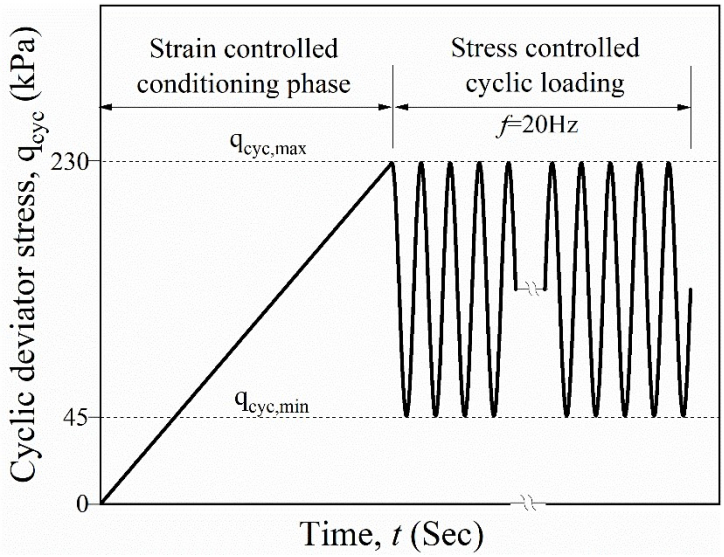

Figure 5.2 Details of the loading procedure

5.3 Void Ratio

The void ratio e of RIBS is calculated using the equation $e = \left(\frac{G_s \gamma_w}{\gamma_d}\right) - 1$, where G_s is the specific gravity of RIBS, γ_w is the unit weight of water, and γ_d is the dry unit weight. Here $\gamma_d = m_s/V$, where m_s is the mass of solids and V is the total volume.

Figure 5.3 shows the void ratio (e) of the specimens at the beginning of the test (e_i), after the conditioning phase (e_0), and at the end of the test (e_f). It is obvious that during the conditioning phase, the materials in all the samples are transformed to a denser granular assembly from their initial state, and the corresponding reduction in the void ratio is significant in relation to the increased rubber content. At the end of the tests, all the specimens have attained a void ratio of e_f, between 0.78-0.76, whereas the specimens after the conditioning phase (e_0) vary from 0.81-0.78. It was previously observed that under cyclic loading, granular material with a lower initial void ratio gave a smaller settlement than the granular material with a higher initial void ratio (Jeffs and Tew, 1991; Selig and Waters, 1994). It was therefore advantage that the RIBS reach a lower void

ratio under similar initial loading conditions (during the conditioning phase) and become more densified compared to the conventional ballast. Here the term "densification" refers to the irreversible rearrangement of grain configurations that is associated with volumetric strain.

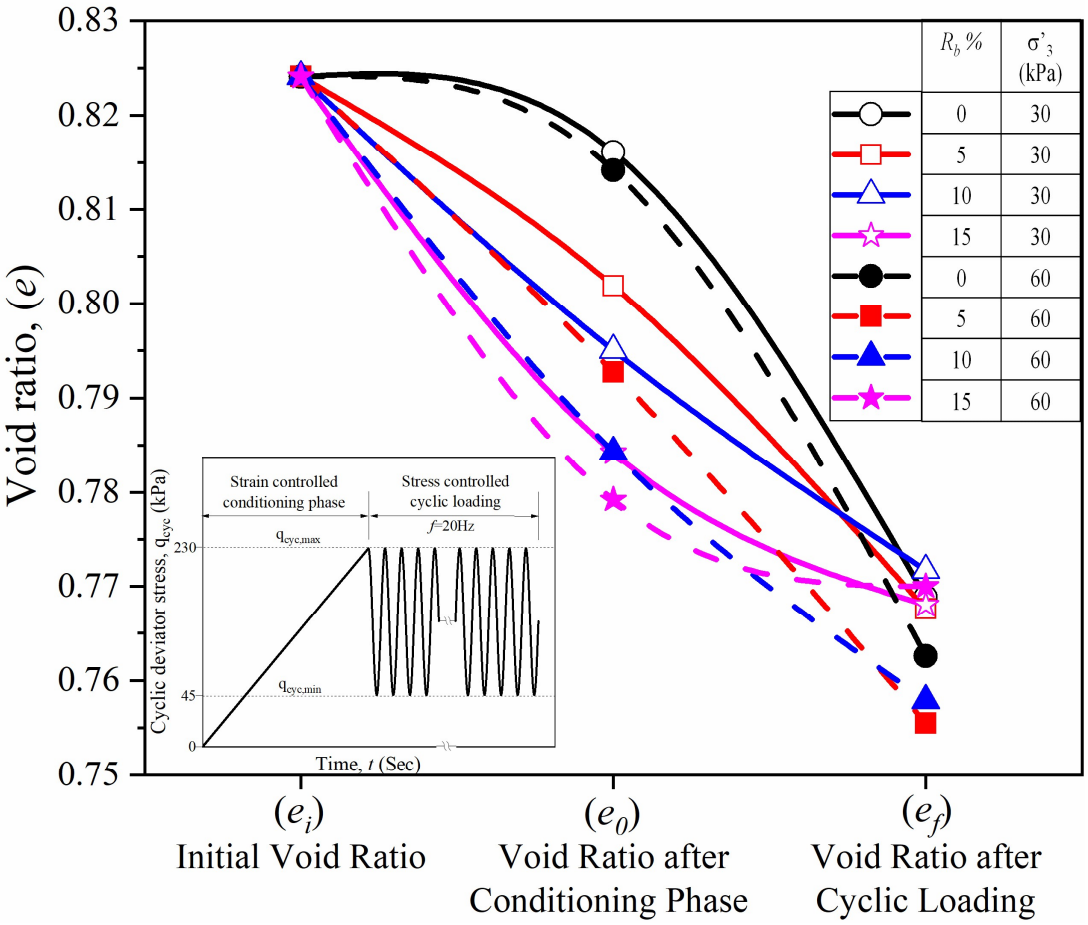

Figure 5.3 Void ratio (e) of the specimens at the beginning of the test (e_i), after the conditioning phase (e_0) and at the end of the test (e_f)

5.4 Permanent Deformation Behaviour

5.4.1 Axial strain

The initial axial deformation observed in the conditioning phase (ε_i) against R_b% for each specimen are shown in Figure 5.4.

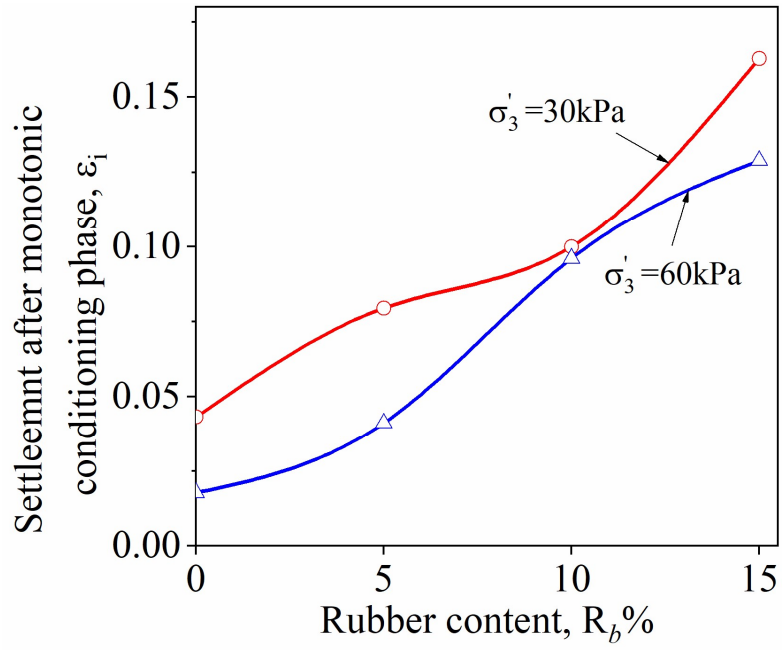

Figure 5.4 Permanent axial deformation after the monotonic conditioning phase ε_i

It is clear that an increase in R_b leads to an increase in ε_i which forms a more densified granular assembly before applying cyclic loads. This phenomenon admits the initial compressions observed in RIBS mixtures under monotonic loading discussed in section 4.2. Similar to the pure ballast, initial axial strains of RIBS decrease with the increased confining pressure, as the increased confining pressure controls the material dilation.

Figures 5.5 (a-b) present the permanent axial strain with the number of cycles (semi-logarithmic scale) for the specimens subjected to confining pressures of 30 and 60 kPa for different amounts of R_b%. By the end of the cyclic loading, the axial strain of RIBS

with R_b=5% is almost similar to pure ballast at σ'_3 =30 kPa, while the reductions in the axial strain for RIBS with R_b=10% and 15% are 23% and 65%, respectively. For a confining pressure of 60 kPa, the reductions in the axial strain at the end of the test for R_b=10% and 15% are around 52% and 63% compared to pure ballast. Also, an increase in the confining pressure decreases the axial strains of all the samples, irrespective of the rubber content. Unlike under static loading, the axial strain response for long-term cyclic loading (after 400,000 cycles) turns out the other way, indicating the lowest axial strains for the samples with increased rubber contents (R_b=15%). This is attributed to the rapid densification of test specimens with higher rubber contents during the initial loading, after which further cyclic loading cannot generate significant compression. Moreover, reduced ballast degradation and increased damping property due to the higher rubber contents are also the reasons for the reduced deformation; this will be discussed further in later sections.

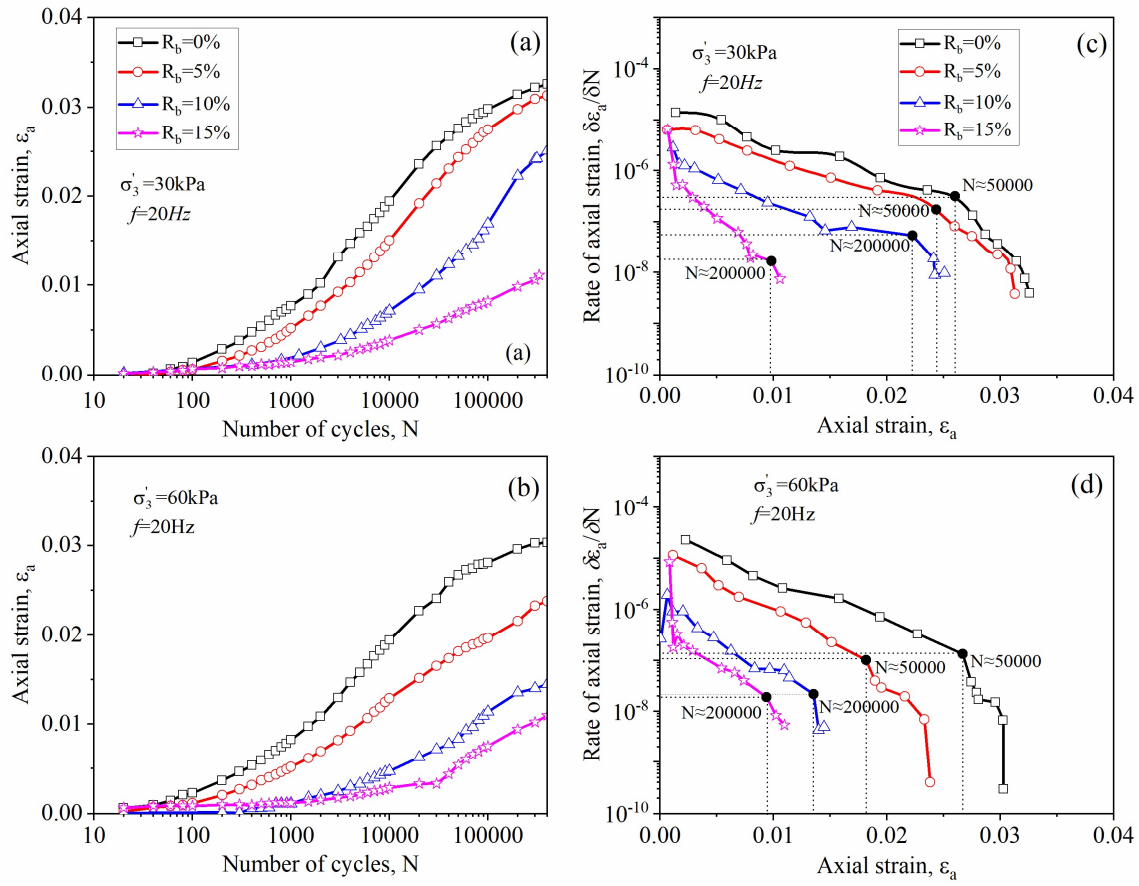

Figure 5.5 (a-b) Axial strain response of RIBS mixtures under effective confining pressures: (a) 30 kPa (b) 60 kPa; (c-d) rate of axial strain variation of RIBS mixtures under effective confining pressures: (c) 30 kPa (d) 60 kPa

The failure criteria of specimens under drained stress-controlled cyclic loading is different from the monotonic loading that takes place by exceeding the failure stress. Werkmeister et al., (2005) reported a new shakedown mechanism to study the deformation of material under repeated loads, and later Sun et al., (2014) extended the idea of a shakedown mechanism for railway ballast. When progressively decreasing plastic axial strain rate eventually stabilises and leads to an asymptotic value in response to cyclic loading, the ballast achieves a state of 'plastic shakedown'. Pure ballast tested in the current study reached the plastic shakedown state by attaining a stable permanent deformation rate with an increased axial strain. This agrees with Sun et al., (2014) where pure ballast was tested under similar conditions to the current study (σ'_3 = 30 kPa, q_{cyc}

$_{max}$ = 230 kPa and frequency of 20 Hz). Figure 5.5 (c-d) shows the permanent axial strain rate ($\delta\varepsilon_a/\delta N$) changes with the axial strain for RIBS under σ'_3=30 and 60 kPa. From Figure 5.5(c-d) it is clear that when R_b% increases, the permanent axial strain rate ($\delta\varepsilon_a/\delta N$) curves move clockwise, indicating RIBS specimens, $\delta\varepsilon_a/\delta N$ progressively decreases to a fairly small plastic axial strain rate (up to around 10^{-8}) and attains a stable rate at a reduced axial strain. Hence the behaviour of RIBS can also be categorised into the plastic shakedown state irrespective of the amount of rubber. In design, the state of plastic shakedown is permitted thus the risk of failure due to excessive settlements is lesser in RIBS compared to the conventional ballast subjected to similar conditions. The approximate points where the RIBS reach the plastic shakedown (no more accumulation of plastic strain) are marked in Figures 5.5(c-d) as solid circles and the corresponding approximate number of cycles are indicated for each curve. It is clear that RIBS with $R_b \geq$10%, the rate of permanent axial deformation gradually reaches the plastic shakedown state after 200,000 cycles while for pure ballast and RIBS with R_b=5%, the rate of permanent axial deformation reaches the plastic shakedown after 50,000 cycles. This means attaining the plastic shakedown is delayed when the rubber content, $R_b \geq$10%. Accumulation of plastic strain at a slower rate is preferred in practice in order to reduce the track maintenance cycles which are required when the accumulated plastic deformation exceeds the tolerable limit. Also, attaining the shakedown state makes the material stiffer because there is no more plastic deformation in terms of grain breakage and creep of rubber particles. Following the mechanism suggested by Tian and Senetakis (2021), it is clear that the deformation due to the increased grain breakage is expected to be prominent in pure ballast, whereas rubber-induced creep deformations can dominate the plastic deformation in RIBS. In other words, creep influence on RIBS may further increase the performance and longevity of the track.

As discussed in section 2.5, various empirical models were developed to predict the permanent deformation of conventional ballast mainly based on deformation incurred after the first load cycle, $\varepsilon_{a,1}$ and the number of load cycles, *N* (Table 2.3). However, existing models are not applicable for ballast mixed with rubber due to the considerable irrecoverable particle rearrangement observed during the first application of maximum cyclic load. Since this observed initial axial deformation is comparatively higher in RIBS (R_b>0), it is convenient to consider two different ranges for axial deformation, i.e., axial deformation after the monotonic conditioning phase ε_i and deformation under cyclic loading ε_a.

It is observed that the permanent axial deformations (ε_a) of RIBS under cyclic loads against the number of cycles can be adequately represented using general hyperbolic relationships (Figure 5.6).

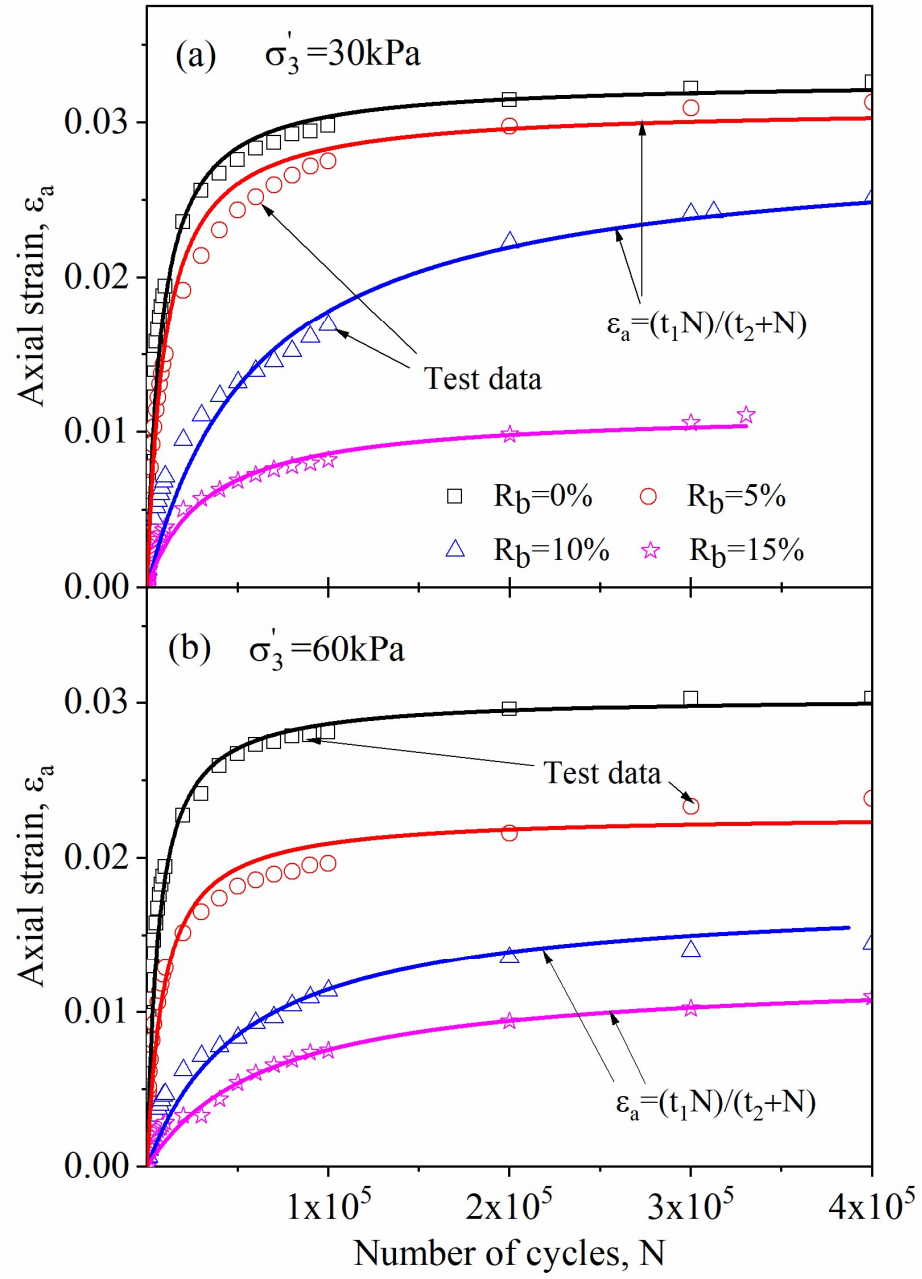

Figure 5.6 Empirical modelling for permanent axial deformation under cyclic loads

Accordingly, the empirical equation for ε_a can be written as $\varepsilon_a = t_1 N/(t_2 + N)$ where t_1 and t_2 are empirical parameters. The model regression parameters can be found in Table 5.1.

Table 5.1 Empirical parameters of the model for permanent axial deformation

R_b (%)	σ'_3	t_1	t_2	R^2
0	30	0.0327	7617	0.97
5	30	0.0310	9506	0.98
10	30	0.0286	60708	0.97
15	30	0.0114	3224	0.96
0	60	0.0304	6228	0.97
5	60	0.0228	9026	0.95
10	60	0.0177	53702	0.94
15	60	0.0126	65979	0.99

5.4.2 Volumetric strain

As shown in Figures 5.7(a-b), an increase of rubber in the RIBS reduces the volumetric strain against the number of cycles indicating that increased rubber in RIBS reduces the ballast dilation. The reason can be that the RIBS specimens undergo increased initial compression with increasing rubber contents during the conditioning phase, thus resulting in effective particle interlocking. As rubber particles are more compressible than rock aggregates, it is not surprising that the overall dilation of the granular mass is contained during the loading phase. As shown in Figures 5.7(a-b), volumetric strain variation with the number of cycles (plotted in log scale) follows two distinct zones considering the slope of the curves. Zone A is the small-strain region where the volumetric strains are small (0-15% of total volumetric strain) and specimens are stable. After several loading cycles (i.e., N=1000 and N= 200 when the samples are subjected to 30 kPa and 60 kPa confining pressures, respectively), the data plots in Zone A swiftly merge into quasi-concave shapes at larger strains as indicated by Zone B. With the increase of confining pressure, Zones A narrows down with fewer cycles while Zone B becomes wider with the increased number of cycles.

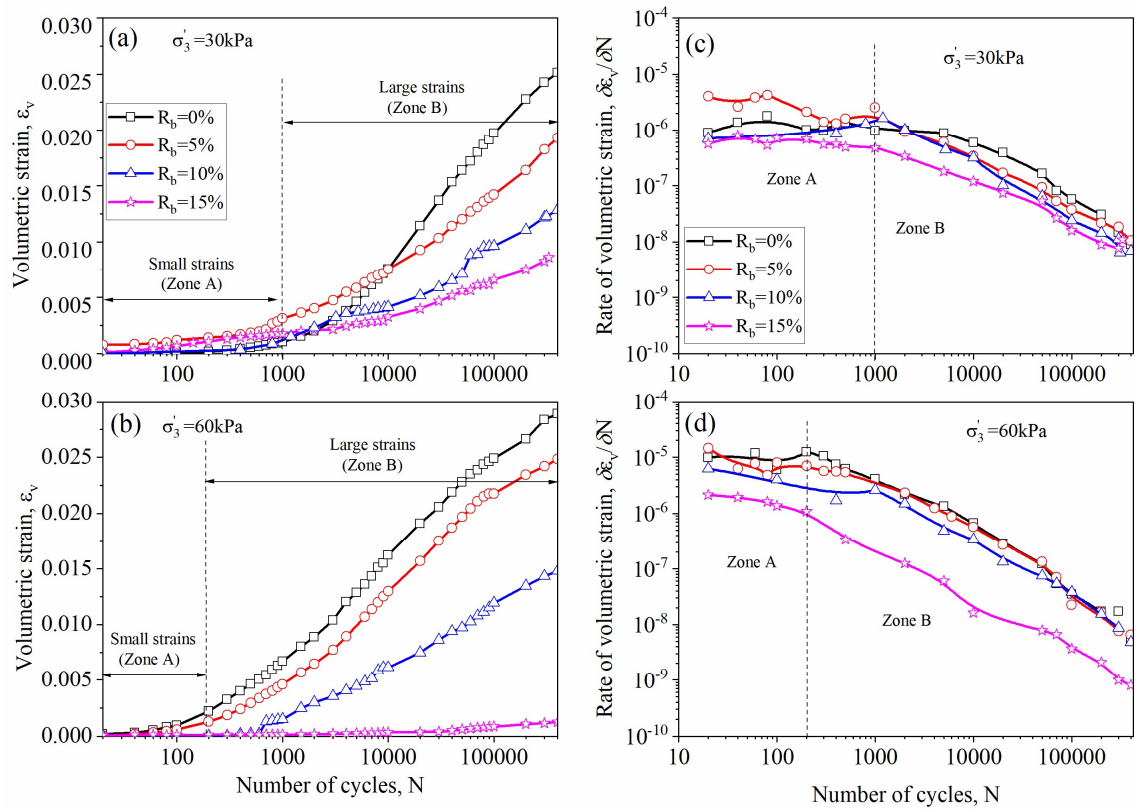

Figure 5.7 (a-b) Volumetric strains (dilation) of RIBS mixtures under effective confining pressures: (a) 30 kPa (b) 60 kPa; (c-d) volumetric strain rates with respect to number of cycles under effective confining pressures: (c) 30 kPa (d) 60 kPa

Figures 5.7(c-d) represent the rate of change in volumetric strain ($\delta\varepsilon_v/\delta N$) against the number of cycles that can differentiate these zones, where the curves are almost flat and stable in Zone A. At the beginning of Zone B, the data plots indicate a downward trend, and it is observed that the change in volumetric strain of Zone B decreases from around 10^{-5} to 10^{-9}. The volumetric strains at zone A (quasi-stable) are very small and can be neglected ($\varepsilon_v < 0.25\%$). Quasi-stable strains usually do not make an unfavourable effect on track deformations and passenger comfort. Therefore, Zone A is very sound in terms of stability. Zone B exhibits more significant volumetric strain (dilation) levels and still increases the volumetric strain even after 400,000 cycles. Therefore, Zone B is beyond the state of equilibrium; thus, it can cause considerable track instability. By mixing the

ballast with granulated rubber, the volumetric strain in Zone B decreases significantly, hence increasing the stability of the track.

5.5 Resilient Modulus

Resilient modulus (M_R) of ballast is a key parameter in railway design because it indicates the elastic response of granular material under repeated loads. M_R is defined as the ratio of the applied cyclic stress (Δq_{cyc}) to the recoverable strain (ε_{rec}), and the definition can be found in Figure 5.8.

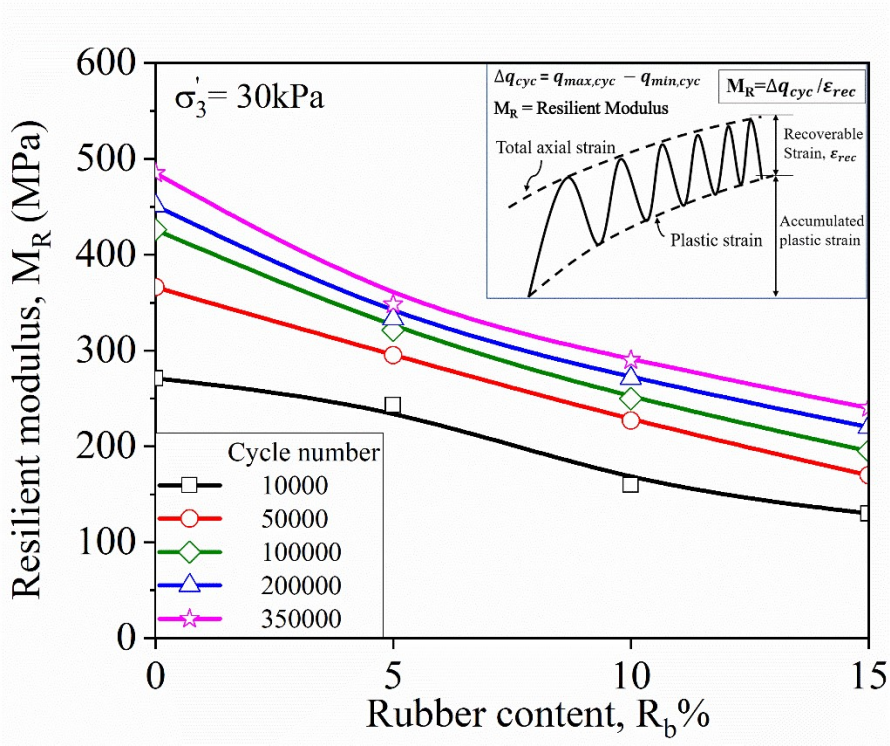

Figure 5.8 Variation of M_R of RIBS mixtures against the rubber content, R_b%

Increased reversible deformation is one of the distinctive features of rubber; hence RIBS with increased rubber shows increased recoverable deformations in each cycle compared to conventional ballast. Therefore, as shown in Figure 5.8, M_R decreases with the

increased content of R_b% in the RIBS (i.e., After around 100000 cycles M_R decreases approximately 25%, 40%, and 50% for RIBS with R_b=5%, 10%, and 15% respectively). All the specimens are gradually densifying with the increased number of cycles; hence the changing of M_R after around 100,000 cycles is insignificant (Figure 5.9).

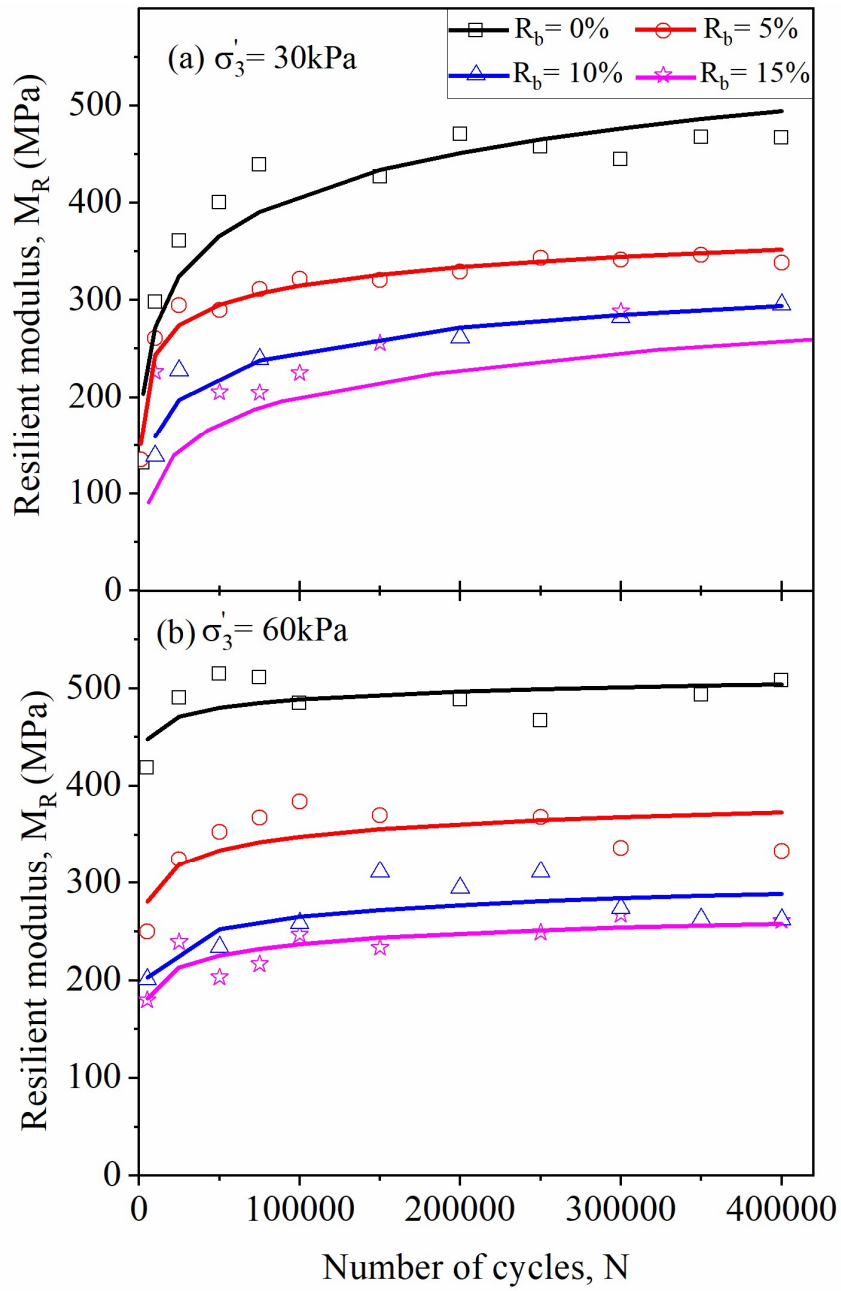

Figure 5.9 Variation of resilient modulus of RIBS mixtures against the number of cycles under effective confining pressures: (a) 30 kPa (b) 60 kPa

Figures 5.9 a and 5.9 b show a slight increase of M_R for all the samples when the effective confining pressure is increased from 30 kPa to 60 kPa. A similar observation was also reported by (Indraratna et al., 2009; Hicks, 1970). This is because of the reduced particle sliding and rolling due to increased stress levels at the ballast contacts (Ngo et al., 2021). All the specimens are gradually densifying with the increased number of cycles, hence the M_R increases with the decreasing rate and tends to attain a stable value after around 100,000 cycles (Figures 5.9 a-b). Generally, the M_R of the pure ballast stabilises at a value of larger than 250 MPa when σ'_3> 30 and $q_{cyc,max}$ >230 kPa (Indraratna et al., 2009). Therefore, the increase of rubber content R_b>10% may not be acceptable for the use of RIBS in general tracks.

5.6 Damping Ratio and Energy Dissipation Capacity

The damping ratio, D, is an important parameter widely used in dynamic analysis to evaluate the efficiency of energy dissipation for granular materials. As shown in Figure 5.10, the damping ratio can be computed by the equation, $D = \frac{A_L}{4\pi A_T}$ where A_L is the area enclosed by the hysteresis loop and A_T is the area of the triangle. Here, the loop area A_L is the measure of dissipated energy per unit volume during a cycle (E'_d), and the triangular area A_T represents the stored elastic energy (Madhusudhan et al., 2017).

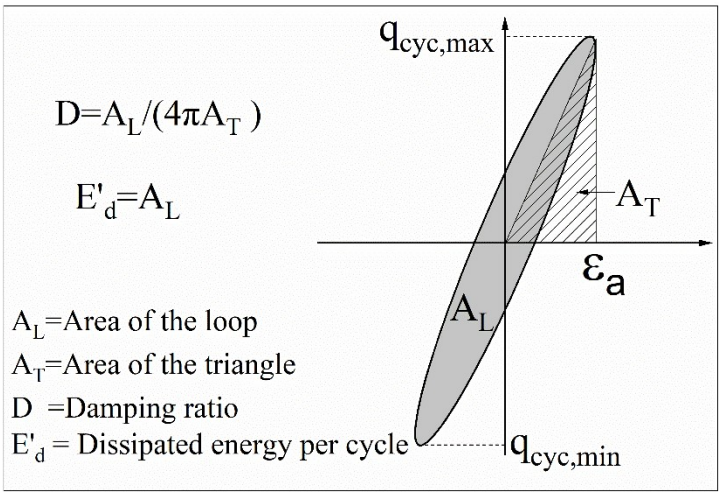

Figure 5.10 Definition of the damping ratio and the dissipated energy per cycle

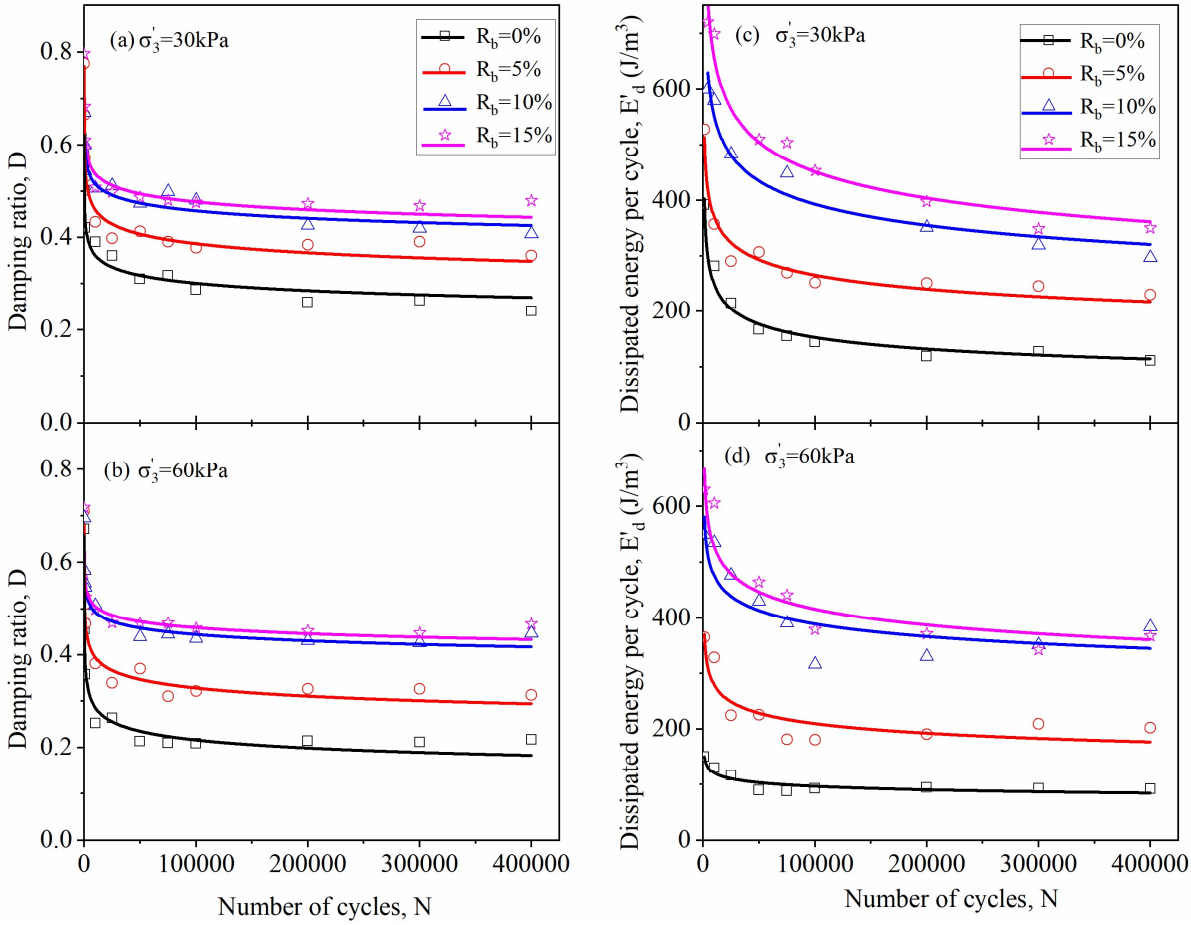

Figure 5.11 (a-b) Variation of the damping ratio against the number of cycles under effective confining pressures: (a) 30 kPa, (b) 60 kPa; (c-d) variation of dissipation energy against the number of cycles under effective confining pressures: (c) 30 kPa, (d) 60 kPa

The damping ratio (D) against the number of cycles (N) and the energy dissipated per cycle (E'_d) against the number of cycles (N) are shown in Figures 5.11(a-b) and Figure 5.11(c-d) respectively. An increase in rubber content in the RIBS increases the damping ratio as well as the energy dissipation, and the damping ratio of all the specimens attains a stable stage after around 100,000 cycles. The nature of the rubber is highly elastic and mainly contributes to the increased damping properties of RIBS with increased rubber contents. The damping ratios of RIBS are larger than that of pure ballast because the elasticity of rubber granules facilitates the rearrangement of particles and relative movements. Therefore, increased energy dissipation is observed for RIBS with $R_b \geq 5\%$. Figures 5.11(a-d) show that no distinctive increase can be observed for damping ratio and energy dissipation when R_b>10%. The reason can be that the increased rubber content in the RIBS ultimately leads to a more rubber-like material that deviates from the behaviour of an unbonded granular medium. However, an increase in confining pressure decreases the damping ratio and energy dissipation. Increased confining pressures relatively reduce the particle movement in granular media due to the increased interparticle friction; hence the dissipated energy reduces.

5.7 Ballast Degradation under Cyclic Loading

Considering the importance of quantifying ballast breakage, Indraratna et al., (2005) introduced a method specifically for ballast material to evaluate particle breakage, namely, the Ballast Breakage Index (BBI). The definition of BBI was discussed in section 2.4, it is based on the particle fractions that passed through a range of sieves before and after the test.

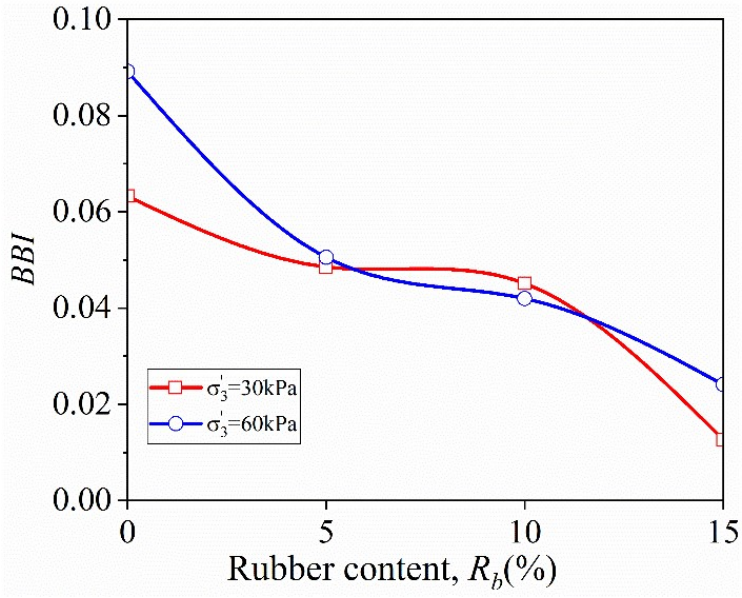

Figure 5.12 Influence of R_b on Ballast Breakage Index, BBI

Figure 5.12 shows that an increase of rubber content in the RIBS mixture up to 5% considerably decrease the *BBI* (43% and 23% reduction in *BBI* under the confining pressures of 60 kPa and 30 kPa respectively); however, a further reduction in the *BBI* is insignificant when the rubber content increases from 5% to 10% (17% and 7% further reduction under the confining pressures of 60 kPa and 30 kPa respectively). Again, further addition of 5% rubber (R_b=15%) provides a considerable reduction in *BBI*. Therefore, the pattern of particle breakage can be characterised by three distinct zones of degradation: (i) $R_b \leq 5\%$: rubber particles predominantly act as a void filler, thus reducing abrasion between ballast particles with a notable reduction in ballast breakage; (ii) 5%< R_b <10%: ballast breakage is less sensitive to the variation of rubber amount, as the initial 5% rubber content had already fulfilled much of its role as a void filler within the fabric of RIBS; (iii) R_b>10%: rubber particles replace a significant fraction of the breakable ballast particles apart from void filling, thus enabling a significant reduction in *BBI*.

Figure 5.13 shows the patterns of ballast degradation observed during testing, and they can be classified into three categories: (a) angular corner breakage or abrasion, (b) grinding or wearing away from the surface or attrition, and (c) splitting into two or more equal particles. This is in agreement with previous studies on ballast e.g. Lees and Kennedy (1975); Qi and Indraratna (2020).

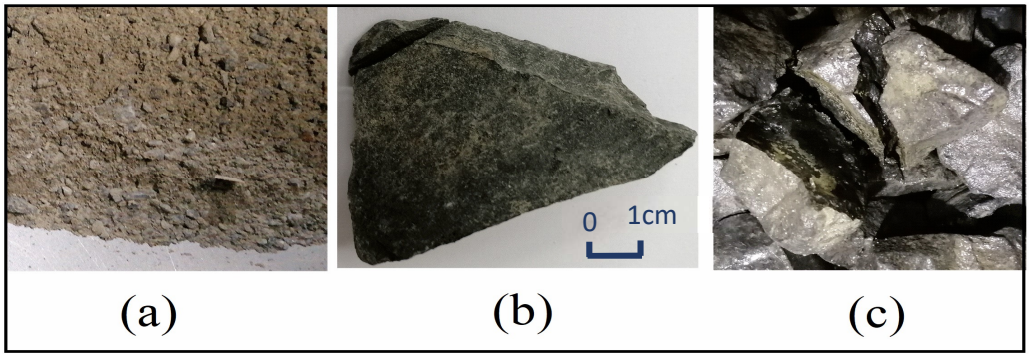

Figure 5.13 Patterns of ballast breakage

As discussed, increasing the rubber content up to 15% fills not only the voids but also replaces some of the breakable ballast particles with rubber, and these particles may contribute to a more uniform contact force distribution. In this case, a higher rubber content (i.e., 15%) may reduce the shear strength of the ballast layer, where significantly reduced peak deviator stresses were observed for similar specimens with R_b=15% under monotonic loads. Therefore, RIBS with increased rubber (R_b >10%) may not be practical for the tracks that are subjected to increased axle loads (>25 tonnes).

5.8 Chapter Summary

This chapter described the response of RIBS under cyclic loads and compared it with conventional ballast material. Laboratory tests reveal that RIBS enhances the ballast performance generally but at the same time slightly compromises some of the important

properties (i.e., stiffness, initial settlements, and resilient modulus) to some extent. This chapter further discusses the particle rearrangement during the conditioning phase and its effect on the performance of RIBS under cyclic loads. Ballast breakage under cyclic loading is explained in detail while the influence of rubber on particle breakage is also included.

CHAPTER SIX

6 ASSESSING THE OPTIMAL RUBBER CONTENT

6.1 Introduction

Chapter 4 involved the investigation of geotechnical properties such as the friction angle, dilation angle, shear strength, stress-strain, and the degradation response and stress dilation behaviour) of mixtures of ballast and rubber granules, i.e. Rubber Intermixed Ballast System (RIBS) by conducting a series of large-scale static triaxial tests with different rubber contents (0–15% by weight) at effective confining pressures of 10, 30, and 60 kPa. Furthermore, in Chapter 5, the influence of rubber on the initial compaction characteristics, material resiliency, damping characteristics, energy absorption, particle breakage, and shakedown behaviour of RIBS under cyclic loads at effective confining pressures of 30 and 60 kPa was examined.

In Chapter 3, it was proposed that rubber granules from 9.5 mm to 19.5 mm be used to replace ballast particles of the same size, in accordance with the nominal 60 grade specifications for the current Australian Standard for ballast (AS2758.7, 2015). In essence, laboratory tests reveal that while RIBS generally enhances the ballast performance it also compromises important properties such as stiffness, initial settlement,

and resilient modulus to some extent. This is why care is needed when choosing the correct amount of rubber in RIBS to optimise ballast performance.

This chapter describes the assessment of optimal rubber content ($R_b\%$) for the RIBS mixture by evaluating the RIBS with different $R_b\%$ ensuring similar or better performance than conventional ballast.

6.2 Conventional Ballast as the Reference

Ballast consists of coarse angular aggregates whose primary purpose is to stabilise rail superstructure. In Australian rail tracks, natural or crushed stones to thicknesses of 150-300mm are generally used as the ballast layer.

The functions of ballast are as follows (Indraratna et al., 2011),

- Provide a strong load-bearing platform with adequate lateral and vertical support to stabilise the sleepers
- Transfer heavy stresses at the sleeper/ballast interface to the subballast and subgrade
- Provide sufficient dynamic resiliency for the entire track
- Ensure minimal plastic deformation to the track structure during typical maintenance cycles
- Provide adequate permeability for drainage
- Facilitate maintenance operations
- Limit the growth of vegetation on the tracks
- Absorb noise and vibration

- Provide adequate electrical resistance

The nominal dimensions of a ballast profile can vary with different classes of track, but they are mainly based on passenger and freight traffic, and the ground conditions. A typical track cross-section of the ballast profile is shown in Figure 6.1.

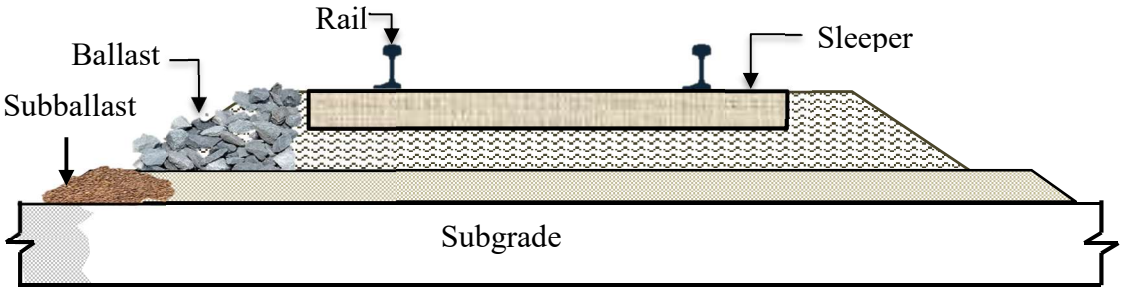

Figure 6.1 Typical ballasted track cross-section

As discussed in previous chapters, parameters such as the modulus degradation, friction angle, dilatancy angle, deformation, and the resilient modulus and ballast breakage control the material stiffness, bearing capacity, lateral/vertical deformation, resiliency, and drainage capacity, etc. In order to use RIBS as an alternative ballast, the parameters that control the functions of material must be evaluated in real-time. A design criterion is therefore introduced to assess the optimum amount of rubber in a RIBS mixture while considering the effective friction angle, dilatancy angle, ballast breakage, as well as the energy absorption, and modulus degradation at the peak deviator stress ratio. Moreover, the proposed optimum amount of rubber was further recognised and verified by evaluating its overall deformation and degradation under cyclic loading.

6.3 Proposed Acceptance Criteria for RIBS

Five levels of acceptance are proposed here to determine the optimum amount of rubber in the RIBS, while aiming towards a reasonably steady condition over the long term.

Step 1 Frictional shear strength and dilation angle.

The effective friction angle (φ_{ef}) is one of the governing factors used to determine the bearing capacity of the ballast layer and the dilation angle (ψ) represents the dilation of the ballast. It is expected that RIBS with an optimal rubber content should have φ_{ef} of not less than pure ballast (Latite basalt) 46°–55° (Indraratna et al., 2011; Salim, 2004), while the ψ of RIBS is to be less than ballast to control dilation.

Step 2 Axial strain at peak stress ratio.

The laboratory test data indicates that the axial strain of pure ballast at the peak stress ratio is around 0.1 under typical track confining pressures where σ_3' = 10–30 kPa (Indraratna et al., 2015). To avoid the consequences of excessive settlements of RIBS compared to conventional ballast material, an axial strain of 0.1 at the peak stress ratio is considered to be the tolerable limit for RIBS design criteria under the same confining pressures of 10–30 kPa.

Step 3 Ballast breakage.

The proposed RIBS with rubber should result in a superior performance in terms of ballast breakage, so the *BBI* values of RIBS should not exceed the *BBI* values of pure ballast under the same confining pressures (0.2–0.22; Figure 4.7). Furthermore, it is expected that the addition of rubber could reduce the *BBI* significantly, and then RIBS could

achieve negligible particle breakage (BBI = 0.1) under general track confining pressures up to 60 kPa. In this case, a stricter criterion is adopted where the BBI<0.1 for the selected RIBS.

Step 4 Modulus degradation.

In traditional ballast, the rate of modulus degradation decreases rapidly with the axial strain, and then it stabilises at a low value (0.1–0.12). However, an increase in the amount of rubber in the RIBS mixtures slows down the rate of modulus degradation, thus indicating higher ductility and the potential of RIBS to withstand failure at larger axial strains. It is important to ensure that the RIBS should have improved ductility than the pure ballast, hence the E/E_i at η_{peak} is expected to be over 0.12 and that was satisfied by all the RIBS samples.

Step 5: Energy density.

It is suggested that the proposed RIBS should satisfy the normalised strain energy density where $\hat{E}_d > 1$ to ensure that the energy absorbing capacity of RIBS material is greater than pure ballast in order to minimise ballast degradation and ensure less energy is transmitted to the adjoining substructure layers.

6.4 Optimising the Amount of Rubber

The effective friction angle of rubber-ballast mixtures has been calculated in previous studies (Fathali et al., 2016; Gong et al., 2019), but note that the rubber granules used in previous studies followed similar ballast gradation. The effective friction angle of rubber-ballast mixtures studied in the past, together with this current study, against R_b% is shown

in Figure 6.2. The effective friction angle of conventional ballast material ($R_b = 0$) varies for each study as the aggregate type (e.g. Fathali et al., (2016) used crushed stone of dolomite type whereas latite basalt was used in the current study) and the particle gradation is different. It is clear that an increase in $R_b$compromises the effective friction angle irrespective of the type of rock used as ballast, but the reduction was lower in the current study compared to the past studies. The reason can be that the particle size of rubber granules (9.5-19mm) used in the current study optimised the strength of the ballast- rubber granular assembly. As mentioned in Step 1 in Section 6.3, it is expected the RIBS with an optimal rubber content should have φ_{ef} of not less than pure ballast (Latite basalt) 46°–55°. RIBS with R_b up to 15% satisfies the requirement but any further increase in R_b should not be considered in RIBS (Figure 6.2).

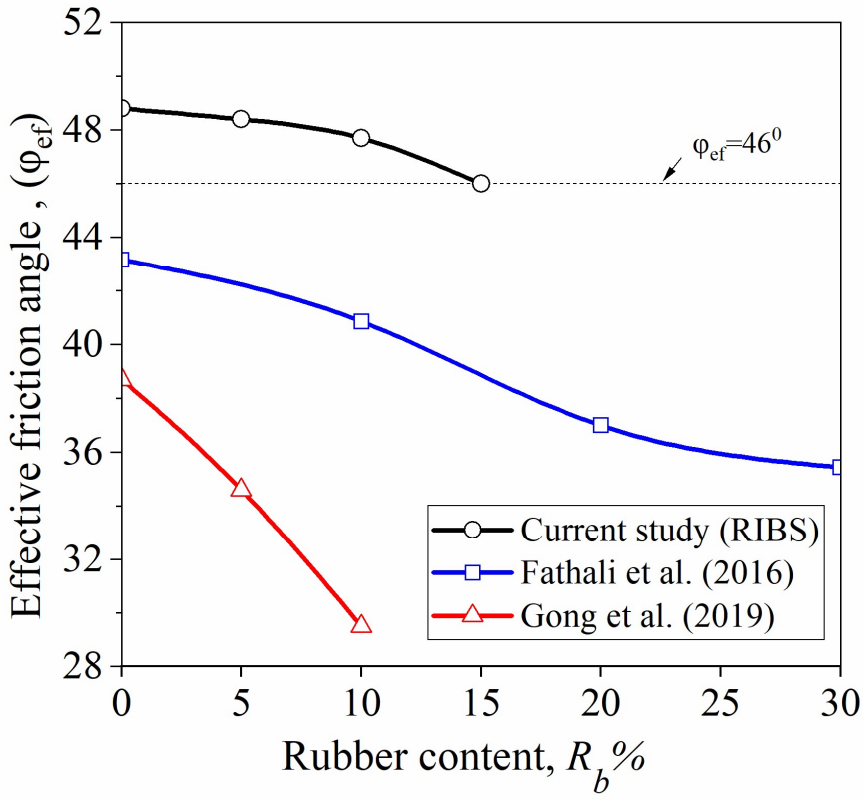

Figure 6.2 Effective friction angle of rubber -ballast mixtures

The dilation angle(ψ) decreases as the amount of rubber increases, and when $R_b > 5\%$, the ψ of RIBS is less than conventional ballast. Having a lower dilation angle is beneficial because it reduces the material dilation which controls lateral deformation.

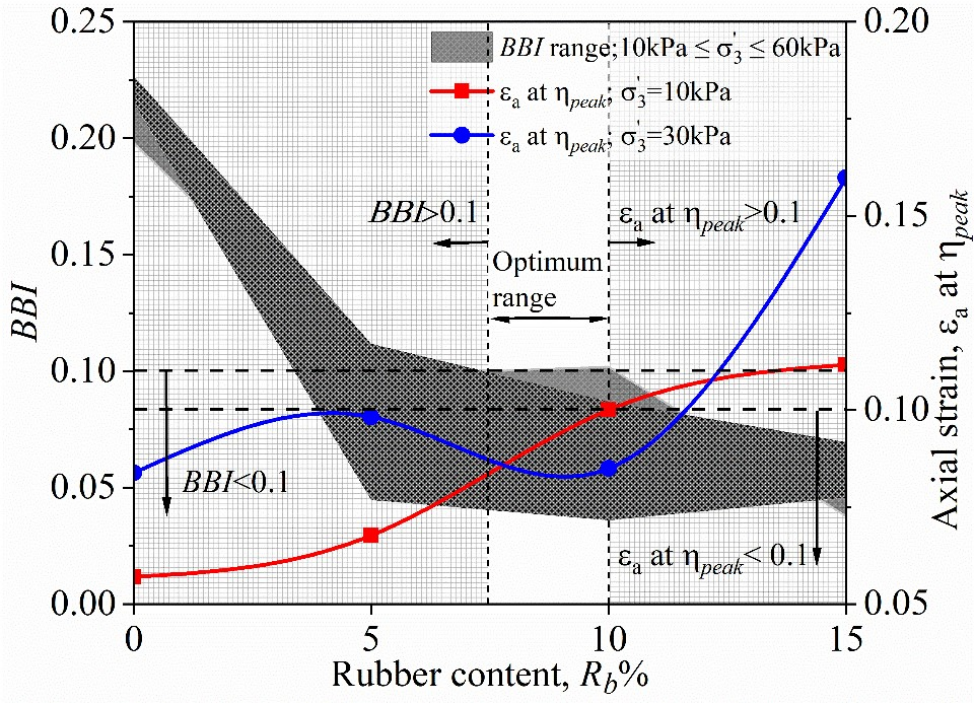

Figure 6.3 Optimisation of the rubber content according to the ballast breakage index and associated axial strain

The optimum amount of rubber in a RIBS mixture that satisfies Step 2 and Step 3 can be assessed as shown in Figure 6.3, which shows how the optimum mixture is justified according to the ballast breakage index and the associated axial strain. When $R_b \geq 5\%$,all the RIBS will present a negligible ballast breakage, i.e., $BBI \leq 0.1$, but when $R_b \geq 10\%$, the axial strain at η_{peak} of RIBS will exceed the acceptable limit of 0.1 under effective confining pressures of 10 kPa to 30 kPa. Here the range of effective confining pressures represents the typical track confining pressures. Therefore, combining the test results of BBI and ε_a at η_{peak}, the acceptable range of rubber should be $7.5 \leq R_b \leq 10\%$.

Moreover, all the RIBS samples showed a greater E/E_i at η_{peak}, and better energy absorption than traditional ballast (Figures 6.4 and 6.5).

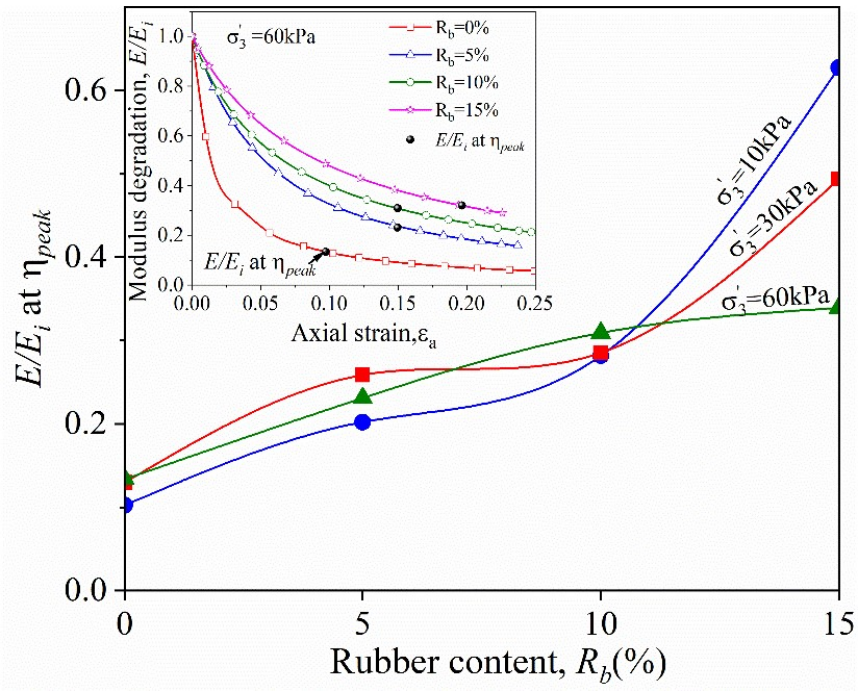

Figure 6.4 Higher E/E_i at η_{peak} compared to the pure ballast

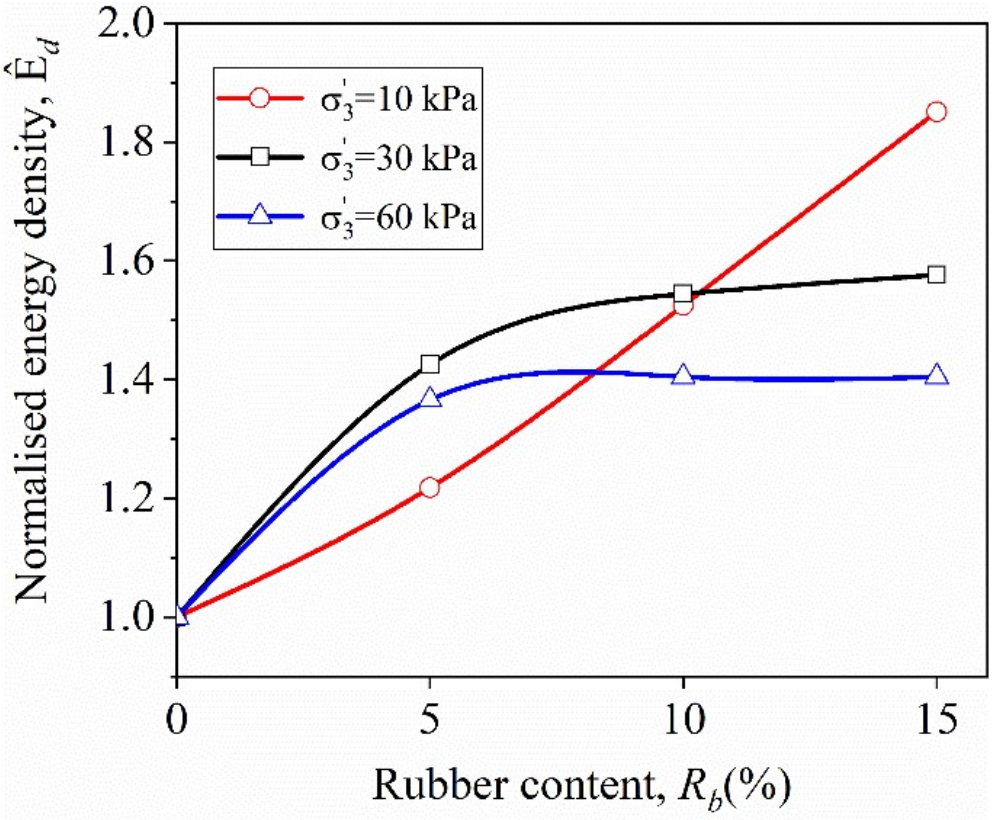

Figure 6.5 Higher energy absorption in RIBS compared to pure ballast

Also, the effective friction angle of RIBS with up to 15% of rubber is within the general range of pure ballast, and all the RIBS samples showed a reduced dilation angle compared to pure ballast. Therefore, by combining the selected results discussed above, under possible real-life confining pressures (10 kPa−30 kPa) tracks are subjected, the optimum percentage of rubber in the RIBS can be confidently prescribed as 10% by weight based on the findings of the monotonic loading results and analysis.

6.5 Justifying the Optimal $R_b\%$ in RIBS Mixture under Cyclic Loading

Monotonic loading indicates that the energy dissipation capacity of RIBS increases with the rubber content, as the granular assembly becomes more ductile due to an increased value of $R_b\%$. For instance, RIBS specimens with 5% rubber under cyclic loading almost double the energy dissipation capacity compared to conventional ballast, and 10 % rubber performs even better by enhancing by almost twice the capacity of 5% RIBS (Figure 6.6). Any further increase in rubber (R_b=15%) does not make a significant contribution to the energy dissipation capacity compared to RIBS with 10% rubber, and it further reduces the resilient modulus. In other words, increasing R_b>10% reduces the resilient modulus M_R by less than 250 MPa, which is generally the minimum recorded for pure ballast from many studies (e.g., Indraratna et al., 2009).

Figure 6.6 shows the energy dissipation capacity per cycle and the resilient modules at N= 200000 against $R_b\%$. Note that the resilient modulus, energy dissipation of each cycle, and the damping ratio attain an approximately stable value after around 100000 cycles (Figure 5.8 and Figure 5.9). An increase in rubber content in RIBS increased the corresponding damping ratio. For example, 10% of rubber almost doubled the damping ratio, but a further increase in rubber content had no discernible impact on the damping ratio.

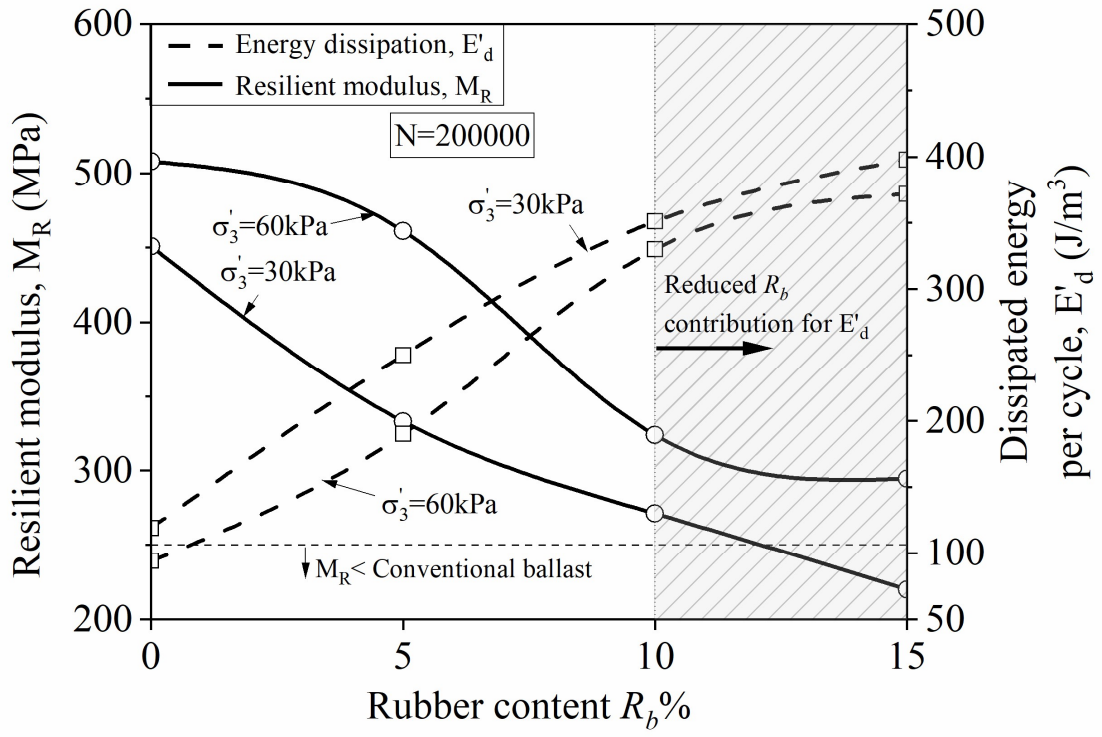

Figure 6.6 Optimisation of the rubber content according to the resilient modulus and energy dissipation per cycle

As discussed earlier (Section 5.7), increasing the rubber content up to 15%, not only fills the voids but also replaces some of the breakable ballast particles with rubber, and these particles may contribute to a more uniform contact force distribution. In this case, a higher rubber content (i.e., 15%) may reduce the shear strength of the ballast layer, where significantly reduced peak deviator stresses were observed for similar specimens with R_b=15% under monotonic loads. Therefore, RIBS with increased rubber (R_b >10%) may not be practical for the tracks that are subjected to increased axle loads (>25 t).

6.6 Drainage Potential

The drainage potential is one of the other major concerns of using RIBS material in real tracks. During testing, even at the lowest void ratio (when the rubber granules are

compressed most), the excess pore water pressures were found to be negligible. Compared to the impervious membrane used in the triaxial specimen, the surrounding boundary of RIBS would not be covered in real tracks, which implies that any infiltrated water could be drained away even more effectively than during laboratory tests. Therefore, an increase in rubber of up to 15% can successfully drain water out of the RIBS assembly, so the proposed R_b =10% satisfies the drainage requirements of the ballast layer. However, geotextile filter layer can be recommended to mitigate the possible risk of drainage performance reduction due to excessive material compression after long term service.

However, since rubber granules are not very heavy, they could be washed out during a flood or heavy rainfall. In this case, conventional ballast should be used in locations that are susceptible to waterlogging, and RIBS should only be placed below the sleeper load-bearing layer.

6.7 Initial Compaction Characteristics

In the RIBS material, there is a trend whereby the initial settlement increases during the conditioning phase as rubber particles are rearranged., but it is possible that sufficient compaction and tamping could reduce any undue initial settlements during the cyclic loading to an admissible limit. This reduced particle breakage and effective particle interlocking during the conditioning phase can make RIBS less compressible formation than a standard ballasted track. It is also identified in this study that, unlike pure ballast, RIBS densifies more under similar initial loading conditions, which ensures there is less settlement during the subsequent application of cyclic loading. The rubber content

R_b=5% in RIBS would not make any significant difference in reducing the axial and volumetric strains under cyclic loads, whereas increasing R_b (by 10 to 15%) and the confining pressure (30 to 60 kPa), reduced the permanent axial strains by 23 to 65%. Increased compaction is needed for pure ballast to decrease its void ratio to the RIBS material ($R_b \geq$5%), a situation that can lead to increased ballast breakage. Therefore, RIBS can be considered expedient in terms of compaction under the same loading while assuring there is less ballast breakage.

In essence, under monotonic and cyclic loads, it was demonstrated that 10% of rubber by weight could be considered as the optimum rubber content to be used in RIBS because any further increase in the rubber content would generate diminishing economic returns in relation to track maintenance.

6.8 Chapter Summary

This chapter contains an approach for optimising the rubber content in the RIBS mixture based on the geotechnical properties (i.e., frictional shear strength, dilation angle, axial strain, ballast breakage, modulus degradation, energy density, resilient modulus and energy absorption under cyclic loading) of RIBS. Then the proposed optimal R_b% was verified with the results from cyclic loading tests for pure ballast and RIBS. Moreover, the advantages of using RIBS with $R_b \geq 5\%$ was discussed in terms of the drainage potential and initial compaction characteristics. As a final note, through this laboratory work, RIBS epitomised its potential as an appropriate blending material to help ballast reduce track deformation and particle breakage under cyclic loading. The test results

demonstrated that 10% by weight of rubber could be considered the optimum rubber content to be used in RIBS.

CHAPTER SEVEN

7 CONSTITUTIVE MODELLING OF BALLAST-RUBBER MIXTURES

7.1 Introduction

Although there are a number of experimental studies in the literature for mixtures of ballast and rubber granules, none of them has attempted to develop a constitutive model that will simulate a stress-strain relationship. It has been of increasing interest in constitutive modelling to model mixtures of rubber and sand or rubber and sub-ballast mixtures based on critical state theory and bounding surface plastic theory (Lee et al., 1999; Youwai and Bergado 2003; Qi et al., 2018), but these models may not be directly applicable to mixtures of rubber and larger rock aggregates such as ballast. This is because as shearing progresses, mixtures of rubber and ballast show strain hardening behaviour rather than the strain-softening behaviour where the host materials are much smaller than the ballast. Often, an exact critical state could not be conveniently identified in a rubber-ballast mixture because the specimens mostly attained a critical state beyond the tested strain limit (>20% axial strain).

Most of the recent advanced constitutive models use elastoplastic or visco-elastoplastic relationships for comparatively larger granular materials such as conventional ballast and

rockfill materials, which means that while the material behaviour can be simulated more realistically, they are much more complicated. Most of these models require comprehensive experiments to derive parameters and complex numerical software simulations. Since this study initiates the constitutive modelling of ballast-rubber mixtures, it is important to form simple constitutive relationships that can be extended in future studies and widely adopted for the current state of research.

Therefore, in this chapter a simple model which adopts the conventional Mohr–Coulomb yield criterion is proposed. Typical stress-strain behaviour is approximated by the hyperbolic stress-strain curve (Duncan and Chang 1970) to obtain the required parameters (i.e., initial tangent modulus (E_i), ultimate deviator stress (q_{ult})) in addition to the conventional triaxial tests conducted for RIBS.

7.2 Strain Softening/Hardening Model

The linear Mohr-Coulomb yield criterion is expressed by:

$$\tau = \sigma \tan \varphi + c \tag{7.1}$$

where τ is the shear strength, σ is the normal stress, and c is the cohesion intercept which is the intercept of the failure envelope. From the Mohr circle, the linear Mohr-Coulomb yield criterion F can be expressed in terms of principal effective stresses as follows:

$$F = \frac{\sigma_1' + \sigma_3'}{2} \sin \varphi_m - \frac{\sigma_1' - \sigma_3'}{2} + c' \cos \varphi_m \tag{7.2}$$

where σ_1' is the major principal stress, σ_3' is the minor principal stress, and φ_m is the mobilised friction angle. Here the mobilised friction angle φ_m is used instead of the

failure friction angle because it is important to consider the change of friction angle as shearing progresses: $c = 0$ is assumed because granular materials have negligible cohesion.

7.2.1 Hardening soil model

As discussed in Chapter 4, the non-linear stress-strain behaviour of RIBS can be approximately represented by the hyperbolic method proposed by Duncan and Chang (1970) (Figure 7.1).

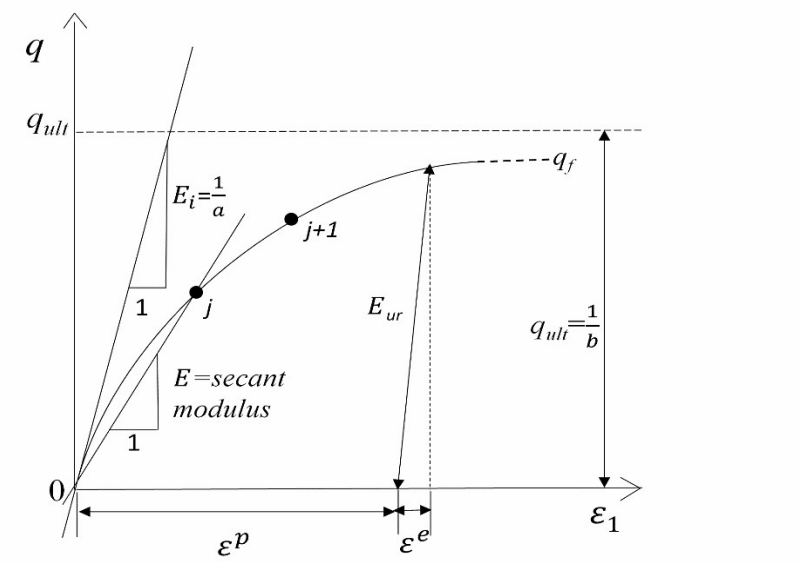

Figure 7.1 Hyperbolic approximation for non-linear stress–strain relationship of soils

The deviator stress $q = (\sigma_1' - \sigma_3')$ can be given by the following equation.

$$q = \frac{\varepsilon_1}{a + b\varepsilon_1} \tag{7.3}$$

where a and b are model parameters determined by curve fitting the experimental data.

In Figure 7.1, based on the hyperbolic fit, $1/a$ is the initial tangent modulus E_i and $1/b$ is the ultimate principal stress difference q_{ult}. Hence, Equation (7.3) can be rewritten as,

$$q = (\sigma_1' - \sigma_3') = \frac{\varepsilon_1}{\frac{1}{E_i} + \frac{\varepsilon_1}{q_{ult}}} \tag{7.4}$$

When $q = q_f$ in Equation (7.2), the Mohr-Coulomb failure criterion is satisfied and plastic yielding occurs.

$$q_f = \frac{2\sin\varphi_p}{(1 - \sin\varphi_p)}\sigma_3' \tag{7.5}$$

where φ_p is the peak friction angle. The failure ratio R_f is the ratio between q_f and q_{ult} and it is obvious that $R_f < 1$.

$$q_{ult} = \frac{q_f}{R_f} = \frac{2\sin\varphi_p}{R_f(1 - \sin\varphi_p)}\sigma_3' \tag{7.6}$$

The peak friction angle φ_p can be calculated from Equation (7.8), and note that φ_p is the maximum mobilised friction angle φ_m.

$$\left(\frac{\sigma_1'}{\sigma_3'}\right)_m = \frac{1 + \sin\varphi_m}{1 - \sin\varphi_m} \tag{7.7}$$

$$\left(\frac{\sigma_1'}{\sigma_3'}\right)_p = \frac{1 + \sin\varphi_p}{1 - \sin\varphi_p} \tag{7.8}$$

The initial tangent modulus E_i of granular materials increases as the confining pressures increase. Figure 7.2a shows the change in the ratio between the initial tangent modulus and the effective confining pressure (E_i/σ_3') with respect to the R_b of the current study.

A similar trend is observed in a previous study (Song et al. 2019) whereby ballast was mixed with tyre-derived aggregates and tested in a direct shear test apparatus at normal pressures of 50-150 kPa (Figure 7.2b). E_i/σ_3' is decreasing as R_b increases. Figure 7.2a shows that in the case of RIBS, the effect of the rubber content, R_b on E_i is significant compared to the approximate confining stresses applicable for railway tracks ($\sigma_3' < 60\ kPa$). Therefore, by considering the influence of both σ_3' and R_b, an equation for the initial tangent modulus can be derived (Equation 7.9).

$$E_i = \sigma_3'(\ a_1\ +\ b_1 \exp(-0.2\ R_b\%)) \tag{7.9}$$

where a_1 and b_1 are the empirical parameters.

By substituting Equations 7.6 and 7.9 in Equation (7.4), and then differentiating, the following equation (the expression of the tangent modulus in the Duncan–Chang model) is obtained for the tangent modulus E_t.

$$\frac{\Delta q}{\Delta \varepsilon_a} = E_t = \sigma_3'(\ \mathrm{a}\ +\ \mathrm{b} \exp(-0.2\ R_b\%)) \times \left[1 - \frac{R_f(1-\sin\phi)(\sigma_1'-\sigma_3')}{2\sigma_3' \sin\phi}\right]^2 \tag{7.10}$$

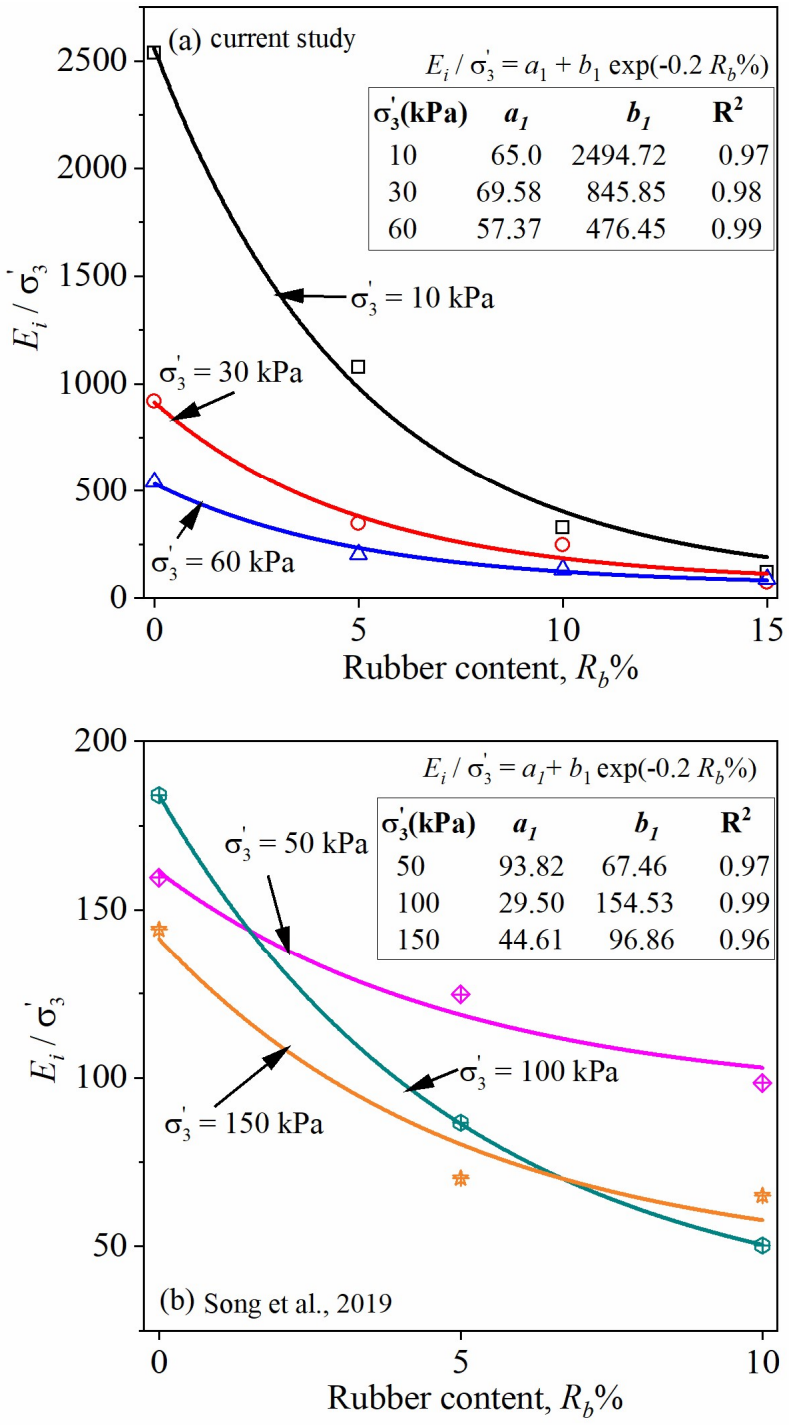

Figure 7.2 Effect of the rubber content (R_b) on $\frac{E_i}{\sigma_3'}$: (a) data from the current study, and (b) data from Song et al., 2019

From Equation 7.6, the following is obtained:

$$\varepsilon_1 = \frac{q}{E_i\left(1 - \frac{q}{q_{ult}}\right)} \tag{7.11}$$

The total axial strain ε_1 consists of the elastic axial strain (ε_1^e) and permanent plastic axial strain $\left(\varepsilon_1^p\right)$. By assuming linear elastic behaviour according to Hooke's elastic relationship during unloading–reloading, ε_1^e can be expressed as:

$$\varepsilon_1^e = \frac{q}{E_{ur}} \tag{7.12}$$

where E_{ur} is the unloading modulus (Figure 7.1). Here, for the hardening soil model, it is assumed that $E_{ur} = 3E_{50}$ where E_{50} is the secant modulus at 50% of the peak deviator stress (q_{peak}). Also,

$$\varepsilon_2^e = \varepsilon_3^e = v\frac{q}{E_{ur}} \tag{7.13}$$

v is Poisson's ratio, which in this study, is assumed to be a constant value of 0.3.

7.2.2 Shear hardening

The shear yield function F^s proposed by Schanz et al., (1999) is modified by adapting the initial tangent modulus(E_i) as in Equation (7.14).

$$F^s = \frac{q}{E_i\left(1 - \frac{q}{q_{ult}}\right)} - \frac{q}{E_{ur}} - \frac{\gamma^p}{2} \tag{7.14}$$

$$\gamma^p = \left(2\varepsilon_1^p - \varepsilon_v^p\right) \approx 2\varepsilon_1^p \tag{7.15}$$

where γ^p is the hardening parameter and ε_v^p is the plastic volumetric strain. In the current study ε_v^p is found to be not significant for RIBS compared to the plastic axial strains.

Only $\pm 0 - 4\%$ of plastic volumetric strains were contractive and dilative volumetric strains, whereas the axial strain was around 20-25%. An increase of γ^p leads to an ultimate shear failure and satisfies the conventional Mohr-Coulomb failure criterion.

7.2.3 Flow rule and plastic potential

One of the limitations of the associated flow rule is the overprediction of dilation. It has already been demonstrated in Chapter 4, that RIBS significantly reduces the dilation compared to pure ballast because of the inclusion of rubber. Therefore, in the current model, a non-associated type flow rule is used accommodating the mobilised dilation angle (ψ_m) instead of mobilised friction angle (φ_m). The relationship between the rate of plastic volumetric strain $\left(\dot{\varepsilon}_v^p\right)$ and the rate of plastic shear strain ($\dot{\gamma}^p$) is similar to all the plasticity models, including the hardening soil models, so the flow rule can be written as:

$$\dot{\varepsilon}_v^p = \sin\psi_m \, \dot{\gamma}^p \tag{7.16}$$

The stress dilatancy theory (Rowe 1962) for triaxial conditions was supplemented by Schanz and Vermeer (1996), in order to obtain a relationship between the friction angle and the dilatancy angle. Thus, the mobilised dilation angle (ψ_m) is expressed as:

$$\sin\psi_m = \frac{\sin\varphi_m - \sin\varphi_{cv}}{1 - \sin\varphi_m \sin\varphi_{cv}} \tag{7.17}$$

φ_{cv} is the critical state friction angle.

As mentioned previously, introducing rubber into ballast material delayed the specimens from attaining the critical stress state and also diminished the strain-softening behaviour. Thus, identifying the precise critical state point for RIBS ($R_b > 10\%$) can be difficult due to the strain limitations of conventional triaxial test apparatus. Luong and MP (1982) indicated that for granular materials the phase transformation state (where the dilatancy d=0) is fairly similar to the critical state. In the current study it is identified that determining the phase transformation state for RIBS is far more accurate than the critical state and it is more practical to use the mobilised friction angle at the phase transformation ($\varphi_{d=0}$) state to replace the mobilised friction angle at the critical state (φ_{cv}).

A modification factor R_m ($R_m < 1$) is introduced in the Equation (7.18); it can be obtained by several trial and error cycles and by comparing them with the test data. Accordingly, Equation (7.17) is modified for the current study as in Equation (7.18).

$$\sin\psi_m = R_m\left(\frac{\sin\varphi_m - \sin\varphi_{d=0}}{1 - \sin\varphi_m \sin\varphi_{d=0}}\right) \tag{7.18}$$

The modification factor R_m in Equation (7.18) depends on the confining pressure (σ_3') and the rubber content (R_b). Therefore R_m can be expressed as in the Equation (7.19), where $k1$ varies with R_b at a given confining pressure and $k2$ varies with σ_3'.

$$R_m = k1 \times k2 \tag{7.19}$$

$$k1 = \alpha 1 \times R_b + \beta 1 \tag{7.20}$$

$$k2 = \alpha 2 \times R_b + \beta 2 \tag{7.21}$$

Equations (7.20) and (7.21) are the empirical equations derived from the test results, where $\alpha 1$, $\alpha 1$, $\beta 1$, and $\beta 2$ are the empirical parameters. Note that Equations (7.20) and (7.21) are stated here to demonstrate the influence of R_b and σ_3', but these two equations have not been used in the simulations to calculate R_m. Instead, a few trial and error cycles were used to calculate R_m and $k1$ and $k2$ were back-calculated. As shown in Figure 7.3 (a-b), $k1$ decreases linearly as R_b increases, and $k1$ increases linearly as σ_3' increases.

Figure 7.3 (a-b) shows the linear variation of $k1$ and $k2$ with respect to R_b and σ_3' by examing data from the current study and Song et al., (2019).

φ_m for RIBS can also be defined in terms of the current stress state (c=0), hence,

$$\sin \varphi_m = \frac{\sigma_1 - \sigma_3}{\sigma_1 + \sigma_3} \tag{7.21}$$

$$\varphi_m = sin^{-1} \frac{q}{q + 2\sigma_3'} \tag{7.22}$$

The plastic potential function g is given by:

$$g = \frac{\sigma_1' + \sigma_3'}{2} \sin \psi_m - \frac{\sigma_1' - \sigma_3'}{2} \tag{7.23}$$

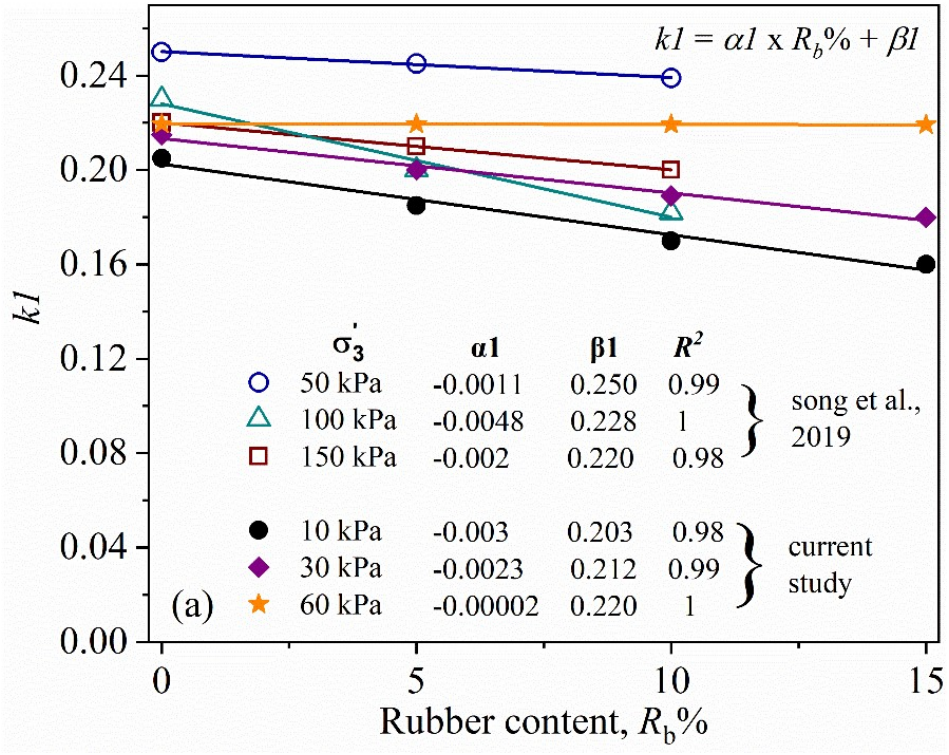

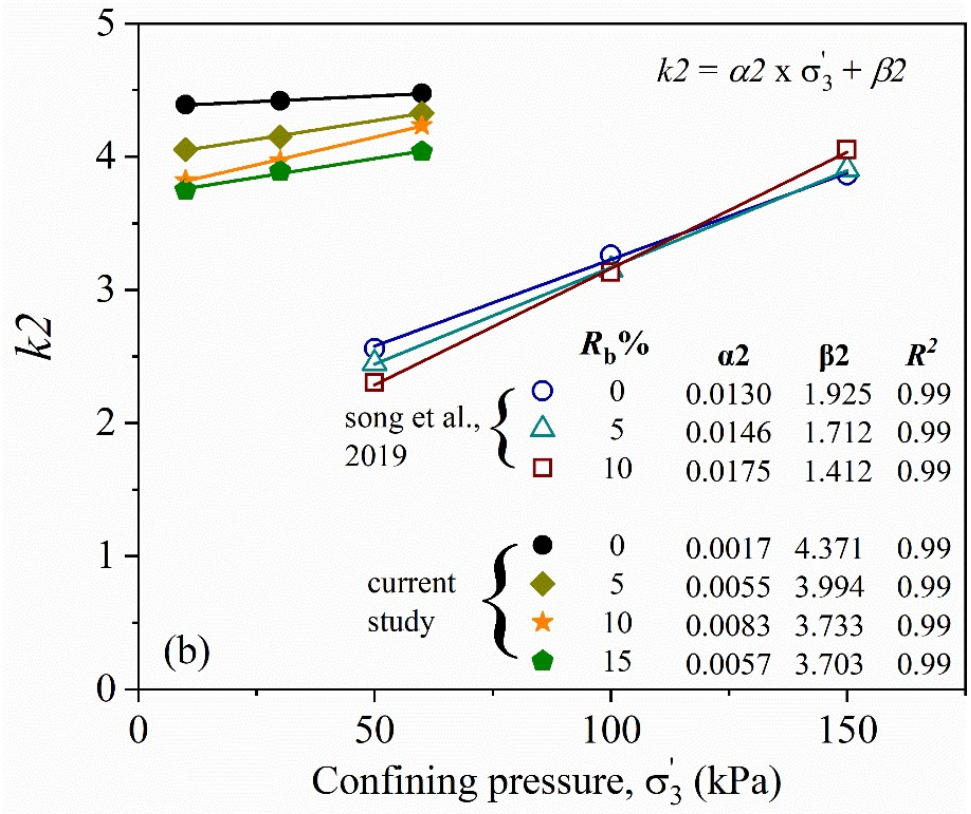

Figure 7.3 (a) The linear variation of $k1$ against R_b (b) The linear variation of $k2$ against σ_3'

7.3 Model Validation

The proposed model was validated by comparing the test data with the model prediction. In addition to the current study, test data from Song et al., (2019) was also used to validate the proposed model. Even though several other studies are available in literature for mixtures of ballast and rubber, no one studied the strain-strain behaviour in triaxial space or under controlled confining pressures. Song et al., (2019) studied ballast with TDA by utilising large-scale direct shear test apparatus and obtained plots for shear stress against shear strain and vertical strain against the horizontal strain. These results were used for model validation by approximating them into the stress-strain behaviour (ex. $\tau = q/2$). Here, the normal stresses (σ) applied in the direct shear test were simulated to the effective confining pressure (σ_3') in the triaxial tests.

7.3.1 Model parameters and calibration

The parameters for the verification of the proposed model using data from the current study and the study by Song et al., (2019), are presented in Table 7.1. Two parameters (a and b) were introduced for calculating the initial tangent modulus (E_i) using Equation (7.9). As discussed in Section 7.2.1, the initial tangent modulus (E_i) can be calculated from the triaxial test results. Figure 7.4 shows that the predicted E_i from Equation (7.9) agree with the E_i obtained from the triaxial tests .

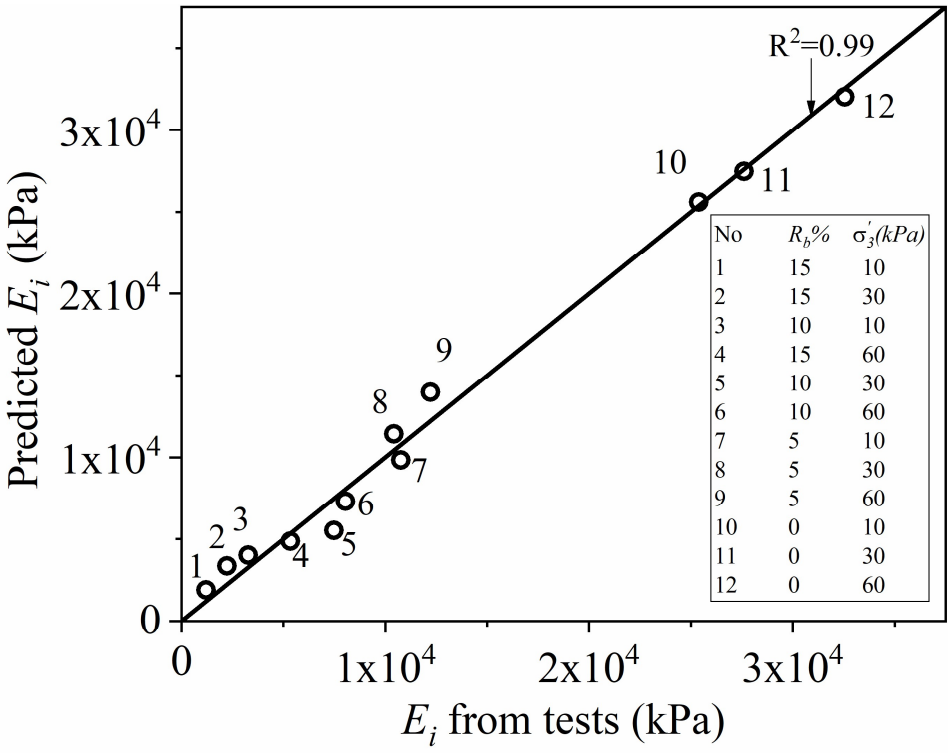

Figure 7.4 Predicted E_i versus E_i from tests

The peak friction angle was obtained from Equation (7.8), and the value for the failure ratio R_f specified for each type of material is also indicated in Table 7.1.

Table 7.1 Model parameters used for the validation

Model properties	Parameters	Current study				Song et al., (2019)		
		Ballast (Latite Basalt)	Ballast with 5% rubber	Ballast with 10% rubber	Ballast with 15% rubber	Ballast	Ballast with 5% rubber	Ballast with 10% rubber
Test details	σ_3'(kPa)	10/30/60	10/30/60	10/30/60	10/30/60	-	-	-
	Normal stress (kPa)	-	-	-	-	50/100/150	50/100/150	50/100/150
Initial tangent modulus (E_i)	a	65/69.58/57.37	65/69.58/57.37	65/69.58/57.37	65/69.6/57.4	93.82/29.50/44.61	93.82/29.50/44.61	93.82/29.50/44.61
	b	2494.72/845.85/476.45	2494.72/845.85/476.45	2494.72/845.85/476.45	2494.7/845.8/476.4	67.46/154.53/96.86	67.46/154.53/96.86	67.46/154.53/96.86
At mohr-Coulomb yield criterion (q_f)	φ_p	64.3/57.0/52.6	63.0/56.3/53.1	58.8/52.0/50.2	58.0/50.4/48.7	41.8/34.7/32.7	40.1/35.2/31.7	37.4/33.8/28.2
	R_f	0.99	0.98	0.95	0.9	0.99	0.98	0.95
Elasticity	E_{50} (MPa)	15.0/14.2/14.1	3.14/6.36/4.96	1.43/3.77/4.36	0.80/1.54/3.27	3.54/9.16/11.9	3.56/5.04/5.98	2.80/3.15/7.11
	v	0.3	0.3	0.3	0.3	0.3	0.3	0.3
Flow rule	$\varphi_{d=0}$	58.9/45.9/46.6	52.3/49.4/44.2	50.6/47.8/44.9	51.0/44.0/45.5	33.0/25.1/26.6	25.9/25.2/29.6	24.0/29.6/27.3
	R_m	0.9/0.95/0.98	0.75/0.83/0.95	0.65/0.75/0.94	0.6/0.7/0.9	0.64/0.75/0.85	0.6/0.63/0.82	0.55/0.57/0.81

7.3.2 Model validation using test data

The proposed constitutive model was validated by comparing the test data with the model prediction. In addition to the test data from the current study, independent test data from Song et al., (2019) was also used for model validation. Model equations were simulated and plotted using MATLAB numerical software. Figure 7.5 shows the stress response from the model predictions and comparison with the test results for RIBS and pure ballast, at confining pressures of 10, 30 and 60kPa. The deviator stress versus axial strain behaviour was captured very well for the specimen tested under σ_3' = 10 kPa and 30 kPa. There was a slight deviation for the specimens at σ_3' = 60 kPa. In terms of the stress response, the proposed model fits well with the experimental results of Song et al., (2019), where tests were carried out at σ_3' = 50 kPa, 100 kPa and 150 kPa (Figure 7.6).

Figure 7.7 compares the constitutive model prediction for volumetric strain curves with the test data. In Figure 7.8, the independent test data from Song et al., (2019) is compared with the proposed model simulation. The model prediction fits quite well with test data, despite the slight deviations observed initially.

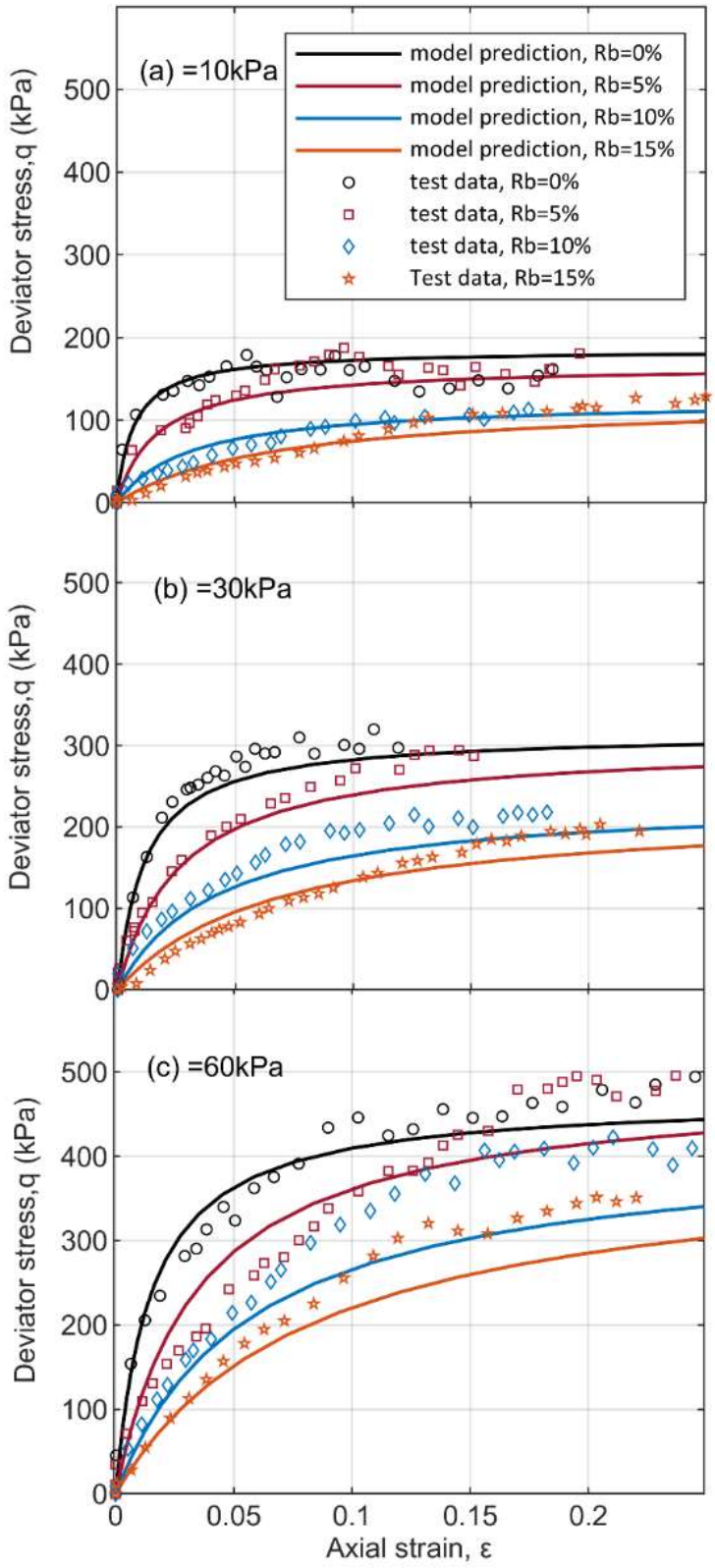

Figure 7.5 Deviator stress-axial strain curves from the test results and model predictions for pure ballast and RIBS with different R_b contents: (a) σ_3' =10 kPa; (b) σ_3' =30 kPa; (c) σ_3' =60 kPa.

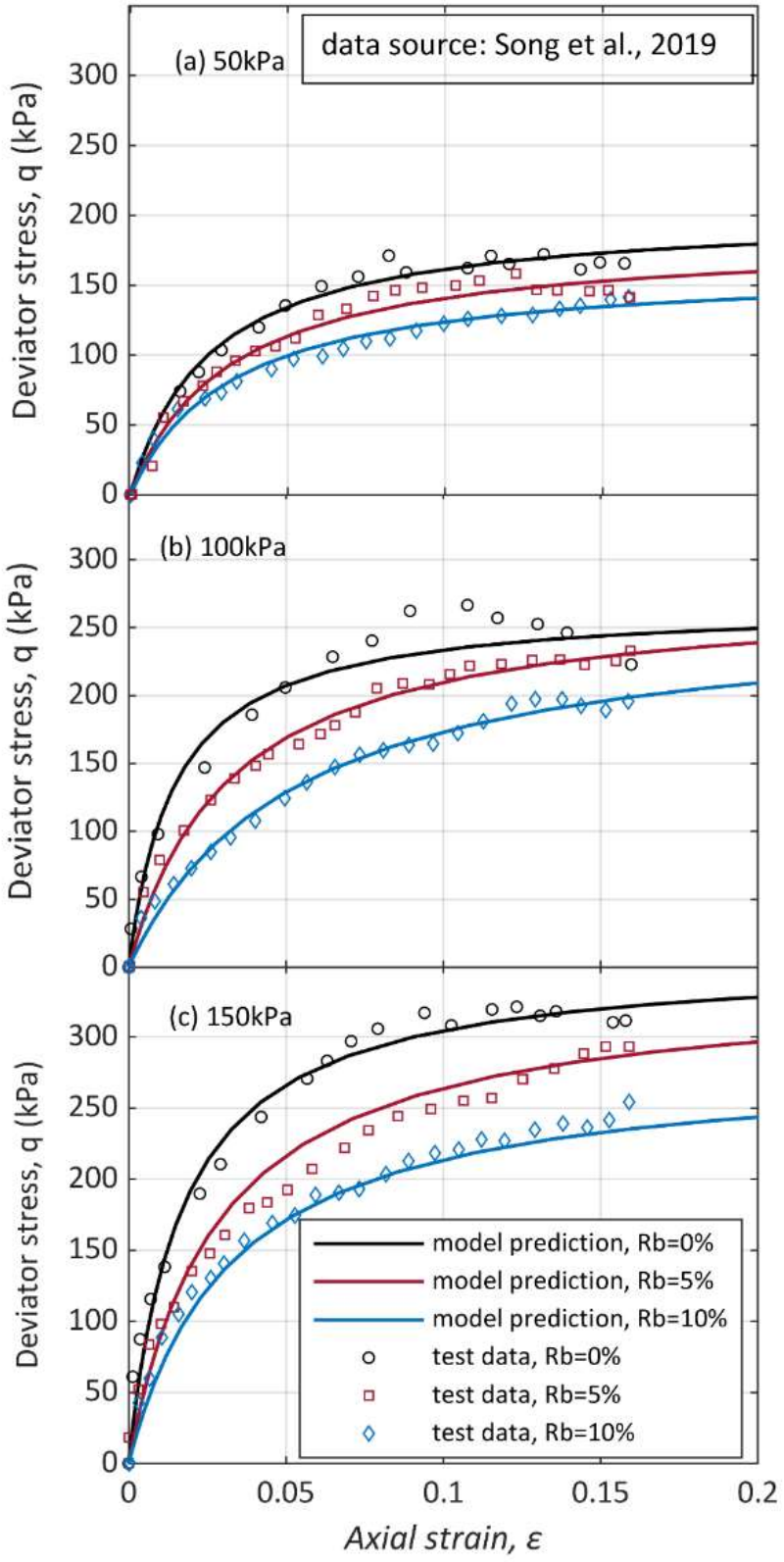

Figure 7.6 Deviator stress-axial strain curves from the test results and model predictions for pure ballast and rubber-ballast mixtures with different R_b contents (test data from: Song et al., 2019) (a) σ =50 kPa; (b) σ =100 kPa; (c) σ =150 kPa.

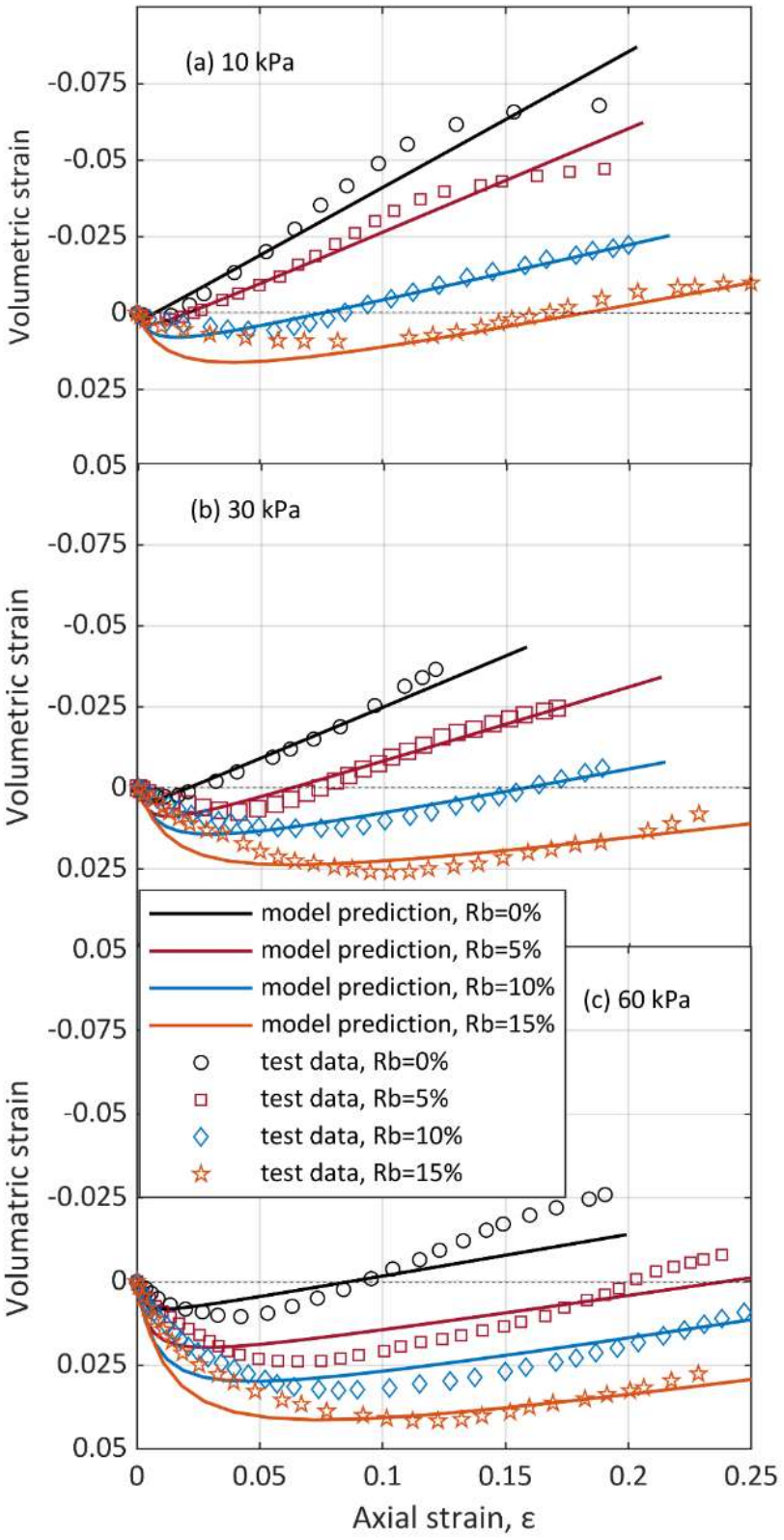

Figure 7.7 Volumetric strain-axial strain curves from the test results and model predictions for pure ballast and RIBS with different R_b contents: (a) σ_3' =10 kPa; (b) σ_3' =30 kPa; (c) σ_3' =60 kPa.

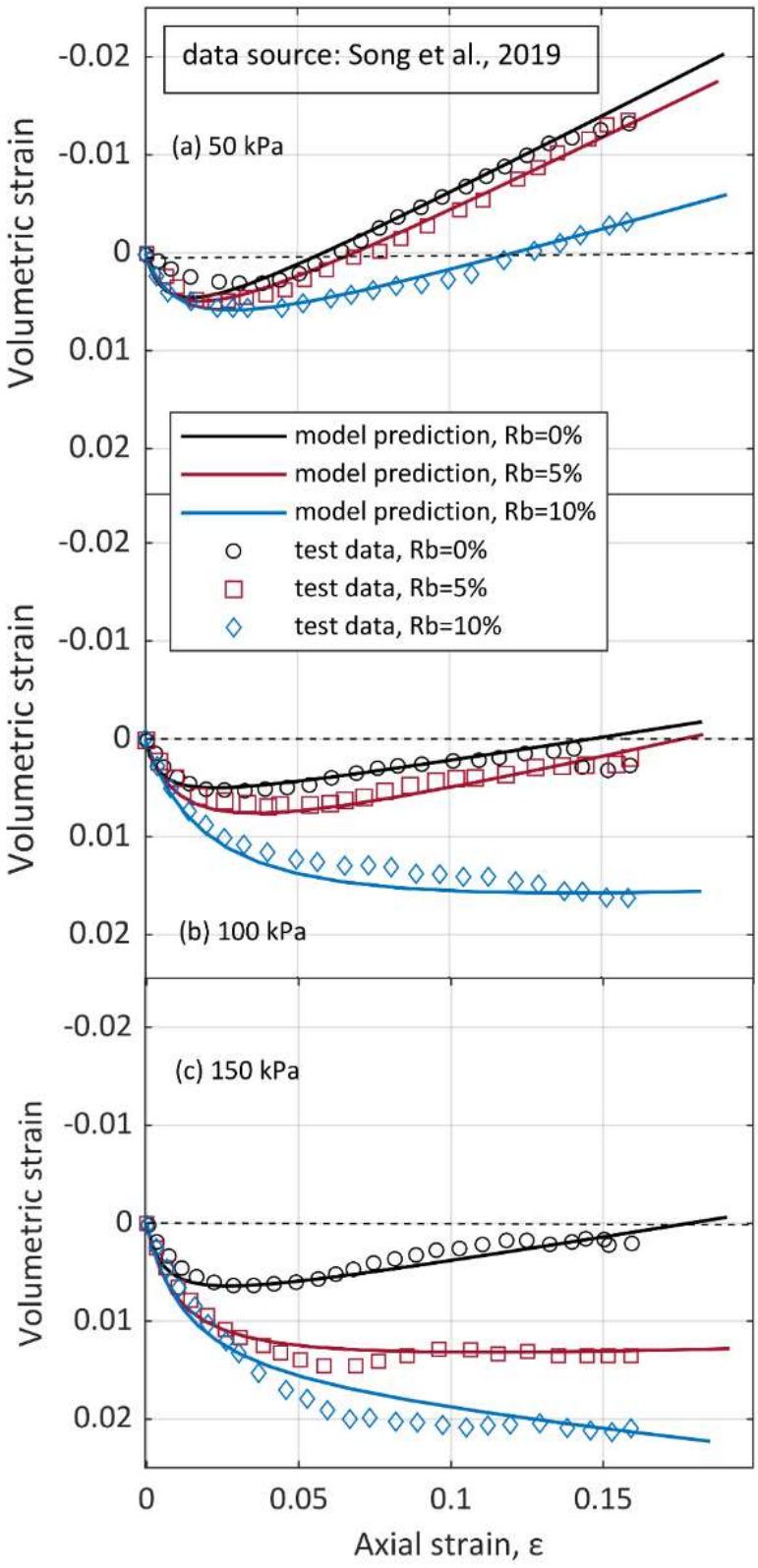

Figure 7.8 Volumetric strain- axial strain curves from the test results and model predictions for pure ballast and rubber-ballast mixtures with different R_b contents (test data from: Song et al., 2019): (a) σ =50 kPa; (b) σ =100 kPa; (c) σ =150 kPa.

7.4 Model Limitations

Slight deviation can be observed in the stress and strain curves at larger confining pressures (σ_3' = 60 kPa), possibly due to the simplicity of the model, approximations for parameters from the Duncan and Chang (1970) model, and approximate modification parameters introduced in the current study.

It can be observed that even at the ultimate deviator stress, the volumetric strains seem to be increasing further. Therefore, the current model is limited to small axial strains ($\varepsilon_a < 0.2$), albeit the applicable strain range could represent the general serviceability strain limits of practical applications (ex. allowable track settlements)

7.5 Chapter Summary

A simple constitutive model was introduced for mixtures of rubber and ballast by adopting the Mohr-Coulomb failure criterion. The model was developed to capture the stress-strain response of ballast materials mixed with rubber (including pure ballast) under static loading conditions. Numerical simulations (adopting MATLAB software) were carried out for model verification using test data from the current study and from an independent study. It was found that the model predictions adequately simulated the actual test results. This model could be developed further by introducing a cut-off limit to avoid continuous volume change even after attaining the critical state and smoothing the strain curves at larger stains.

CHAPTER EIGHT

8 PRACTICAL APPLICATIONS AND LIMITATIONS

8.1 Introduction

This chapter describes the practical applications and limitations of the Rubber Intermixed Ballast System (RIBS) to help for a better understanding of this current study.

8.2 Practical Application of RIBS in a Trial Track

The implementation of R & D outcomes of RIBS from laboratory to practice was proposed as a collaborative project with Sydney Trains, Australia. The trial track constructed at Chullora Technology Precinct includes a section with and without rubber granules in the ballast layer so that the performance of this RIBS track can be compared with a conventional ballasted track. As recommended in Chapter 6, R_b =10% by weight was used in the RIBS section of the field trial.

8.2.1 Design of track

It was proposed that a 20 m long instrumented track section be constructed with RIBS material by replacing a 150 mm thick layer of ballast in the conventional rail substructure and then comparing its performance with the conventional track. A 20 m long section of instrumented reference track (only used conventional ballast) section was also constructed more than 30m away from the track section of RIBS to enable the boundary conditions of both these tracks to perform independently. A distance of 30m from each end of the trial track was maintained with the same track formation to enable the train to accelerate and decelerate before connecting the new track to the existing long track. The reason for this is so that each train can maintain a constant speed as they pass over the instrumented sections of track.

A site investigation was carried out to obtain the soil profile and relevant ground characteristics needed for the track design. Based on ground investigation data, it was found that a thin surficial stratum of sandy-silty clay and clayey sands (unsaturated) were underlain by weathered shale and interspersed claystone, with a relatively stiff clay stratum existing at greater depths; hence, the subgrade up to a depth of 5m or so can be considered as a relatively stiff formation. A soil sample refusal at the respective location was visible as in Figure 8.1.

Figure 8.1 Soil sampling refusal at proposed RIBS section of track

The operating class of the track is a freight siding (T5) where the design criteria considered 25-tonne wagon axle loading with an assumed maximum speed of 80 km/h over a design life of 20 years with total traffic of 5 MGT/year. Details of the design calculations for the RIBS track are given in Appendix B.

Based on the analysis, typical ballast and capping thickness were approximately 250-300 mm and 150-200 mm, respectively. Since the permitted train speed at the site is within 15 km/hour, the ballast was reduced to 250 mm thick, and was placed over a 150mm thick compacted capping layer; and the thickness of both layers was uniform across the entire trial track. A granular drainage layer was laid on the bottom of the excavation (beneath the capping layer). The dimensions of the track were chosen after referring to the code of practice (Section 4 -Ballast) issued by the Australian rail track cooperation (ARTC), it is in line with the T HR TR 00192 ST Ballast specifications set out by Transport for NSW.

Instrumentation and monitoring play a vital role in field trials because evaluating the performance of the track depends predominantly on instrumentation and monitoring. To evaluate the performance of each layer separately in terms of deformation, dilation, stress transformation (energy absorption), and vibration, different types of instruments were proposed, as shown in Table 8.1. The symbols used for the identification and level of

placement are also given in Table 8.1. Note that the arrangement for the instrumentation proposed for the RIBS section and the reference section are the same. The pressure cells, extensometer, and accelerometer of each section are connected to the data acquisition of the section, namely DAQ RIBS and DAQ REF. Figure 8.2 shows a plan view and a cross-section of the instrumented RIBS track. The settlement pegs are designed to measure the vertical deformation of the track (settlement) so the level of the settlement peg can be read manually or taken by a camera. A set of settlement pegs were used for manual reading and a separate sets of settlement pegs were used for monitoring using a wide-angle PTZ camera.

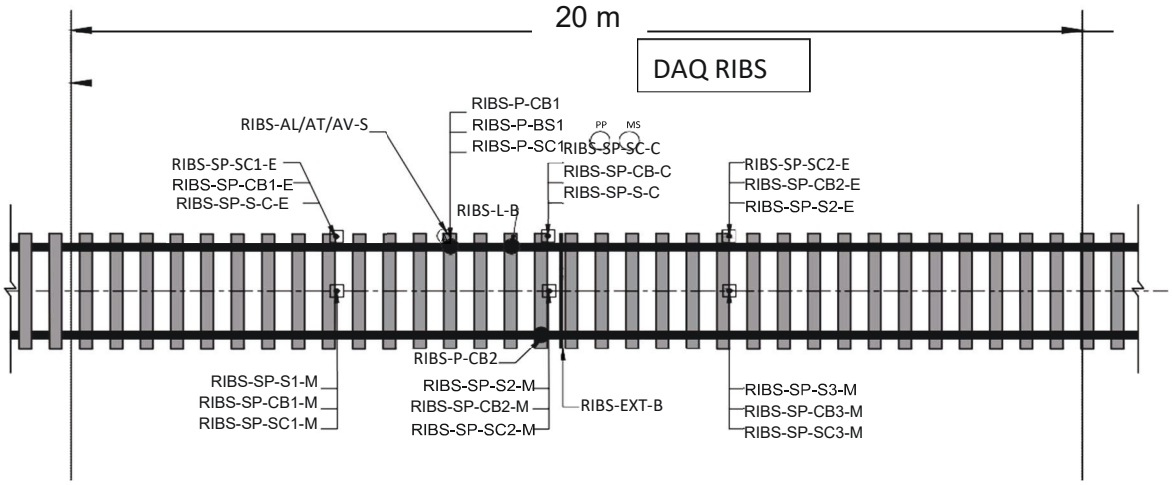

INSTRUMENTATION - (PLAN VIEW)
SCALE: 1:100

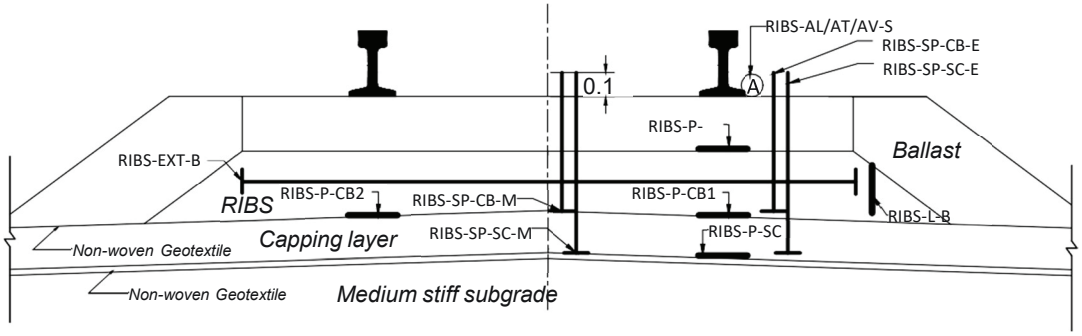

INSTRUMENTATION - (CROSS-SECTION)
SCALE: 1:20

Figure 8.2 Plan view and cross-section of instrumentation

Table 8.1 List of the instruments

Location of the instrument	Sensor	Sensor name	Number of Instruments
Subgrade (in the ground)	Moisture sensor	RIBS-MS-G-17.910	1
	Pore Pressure Transducers	RIBS-PP-G-17.910	1
Subgrade -capping interface	Settlement peg (Camera)	RIBS-SP-SC-17.910	1
	Settlement peg (Manual)	RIBS-SP-SC-17.906 RIBS-SP-SC-17.914	2
	Vertical Pressure sensor	RIBS-P-SC-17.908	1
Capping-ballast interface	Settlement Peg (Camera)	RIBS-SP-CB-17.910	1
	Settlement peg (manual)	RIBS-SP-CB-17.906 RIBS-SP-CB-17.914	2
	Vertical Pressure sensor	RIBS-P-CB-17.908 RIBS-P-CB-17.910	2
In ballast/RIBS	In ballast extensometer	RIBS-EXT-B-17.912	1
	Horizontal pressure plate	RIBS-L-B-17.912	1
Ballast-sleeper interface	Vertical Pressure sensor	RIBS-P-BS-17.908	1
Sleeper and rail position	Target on sleeper (Camera)	RIBS-SP-S-17.910	1
	3-axis Accelerometer at Rail	RIBS-AL-S-17.908 RIBS-AT-S-17.908 RIBS-AV-S-17.908	1

Notations:

MS: Moisture sensor

PP: Pore pressure transducer

SP: Settlement Peg

P: Pressure cell (Vertical stresses)

L: Pressure cell (Horizontal stresses)

EXT: Extensometer

AL/AT/AV: Accelerometer (Longitudinal, Transverse and Vertical directions)

G: Ground

SC: Subgrade-capping interface

CB: Capping-ballast interface

B-Ballast S-Sleeper C-Camera

M-Middle of the track E-Edge of the track

8.2.2 Construction of track

Construction commenced by mixing the materials (ballast and rubber granules) for RIBS. A Volumetric Mixer was first calibrated with each type of material to calculate the gate openings needed to blend the two products to the desired mix proportion. The inlet gates were then set and the materials were loaded into two bins and blended with a mixing augur. The RIBS material (ballast with 10% rubber by weight) coming from the outlet was moved to a stockpile for use in the track. Figure 8.3 (a-b) shows the materials being mixed onsite.

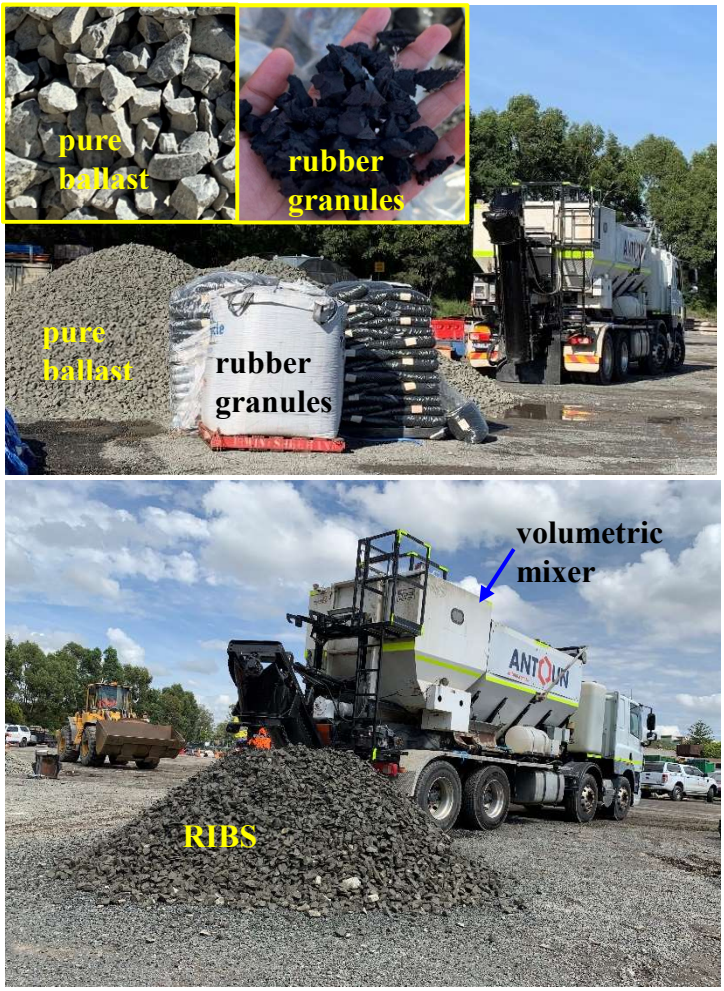

Figure 8.3 Mixing the ballast and rubber granules at the site (a) the materials before mixing, and (b) volumetric mixer while producing RIBS

The next step was site clearing by removing the old track at the same location. Excavations continued up to the designed bottom level of the track formation, and then the condition of the soil at the bottom of the excavation was assessed. Figure 8.4 (a) shows the excavation and the ground condition of the proposed track. Even though the water table was not encountered during the excavation or site investigation, the area is prone to accumulate surface runoff water from the surrounding area, so a granular drainage layer was placed at the top of the subgrade and a cess drain (150 mm diameter pipe) was constructed at the edge of the track to divert the water into a nearby culvert (Figure 8.4 (b)). A nonwoven geotextile layer was placed in between the subgrade and drainage interface to prevent subgrade fines and slurry from migrating up into the drainage layer.

Figure 8.4 Ground preparation (a) excavation starts from the centreline of the track, and (b) the drainage layer on top of the subgrade is separated by a non-woven geotextile

After completing the drainage layer, 150 mm thick capping material was placed in situ such that the top surface maintained 2% slope towards the drainage pipe. The particle size distribution of the capping material is shown in Figure 8.5. The capping was compacted to more than 98% of its maximum dry density (MDD = 2200 kg/m^3). Non-destructive density testing was carried out using nuclear density gauge for the capping density check as shown in Figure 8.6. As shown in Figure 8.5, the capping material contains around 15% of fine particles (the percentage passing through $0.75\mu m \approx 15\%$). To ensure that the ballast could not be contaminated with fines from the capping layer and drain out water into the cess drain, a layer of Bidim A44 nonwoven geotextile was placed between the capping layer and the ballast interface.

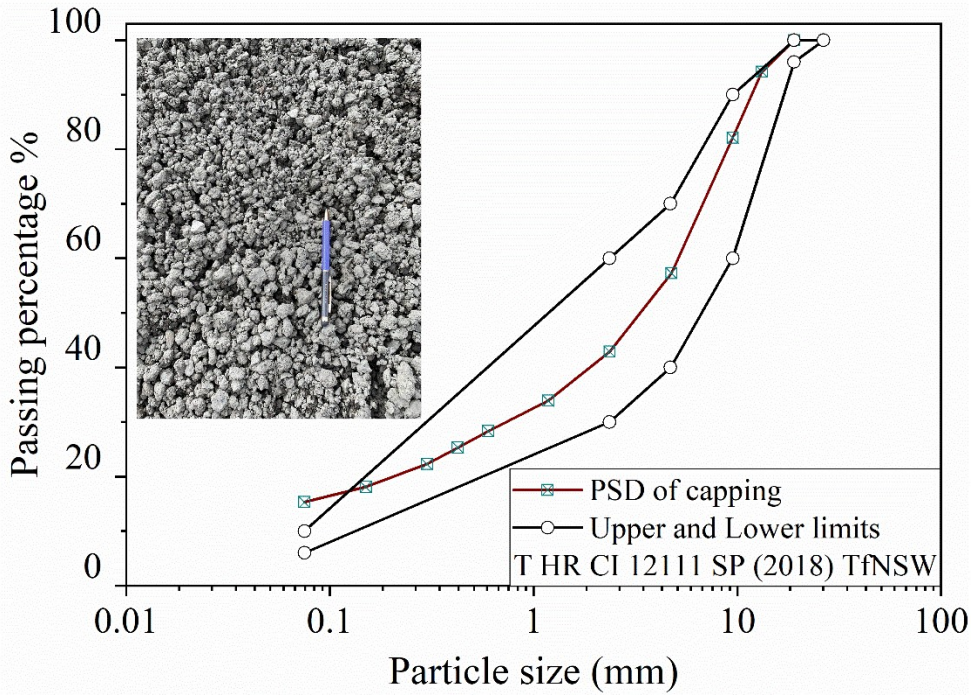

Figure 8.5 Particle size distribution of capping material

Figure 8.6 Non-destructive density testing for the capping layer

After completing the capping layer, a 150 mm thick RIBS layer was laid and compacted to a maximum dry density of 1450 kg/m^3 to replace the bottom ballast layer. An approximately 100 mm thick layer of pure ballast was placed on top of the RIBS layer, and then the sleepers were laid. In the final stage, the construction of the rails, placement of crib/shoulder ballast, and ballast tamping were carried out. Note that the instruments were placed at predetermined locations (Table 8.1) while the track substructure was being constructed in stages. Solar and battery-powered data acquisition is located close to the instrumentation points and away from the live track (Figure 8.7). Figure 8.8 (a-e) shows the stages of the track construction.

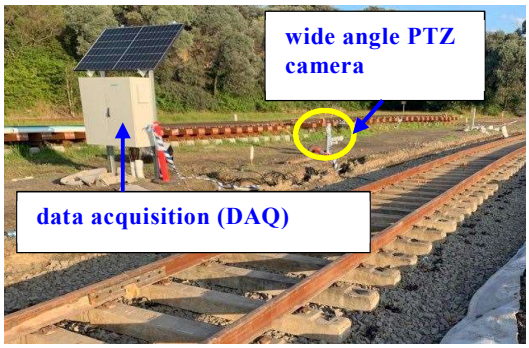

Figure 8.7 Data acquisition system

(a) compacted capping

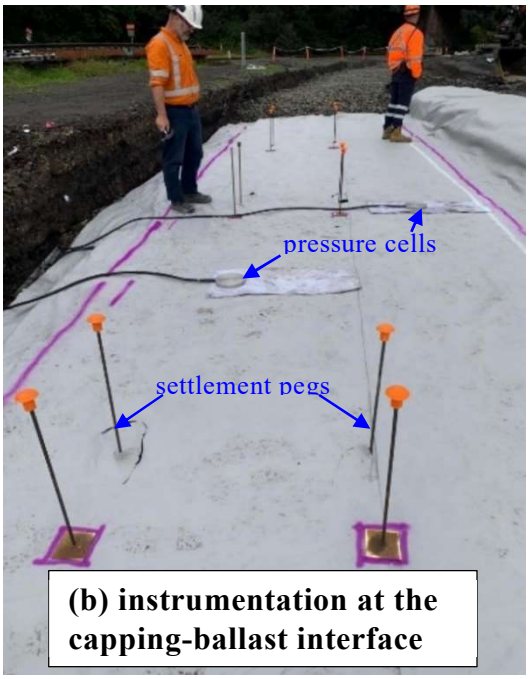

(b) instrumentation at the capping-ballast interface

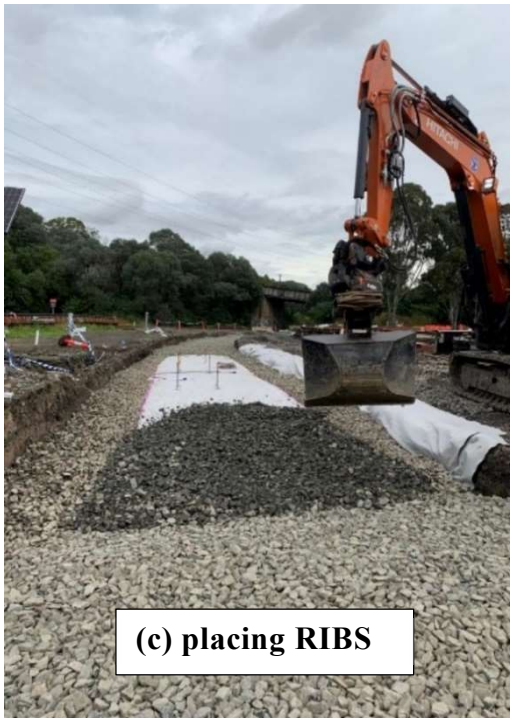

(c) placing RIBS

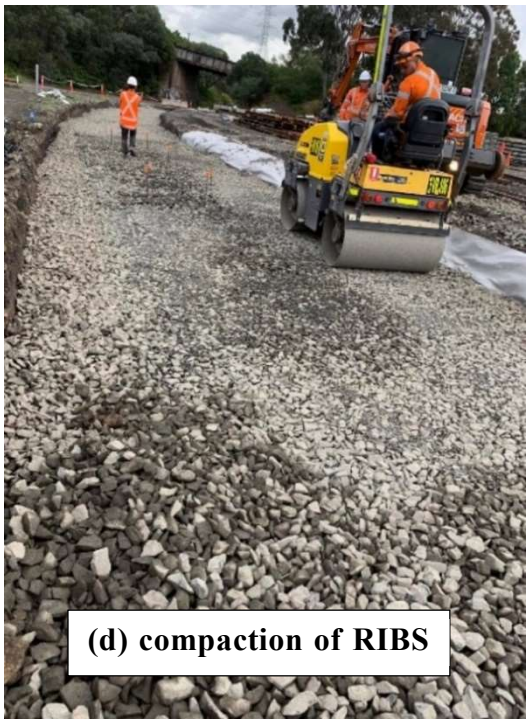

(d) compaction of RIBS

Figure 8.8 Stages of RIBS track construction

8.2.3 Observations and considerations during construction

During laboratory testing, the initial settlement increased during the conditioning phase as the rubber particles compressed, however, sufficient compaction and tamping could reduce any undue initial settlement to an admissible limit (Chapter 5). The reduction in particle breakage and effective particle interlocking during compaction could make RIBS less compressible compared to a standard ballasted track. Similarly, after compacting the ballast/RIBS in the field, a well-interlocked particle arrangement was observed in the RIBS layer compared to the conventional ballast layer in the reference track section. This can be considered as an irreversible particle rearrangement during compaction because the material did not bounce back after the roller passed over. Therefore, it is expected that RIBS with $R_b = 10\%$, reduce the deformation of ballast over the long term, as revealed by the laboratory findings.

As was also identified in this study, increased compaction caused increased ballast breakage in the reference section, whereas RIBS is expedient in terms of compaction to a reduced void ratio while assuring less ballast breakage.

8.2.4 Monitoring and test outcomes

Although it was supposed to collect data from the field trial and include complete real time track analysis in this thesis, the COVID-19 restrictions implemented in NSW, Australia terminated construction for a long time, which delayed the loading and collection of field data; therefore, field data cannot be shown at this stage.

8.3 Limitations of RIBS

Laboratory tests revealed that while RIBS generally enhances the performance of ballast, the stiffness, initial settlement, and resilient modulus are compromised to some extent. Therefore, particular attention is needed to select the right amount of rubber in RIBS that will optimise the performance of ballast.

As discussed in Chapter 5, increasing the amount of rubber by up to 15% will not only fill the voids, it will also replace some of the broken particles of ballast with rubber, and these particles may contribute to a more uniform contact force distribution. Thus, the peak deviator stresses for similar specimens with R_b=15% had decreased significantly. In this case, R_b >10% may reduce the shear strength of the ballast layer; Therefore, RIBS R_b >10% of rubber without any amplification may not be practical for tracks that will be subjected to increased axle loads (>25 tonnes). However, this limitation can be avoided

in practice due to the compaction characteristics of RIBS under tamping and initial loading cycles.

However, since rubber granules are light, comparatively, they could be washed away by a flood or heavy rainfall. In this case, for locations that are susceptible to waterlogging, conventional ballast material could be used as crib ballast while RIBS are only placed below the sleeper load-bearing layer.

Mixing larger quantities of rubber granules for field applications should be done carefully because it may be directed to undesired outputs. It is important to avoid mixing two granular materials under wet conditions because wet rubber granules can remain as lumps in the mixture, and that affects the uniformity. Also, dropping the mixture from a considerable height can segregate lightweight rubber granules to some extent. Mixed material discharged from the outlet (at the end of the mixing augur) of the volumetric mixer was collected from a reduced height (<1 m).

Minor segregation of rubber particles was observed when the RIBS material was placed on the track, which could be due to the size of the rubber particles used in the field trial. Since the commercially available range of rubber granules is 8-15 mm instead of 9.5-19 mm, the rubber particles used in the field were somewhat smaller than desired. It was also difficult to remove and replace ballast particles with the same size rubber granules because the contractor provided pure ballast which complied with T HR TR 00192 ST Ballast - Transport for NSW as well as AS 2758.7:2015. Therefore, rubber granules were added to the ballast for the field trial without replacing them with the same size ballast particles. However, after adding $R_b = 10\%$ to the pure ballast, which had gradation of an approximate average of the upper and lower limits of particle size distribution curves,

it still complied with the AS 2758.7:2015 ballast specifications. So that the ultimate probable particle size distribution of RIBS in the field trial is shown in Figure 8.9.

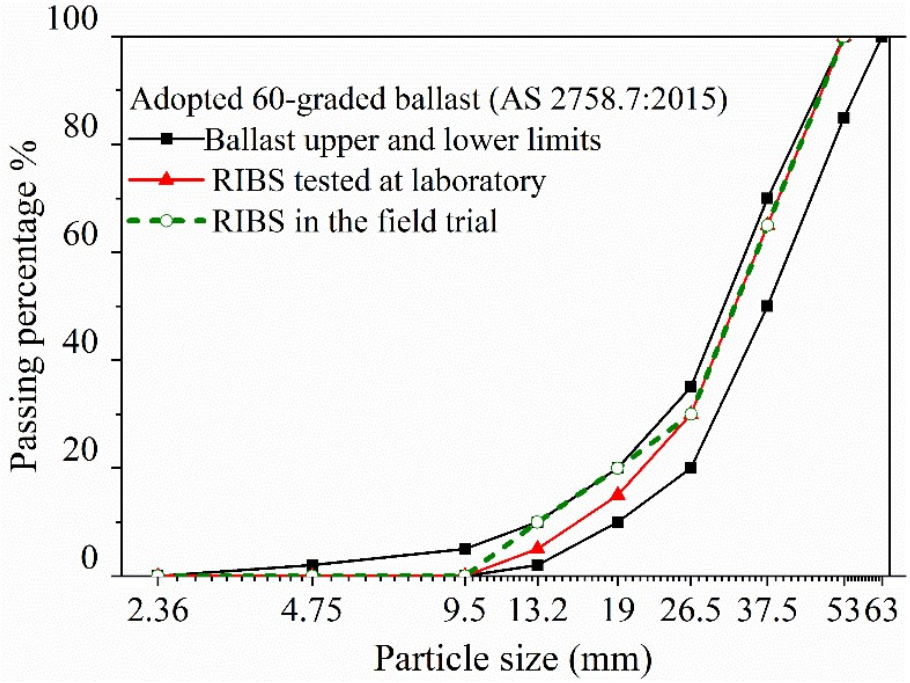

Figure 8.9 Particle size distribution of RIBS in the field trial

8.4 Chapter Summary

This chapter describes an example of the practical application of RIBS material in real tracks. The field trial was an industry collaborative project with Sydney Trains, Australia. The track has a 20 m long instrumented RIBS section and a 20 m long instrumented conventional track section (as a reference) to compare the performance of RIBS track. In addition to describing the design and construction of a trial track, the chapter included the observations and considerations experienced during the construction phase. Furthermore, the limitations of the proposed new material, (Rubber Intermixed Ballast System-RIBS) were discussed based on the outcomes of laboratory testing and field trial construction.

CHAPTER NINE

9 CONCLUSIONS AND RECOMMENDATIONS

9.1 Introduction

This chapter concludes the main findings related to the behaviour of the Rubber Intermixed Ballast System (RIBS), including the geotechnical responses under static and cyclic loading, the optimal rubber content in the RIBS mixture, constitutive modelling, and practical applications and limitations of RIBS. Recommendations for future work on RIBS are also discussed.

9.2 Geotechnical Characteristics of RIBS under Static Loading

The following salient findings regarding the geotechnical characteristics of RIBS could be drawn from the static triaxial loading tests (relation to Chapters 3 and 4):

1. The inclusion of rubber offered a significant reduction in ballast breakage, with more than 70% reduction in the breakage of coarser ballast particles (>38 mm) in all the RIBS mixtures.

2. Under the same effective confining pressure, the peak deviator stress q_{peak} of RIBS decreased when the amount of rubber, R_b > 5%; however, this reduction in strength (i.e., the drop in q_{peak} = 27% and 34% for RIBS with R_b = 10% and 15% at σ_3' = 30 kPa) was certainly tolerable in relation to the obvious benefits of having less particle breakage.

3. RIBS with an increased amount of rubber at larger effective confining pressures initially demonstrated larger volumetric contraction, however, the increased amount of rubber reduced dilation significantly compared to pure ballast, thereby improving track stability from a real-life perspective.

4. The modulus degradation gradually declined as the amount of rubber was increased up to the optimum of 10% by weight; the mix remained stable at larger axial strains. This implied that the rubber helped to increase the ductility of the mix, so in reality the track is expected to be more resilient while attaining a stable settlement.

5. There was only a minor reduction in the effective friction angle (<6%) of the RIBS mixtures when the amount of rubber increased from 0 to 15%. This was mainly because the rubber fraction (9.5–19 mm) was of the same size and similar angularity as the replaced natural rockfill fraction. The decreased angle of shearing resistance could be attributed to the reduced particle hardness and surface roughness of the rubber particles compared to quarried natural rock aggregates.

6. When R_b=10%, RIBS showed similar stress-dilation behaviour with the increasing effective confining pressure while indicating at least a 50% reduction in the dilation angle compared to pure ballast at confining pressures, $\sigma_3' \geq 30$ kPa.

7. A 10% increase in the amount of rubber increased the strain energy density of RIBS by around 15%, in contrast to pure ballast, with the benefit of absorbing the energy transferred to the substructure, thus reducing track deterioration. However, at larger confining pressures ($\sigma_3' \geq 60$ kPa) the strain energy density was likely to remain steady with a more than 5% increase in rubber.

9.3 The Response of RIBS under Cyclic Loading

Large-scale cyclic triaxial tests were carried out to investigate the dynamic properties of RIBS with varying rubber contents (0-15% by weight), and its associated behaviour (i.e., deformation, resilient modulus, damping ratio, ballast breakage) when subjected to different confining pressures (30 and 60 kPa) under a loading frequency of 20 Hz. The following conclusions can be drawn based on the test results (based on Chapter 5).

1. This study confirmed that during the conditioning phase (strain controlled static loading up to the maximum cyclic stress), RIBS attained a denser granular assembly attributed to the compression of rubber granules, i.e., resulting in a reduced void ratio. Compared to pure ballast ($R_b = 0\%$), the reduction in the void ratio of the RIBS test specimens was approximately 3, 4, and 5 times for R_b =5, 10, and 15%, respectively. This densification contributed to reduce the permanent axial strains by 23 to 65%; this corresponded to increasing values of R_b (10 to 15%) and confining pressure (30 to 60 kPa).

2. Although all the test specimens reached plastic shakedown at an axial strain between 1% and 3%, the addition of rubber delayed the specimens from attaining shakedown (At $N \approx 50{,}000$ for pure ballast and $N \approx 200{,}000$ for RIBS with $R_b = 10\%$). From a practical perspective, the accumulation of plastic strain at a slower rate in RIBS than pure ballast is beneficial in making the track maintenance cycles less frequent and more cost effective.

3. The addition of rubber and the subsequent increase in confining pressure reduced the volumetric strain (dilation) of the RIBS specimens. These specimens could be categorised into two distinct zones, namely, Zone A (quasi-stable) at small strains and Zone B at larger volumetric strains that correspond to a greater number of loading cycles. This led to the conclusion that ballast tracks might compromise stability in the long run (Zone B), but the addition of even a small percentage of rubber in RIBS to contain excessive volumetric strain (dilation) could be considered an obvious benefit.

4. An increase in rubber content in RIBS increased the corresponding damping ratio and the energy absorption capacity. For example, 10% of rubber almost doubled the damping ratio and increased the energy dissipation capacity by approximately three times that of pure ballast, while sustaining an adequate resilient modulus (> 250 MPa) for the RIBS material.

5. Under the confining pressure of 30 kPa, the ballast breakage of RIBS reduced by approximately 25%, 30% and 80% as the rubber content increased by 5, 10, and 15%, respectively. The role of rubber particles within RIBS could be identified as threefold: (i) predominantly void filling ($R_b \leq 5\%$), (ii) fulfilling the role of void

filling to an optimum volume within the RIBS fabric ($5\% < R_b \leq 10\%$), and (iii) unbreakable rubber crumbs replacing an equivalent fraction of breakable ballast particles, apart from void filling ($10\% < R_b \leq 15\%$).

9.4 Optimal Amount of Rubber in RIBS Mixtures

1. To optimise these mechanical properties and deformation characteristics without making the blended mix overly compressive, an optimum amount of 10% of rubber by weight is recommended in RIBS because any further increase would generate diminishing economic returns concerning track maintenance.

2. It was also evident from the results that rubber particles ranging from 9.5 to 19 mm and with a similar angularity to ballast aggregates were advantageous, because they reduced the breakage of load-bearing larger aggregates and thus effectively controlled ballast fouling within the granular matrix.

9.5 Constitutive Modelling

A simple constitutive model was proposed (Chapter 7) by adopting the conventional Mohr-Coulomb yield criterion. The following model developments can be presented from the study.

1. The expression for the tangent modulus (E_t) in the Duncan–Chang model (Duncan and Chang 1970) was modified by including the rubber content ($R_b\%$), and the confining pressure (σ_3') in the function for the initial tangent modulus (E_i);

which could be used for granular rubber and rock mixtures with sufficient accuracy.

2. A non-associated type flow rule was adopted to accommodate the mobilised dilation angle (ψ_m) rather than the mobilised friction angle (φ_m) because rubber reduces the dilation angle for RIBS mixtures significantly compared to the friction angle. The relationship between ψ_m and the critical stress friction angle (φ_{cv}) introduced by Schanz and Vermeer (1996) was modified by replacing the φ_{cv} with the friction angle at the phase transformation state ($\varphi_{d=0}$), because rubber-ballast mixtures are more likely to attain the critical state beyond the tested strain limit (>20% axial strain).

3. A modification factor (R_m) was introduced for calculating ψ_m in terms of φ_m and $\varphi_{d=0}$, which could be obtained easily with a few trial and error cycles. The factor R_m was found to depend on R_b% and σ_3'.

4. In this current study, the stress-strain model was verified by the test data and by Song et al., (2019). A considerably good correlation was observed between the test data and the model simulation.

9.6 Practical Applications and Limitations

Based on the outcomes of the design and construction of the field trial (Chapter 8), the following conclusions are presented.

1. Using rubber granules from waste tyres as elastic aggregates blended with traditional ballast particles for rail tracks is practically feasible. Conventional

procedures for track construction could be used to construct a RIBS track, but a specific machine is required to blend the rubber and rock aggregates at the site.

2. It was practical to use a volumetric mixer to mix the two materials (10% by weight of rubber granules and ballast) by calibrating the machine for the correct mixture. To obtain a fairly uniform RIBS mixture, it is recommended that the two materials be mixed in dry conditions and then drop the mixture off at a reduced height (<1 m).

3. As observed in the field trial, the compaction of RIBS in the track resulted in a well-interlocked particle arrangement with minimum particle breakage compared to conventional ballast material. This irreversible arrangement of particles observed in RIBS during compaction could be considered as being permanent but not resilient. This indicated that the compaction stage of RIBS agreed with the conditioning phase of cyclic loading laboratory tests (Chapter 5); therefore, it was expected to reduce the long-term settlement of RIBS tracks compared to conventional ballast tracks.

4. The limitations of these new RIBS materials could be (i) possible segregation if not handled carefully, (ii) difficulties in removing 10% of the selected ballast particles (the same size as rubber particles) from the pure ballast available which complies with the standard, and (iii) rubber particles being washed away if they are used in tracks at areas that can become waterlogged. Particular care is needed to overcome these limitations. For example, reducing the height from which the mixtures fall to the ground to < 1 m, mixing the materials under dry conditions, considering the particle size and percentage of rubber when preparing the rock

aggregates, and using RIBS as bottom ballast while the crib and shoulder ballast remains unchanged.

5. RIBS provided a solution for reusing non-biodegradable waste material from the tyre industry at a low cost as an aggregate in railways, while preserving the natural landscapes.

9.7 Recommendations for Future Works

1. Firstly, it is important to monitor the trial tracks already constructed during for a considerable period during this study and then analyse the performance of the RIBS track section compared to the reference track. These findings will be helpful for stakeholders and interested parties for future practical applications, and academics in the same discipline.

2. The scope of this current study was limited to assessing behaviour under cyclic loading for maximum cyclic stress of 230 kPa, this represents a 25-tonne train axle load. It was also observed that increased R_b decreased q_{peak} so the bearing capacity of RIBS was slightly smaller than pure ballast. Therefore, it is better to study RIBS under increased axial loads (> 25 t) at changing frequencies because the optimum R_b can be changed for higher axle loads.

3. It is suggested that rubber particles in the size range of 19-26.5 mm be tested and analysed because this may help to avoid possible segregation during practical applications (when the falling height of the mixture cannot be controlled). However, increasing the particle size to more than 26.5 mm is not recommended

because the stiffness will be compromised. Moreover, commercially available larger rubber particles miss out on their angularity.

4. Wheel flats create unfavourable impact loads on rail and substructure, therefore it is essential to know how ballast mixed with rubber will perform under impact loads. Unlike under cyclic loading, tracks can experience considerable re-bounce due to the impact loads which will affect the safety and comfort of rail transportation. Therefore, it is recommended that impact loading tests be carried out for RIBS.

5. The constitutive model could be further developed to cut off continuous increases in volumetric strains after attaining the critical state, and also smooth the curves by following the trend of experimental data.

6. FEM modelling can predict material behaviour in advance by simulating changing conditions (i.e., axle load, confining pressure, frequency, the thickness of the RIBS layer, etc.). Therefore, it is suggested that FEM modelling for RIBS be carried out to better understand its engineering applications. Furthermore, DEM modelling is also suggested for studying RIBS granular mixtures because it would help to study particle contact forces, and the deformation/compressibility mechanism of particles, etc.

7. A critical cost-benefit analysis (initial and long term), including the carbon footprint of RIBS replacing conventional ballast material, is recommended because it would inspire the industry to use RIBS in real tracks.

REFERENCES

Abadi, T., Le Pen, L., Zervos, A. and Powrie, W. (2016). "A review and evaluation of ballast settlement models using results from the Southampton Railway Testing Facility (SRTF)." *Procedia engineering*, 143, pp.999-1006.

Ahmed, I. (1991). "Use of waste materials in highway construction."

Allen, J.J. (1973). "The effects of non-constant lateral pressures on the resilient response of granular materials," University of Illinois at Urbana-Champaign.

Anderson, W.F., and Fair, P. (2008). "Behavior of railroad ballast under monotonic and cyclic loading." *J. Geotech. Geoenviron. Eng.*, 134, 316-327.

Arachchige, C. M. K., Indraratna, B**.,** Qi, Y., Vinod, J. S., and Rujikiatkamjorn, C. (2021). "Geotechnical characteristics of a Rubber Intermixed Ballast System". *Acta Geotechnica*., 1-12.

AREMA. (2010). Manual for railway engineering, Vol. 1: Track, Ch. 1: Roadway and ballast. American Railroad Engineering and Maintenance of Way Association (AREMA), Washington, D.C.

Arroyo, M., Lopez-Manchado, M.A., Valentin, J.L. and Carretero, J. (2007). "Morphology/behaviour relationship of nanocomposites based on natural rubber/epoxidized natural rubber blends." *Composites science and technology,* 67(7-8), pp.1330-1339.

ARTC (2012). "Engineering (Track & Civil) Code of Practice-Section 4 Ballast." Australian Rail Track Corporation.

Arulrajah, A., Naeini, M., Mohammadinia, A., Horpibulsuk, S., and Leong, M. (2020). "Recovered plastic and demolition waste blends as railway capping materials." *Transp. Geotech*., 22.

AS (Australian Standards), (2015). "Aggregates and rock for engineering purposes. Part 7: Railway ballast." *AS 2758.7,*Standards Australia.

ASTM (2020). “Methods for consolidated drained triaxial compression test for soils.” *ASTM D7181*. West Conshohocken, PA: ASTM

Aursudkij, B. (2007). “A laboratory study of railway ballast behaviour under traffic loading and tamping maintenance.” Doctoral dissertation, Univ. of Nottingham, England.

Carrascal, I., Casado, J., Diego, S. and Polanco, J. (2010). “Comportamiento mecánico frente a esfuerzos dinámicos de manta elastomérica para la atenuación de vibraciones en ferrocarriles.”

Carrera, A., Coop, M. and Lancellotta, R. (2011). “Influence of grading on the mechanical behaviour of Stava tailings.” *Géotechnique,* 61**,** 935-946.

Chrismer, S. and Selig, E. (1993). “Computer model for ballast maintenance planning.” *Proc. of 5th international heavy haul railway conference,* beijing, china, 1993. 223-227.

Costanzo, N.M., Pita, A.L., Fontseré, V., Ausilio, A., De Ambri, E. and Basei, E. (2016).“NEOBALLAST: seeking for the ballast of the future.” https://www.tecnicavialibre.es/documentos/Articulos/VLTecnica11_Neoballast.pdf

Dafalias, Y.F. (1982). “Bounding surface formulation of soil plasticity.” Soil mechanics-transient and cyclic loads, 253-282.

Dafalias, Y. F., and Popov, E. P. (1975). "A model of nonlinearly hardening materials for complex loading." *Acta Mechanica,* 21(3), 173-192.

Deloitte (2019). Global ELT Management –A global state of knowledge on regulation, management systems, impacts of recovery and technologies.

DEQ. (1989). Rhinehart tire fire dum. Virginia Department of Environmental Quality, Winchester, 1-3.

Diyaljee, V.A. (1987). “Effects of stress history on ballast deformation.” *J. geotech. Eng.,* 113, 909-914.

Duncan, J.M., and Chang, C.Y. (1970). “Nonlinear analysis of stress and strain in soils.” Soil. Mech. Found. Eng.

Edil, T.B. and Bosscher, P.J. (1994). “Engineering properties of tire chips and soil mixtures.” *Geotech. Test. J.,* 17, pp.453-453.

Esmaeili, M., Aela, P. and Hosseini, A. (2017). “Experimental assessment of cyclic behavior of sand-fouled ballast mixed with tire derived aggregates.” *Soil Dyn. Earth. Eng.,* 98, 1-11.

Esmaeili, M., Ebrahimi, H., and Sameni, M. K. (2018). “Experimental and numerical investigation of the dynamic behavior of ballasted track containing ballast mixed with TDA.” *Proc., Inst. Mech. Eng. Part F: J. Rail. Rapid. Transit.,* 232 (1), 297–314.

Esmaeili, M., Zakeri, J. A., Ebrahimi, H., and Sameni, M. K. (2016). “Experimental study on dynamic properties of railway ballast mixed with tire derived aggregate by modal shaker test.” *Adv. Mech. Eng.,* 8 (5), 1687814016640245.

ETRMA (2016). “ETRMA on Safety of recycled rubber infill material.” European tyre and rubber manufacturers Association.

Fathali, M., Esmaeili, M. and Moghadas Nejad, F. (2019). “Influence of tire-derived aggregates mixed with ballast on ground-borne vibrations.” *J. Mod. Transp.,* 27(4), pp.355-363.

Fathali, M., Nejad, F. M., and Esmaeili, M. (2016). “Influence of tire-derived aggregates on the properties of railway ballast material.” *J. Mater. Civ. Eng.,* 29 (1).

Feng, Z., and Sutter, K. (2000). "Dynamic Properties of Granulated Rubber/Sand Mixtures." *Geotech. Test. J.*, 23(3), 338-344.

Fontseré, V., Pita, A.L., Manzo, N. and Ausilio, A. (2016). “NEOBALLAST: new high-performance and long-lasting ballast for sustainable railway infrastructures.” *Trans. Research Proc.,* 14, 1847-1854.

Ghazavi, M. and Sakhi, M.A. (2005). "Influence of optimized tire shreds on shear strength parameters of sand." *Int. J. Geomech.,* 5, 58-65.

Gong, H., Song, W., Huang, B., Shu, X., Han, B., Wu, H., and Zou, J. (2019). "Direct shear properties of railway ballast mixed with tire derived aggregates: Experimental and numerical investigations." *Constr. Build. Mater.,* 200 (Mar), 465–473.

Gulfnews (2021). Kuwait: Fire ripped through 25,000 square meters of Al Sulabiya tire site. https://gulfnews.com/world/gulf/kuwait/kuwait-fire-ripped-through-25000-square-meters-of-al-sulabiya-tire-site-1.74769506

Guo, Y., Markine, V., Qiang, W., Zhang, H., and Jing, G. (2019). "Effects of crumb rubber size and percentage on degradation reduction of railway ballast." *Constr. Build. Mater.,* 212:210-224.

Hardin, B.O., (1985). "Crushing of soil particles." *J. Geotech. Eng.,* 111(10), 1177-1192.

Hazarika, H 2007, 'Structural stability and flexibility during earthquakes using tyres', —a novel application for seismic disaster mitigation. In: Hazarika, Yasuhara, editors. 23–24 March 2007, Yokosuka, Japan Proceedingsoftheinternational workshop on scrap tire derived geomaterials—opportunities and challenges. London: Taylor & Francis Group; pp. 115-125.

Hicks, R. G. 1970. "Factors influencing the resilient properties of granular materials." Doctoral dissertation, Univ. of California, Berkeley, California.

Ho, C.L., Humphrey, D., Hyslip, J.P., and Moorhead, W. (2013). "Use of Recycled Tire Rubber to Modify Track–Substructure Interaction." *Transp. Res. Rec.,* 2374:119-125.

Hussaini, S. K. K., Indraratna, B., and Vinod, J. S. (2015). "Performance assessment of geogrid-reinforced railroad ballast during cyclic loading." *Transp. Geotech.,* 2, 99–107.

Holtz, W.G., and Gibbs, H.J. (1956). "Triaxial shear tests on pervious gravelly soils." *J. Soil Mech. Found. Div,* 82, 867-1-867-22.

Indraratna, B. and Ionescu, D. (2000). "State of the art large scale testing of ballast." CORE 2000 Railway Technology for the 21st Century, Australia: Railway Technical Society of Australasia. 24.1-24.13

Indraratna, B., Ionescu, D., and Christie, H. D. (1998). "Shear behaviour of railway ballast on large-scale triaxial tests." *J. Geotech. Geoenviron. Eng.,* 124(5), 439-449.

Indraratna, B., Khabbaz, M.H., Salim, W. and Christie, D. (2006). "Geotechnical properties of ballast and the role of geosynthetics in rail track stabilisation." *J. Ground Imp.,* 10(3), 91-102.

Indraratna, B., Lackenby, J., and Christie, D. (2005). "Effect of confining pressure on the degradation of ballast under cyclic loading." *Géotechnique,* 55(4), 325–328.

Indraratna, B., and Ngo, T., (2018), "Ballast railroad design: smart-uow approach." *CRC Press.,* UK.

Indraratna, B., and Nimbalkar, S. (2013). "Stress-strain degradation response of railway ballast stabilized with geosynthetics." *J. Geotech. Geoenviron. Eng.,* 139, 684-700.

Indraratna, B., Nimbalkar, S., Christie, D., Rujikiatkamjorn, C. and Vinod, J. (2010). "Field assessment of the performance of a ballasted rail track with and without geosynthetics." *J. Geotech. Geoenviron. Eng.,* 136(7), pp.907-917.

Indraratna, B., Qi, Y. and Heitor, A. (2017). "Evaluating the Properties of Mixtures of Steel Furnace Slag, Coal Wash, and Rubber Crumbs Used as Subballast." ." *J. Mater. Civ. Eng.,* 30, 04017251.

Indraratna, B., and Salim, W. (2002). "Modelling of particle breakage of coarse aggregates incorporating strength and dilatancy." *Proc. Inst. Civ. Eng. Geotech. Eng.,* 155(4):243-252.

Indraratna, B., and Salim, W. (2003). "Deformation and degradation mechanics of recycled ballast stabilised with geosynthetics." *Soils. found.,* 43, 35-46.

Indraratna, B., and Salim, W. (2005). "Mechanics of ballasted rail tracks: a geotechnical perspective." *CRC Press*, UK

Indraratna, B., Salim, W., and Rajikiatkamjorn, C. (2011). "Advanced rail geotechnology: Ballasted track." *CRC Press,* Rotterdam, Netherlands.

Indraratna, B., Sun, Q., and Nimbalkar, S. (2015). "A critical state based constitutive model for the triaxial response of ballast incorporating particle breakage." *Proc XV Panamerican Conf. Soil. Mech. Geotech. Eng.,* 1232-1239.

Indraratna, B., Sun, Q.D., and Nimbalkar, S. (2015). "Observed and predicted behaviour of rail ballast under monotonic loading capturing particle breakage." *Can. Geotech. J.,* 52:73-86.

Indraratna, B., Tennakoon, N., Nimbalkar, S., and Rujikiatkamjorn, C. (2013). "Behaviour of clay-fouled ballast under drained triaxial testing." *Géotechnique*., 63(5):410-419.

Indraratna, B., Vinod, J. S., and Lackenby, J. (2009). "Influence of particle breakage on the resilient modulus of railway ballast." *Géotechnique,* 59(7), 643–646.

Ionescu, D., Indraratna, B. and Christie, H. (1998). "Behaviour of railway ballast under dynamic loads." Thirteenth Southeast Asian Geotechnical Conference., 69-74.

Iwan, W.D. (1967). "On a class of models for the yielding behavior of continuous and composite systems." *J. Appl. Mech*. 34(3): 612-617

Jayasuriya, C., Indraratna, B., and Ngo, T. N. (2019). "Experimental study to examine the role of under sleeper pads for improved performance of ballast under cyclic loading." *Transp. Geotech.*, 19, 61-73.

Jeffs, T., and Tew, G. (1991). A Review of Track Design Procedures–Volume 2: *Sleepers and Ballast.* Railways of Australia, Australia.

Jefferies, M. (1993). “Nor-Sand: a simle critical state model for sand.” *Géotechnique,* 43, 91-103.

Jones, K. (2001). “Back to the trees.” *Proc. of the International Sympnosium On Recycling and Reuse of Used Tyres,* Univ. of Dundee, Thomas Telford, UK, 39-49.

Kaneko, T., Hyodo, M., Nakata, Y., Nyoshi and Hazarika, H. (2013). “Dynamic deformation 660 characteristics and seismic response of tire chip and mixtures with sand.” *J. Japan 661 Society of Civil Engineers, Ser. C* (Geosphere Engineering), 69(1):91-107

Kennedy, J., Woodward, P., Medero, G., and Banimahd, M. (2013). “Reducing railway track settlement using three-dimensional polyurethane polymer reinforcement of the ballast.” *Constr. Build. Mater.,* 44:615-625.

Khoshoei, S.M., Bak, H.M., Abtahi, S.M., Hejazi, M., and Shahbodagh, B. (2021). “Experimental Investigation of the Cyclic Behavior of Steel-Slag Ballast Mixed with Tire-Derived Aggregate.” *J. Mater. Civ. Eng.,* 33:04020468.

Kim, H. K. and Santamarina, J. C. (2008). “Sand–rubber mixtures (large rubber chips).” *Can. Geotech. J.,* 45(10), 1457-1466.

Koohmishi, M. and Azarhoosh, A. (2020). “Hydraulic conductivity of fresh railway ballast mixed with crumb rubber considering size and percentage of crumb rubber as well as aggregate gradation.” *Constr. Build. Mater.,* 241, 118133.

Koohmishi, M. and Azarhoosh, A. (2021). “Degradation of crumb rubber modified railway ballast under impact loading considering aggregate gradation and rubber siz.” *Can. Geotech. J.,* 58, 398-410.

Lackenby, J. (2006). “Triaxial behaviour of ballast and the role of confining pressure under cyclic loading.” Doctoral dissertation, Univ. of Wollongong, Australia.

Lackenby, J., Indraratna, B., Mcdowell, G., and Christie, D. (2007). “Effect of confining pressure on ballast degradation and deformation under cyclic triaxial loading.” *Géotechnique,* 57(6), 527-536.

Lee, J., Salgado, R., Bernal, A. and Lovell, C. (1999). “Shredded tires and rubber-sand as lightweight backfill.” *J. Geotech. Geoenviron. Eng.,* 125, 132-141.

Lee, J.S., Dodds, J. and Santamarina, J. C. (2007). “Behavior of rigid-soft particle mixtures.” *J. mater. Civ. Eng.,* 19, 179-184.

Lee, K.L. and Seed, H.B. (1967). “Drained strength characteristics of sands.” *J. Soil. Mech. Found. Div.,* 93, 117-141.

Lees, G. and Kennedy, C. K. (1975). “Quality, shape and degradation of aggregates.” *Q. J. Eng. Geol.,* 8, 193-209.

Lekarp, F., Isacsson, U. and Dawson, A. (2000). “State of the art. I: Resilient response of unbound aggregates.” *J. transp. Eng.,* 126, 66-75.

Li, D. and Selig, E.T. (1998). “Method for railroad track foundation design. I: Development.” *J. Geotech. Geoenviron. Eng.,*124(4), pp.316-322.

Luong, M. and L. MP (1982). "Mechanical aspects and thermal effects of cohesionless soils under cyclic and transient loading." International Union of Theoretical and Applied Mechanics Symposium., Balkema, DA.

Madhusudhan, B., Boominathan, A. and Banerjee, S. (2017). “Static and large-strain dynamic properties of sand–rubber tire shred mixtures.” *J. Mater. Civ. Eng,* 29, 04017165.

Marachi, N.D. (1969). “Strength and Deformation. Characteristics of Rockfill Materials.” Report No. TE-69-5 to State of California Department of Water Resources.

Marsal, R.J. (1967). “Large-scale testing of rockfill materials.” *Soil. Mech. Found. Div.,* 93(2):27-43.

Marschi, N.D., Chan, C.K., and Seed, H.B. (1972). “Evaluation of properties of rockfill materials.” *Soil. Mech. Found. Div.,* 98(1):95-114.

Mashiri, M., Vinod, J., Sheikh, M.N. and Tsang, H.H. (2015). “Shear strength and dilatancy behaviour of sand–tyre chip mixtures.” *Soils. Found.,* 55**,** 517-528.

Miura, N. and Sukeo, O. (1979). “Particle-crushing of a decomposed granite soil under shear stresses.” *Soils. Found.,* 19, 1-14.

Mroz, Z. (1966). “On forms of constitutive laws for elastic-plastic solids.” Archiwum Mechaniki Stosowanej, 18, 1-34.

Müller, R., (2008). “Under ballast mats (UBM) insertion loss.” UIC-Report, Version, 3, p.04.

Naeini, M., Mohammadinia, A., Arulrajah, A., Horpibulsuk, S., and Leong, M. (2019). “Stiffness and strength characteristics of demolition waste, glass and plastics in railway capping layers.” *Soils. Found.,* 59(6):2238-2253.

Navaratnarajah, S.K. and Indraratna, B. (2017). “Use of rubber mats to improve the deformation and degradation behavior of rail ballast under cyclic loading.” *J. Geotech. Geoenviron. Eng.,* 143(6), p.04017015.

Navaratnarajah, S. K., Indraratna, B. and Ngo, N. T. (2018). “Influence of under sleeper pads on ballast behavior under cyclic loading: experimental and numerical studies.” *J. Geotech. Geoenviron. Eng.,* 144(9).

Ngo, T., Indraratna, B. and Ferreira, F. (2021). “Influence of synthetic inclusions on the degradation and deformation of ballast under heavy-haul cyclic loading*.” Int. J. Rail Transp,* 1-23.

Nova, R. and Hueckel, T. (1981). “A unified approach to the modelling of liquefaction and cyclic mobility of sands.” *Soils. Found.,* 21, 13-28.

Paderno, C. (2010). “Comportement du ballast sous l" action du bourrage et du trafic ferroviaire. Doctoral Dissertation, Swiss Federal Institute of Technology Lausanne, Switzerland.

Park, J., Kim, J. and Edil, T. (1993). "Sorption capacity of shredded waste tires." *Proc. of the International Symposium on Geotechnical Related to the Environment*, A. Balkema, 341-348.

Pender, M. (1978). "A model for the behaviour of overconsolidated soil." *Géotechnique,* 28, 1-25.

Perez, J. L., Kwok, C. and Senetakis, K. (2016). "Effect of rubber size on the behaviour of sand-rubber mixtures: A numerical investigation." *Comput. Geotech.,* 80, 199-214.

Qi, Y. and Indraratna, B. (2020). "Energy-based approach to assess the performance of a granular matrix consisting of recycled rubber, steel-furnace slag, and coal wash." *J. Mater. Civ. Eng,* 32, 04020169.

Qi, Y., and Indraratna, B. (2021). "The influence of rubber inclusion on the dynamic response of rail track." *J. Mater. Civ. Eng.,* 34(2), 04021432.

Qi Y, Indraratna, B. and Tawk, M. (2020). "Use of Recycled Rubber Elements in Track Stabilisation." *Proc Geo-Congress 2020 conf.,* 49-59. Reston: American Society of Civil Engineers.

Qi Y, Indraratna, B. and Vinod, J.S. (2018). "Behavior of steel furnace slag, coal wash, and rubber crumb mixtures with special relevance to stress–dilatancy relation*." J. Mater.Civ. Eng.,* 30, 04018276.

Qian, Y., Lee, S.J., Tutumluer, E., Hashash, Y.M., Mishra, D. and Ghaboussi, J. (2013). "Simulating ballast shear strength from large-scale triaxial tests: Discrete element method." *Transp. Res. Rec.,* 2374, 126-135.

Raymond, G.P., Gaskin, P.N. and Svec, O. (1978). "Selection and performance of railroad ballast." *Railroad track mechanics and technology.* Elsevier.

Raymond, G.P. and Williams, D.R. (1978). "Repeated load triaxial tests on a dolomite ballast". *J. Geotech. Eng. Div.,* 104, 1013-1029.

Remennikov, A., Kaewunruen, S., and Ikaunieks, K. (2006). “Deterioration of dynamic rail pad characteristics.” *Proc., Conf. on Railway Engineering,* Melbourne, Australia.

Roscoe, K.H., Schofield, A. and Wroth, A.P. (1958). “On the yielding of soils.” *Géotechnique,* 8, 22-53.

Rowe, P.W. (1962). “The stress-dilatancy relation for static equilibrium of an assembly of particles in contact.” *Proc. Royal Society of London. Series A. Mathematical and Physical Sciences,* 269, 500-527.

Salim, W. (2004). “Deformation and degradation aspects of ballast and constitutive modeling under cyclic loading,” Doctoral dissertation., Univ. of Wollongong, Australia.

Salim, W. and Indraratna, B. (2004). “A new elastoplastic constitutive model for coarse granular aggregates incorporating particle breakage.” *Can. Geotech. J.,* 41, 657-671.

Schanz, T. and P. Vermeer. (1996). "Angles of friction and dilatancy of sand." *Géotechnique,* 46(1): 145-151.

Schanz, T., Vermeer, P.A. and Bonnier, P.G. (2019). “The hardening soil model: formulation and verification.” *Beyond 2000 in Computational Geotechnics.,* pp. 281-296.

Schofield, A.N. and Wroth, P. (1968). “Critical state soil mechanics”, McGraw-hill London.

Selig, E. T., and Waters, J. M. (1994). Track technology and substructure management, Thomas Telford, London.

Senetakis, K., Anastasiadis, A. and Pitilakis, K. (2012). “Dynamic properties of dry sand/rubber (SRM) and gravel/rubber (GRM) mixtures in a wide range of shearing strain amplitudes.” *Soil Dyn. Earthq. Eng,* 33, 38-53.

Shenton, M. (1978). “Deformation of railway ballast under repeated loading conditions”. Railroad track mechanics and technology. *Elsevier.*

Shenton, M. (1985). “Ballast deformation and track deterioration”. *Track technology,* 253-265.

Siddique, R. and Naik, T.R. (2004). “Properties of concrete containing scrap-tire rubber–an overview.” *Waste management,* 24, 563-569.

Sidhu, K.S., Keeslar, F.L. and Warner, P.O. (2006). “Potential health risks related to tire fire smoke*.” Toxicol. Int,* 13(1), 1-17.

Sol-sánchez, M., Moreno-navarro, F., and Rubio-gámez, M. (2014). “The use ofdeconstructed tires as elastic elements in railway tracks.” *Materials,* 7, 5903-5919.

Sol-Sanchez, M., Moreno-Navarro, F., and Rubio-Gámez, M. C. (2015). “A study into the use of crumb rubber in railway ballast.” *Constr. Build. Mater.,* 75, 19-24.

Song, W., Huang, B., Shu, X., Wu, H., Gong, H., Han, B., and Zou, J. (2019). “Improving damping properties of railway ballast by addition of tire-derived aggregate.” *Transp. Res. Rec.,* 2673, 299-307.

Suiker, A.S.J. (2002). “The mechanical behaviour of ballasted railway tracks.” *Delft University Press,* Netherlands

Sun, Q. (2015). “An elasto-plastic strain-based approach for analysing the behaviour of ballasted rail track.” Doctoral dissertation, Univ. of Wollongong, Australia.

Sun, Q., Indraratna, B., and Nimbalkar, S. (2014). “Effect of cyclic loading frequency on the permanent deformation and degradation of railway ballast.” *Géotechnique,* 64, 746-751.

Sun, Q.D., Indraratna, B. and Nimbalkar, S. (2016). “Deformation and degradation mechanisms of railway ballast under high frequency cyclic loading*.” J. Geotech. Geoenv. Eng.,* 142.

Sweere, G. (1990). “Unbound granular bases for roads:” Doctoral dissertation, University of Delft, Holland, 1990.-429 p.

T HR TR 00192 ST Ballast - Transport for NSW (2018)., Transport Asset Standard Austhority, NSW Australia.

T HR CI 12111 SP Earthwork Materials - Transport for NSW (2018)., Transport Asset Standard Austhority, NSW Australia.

Tawk, M., Qi, Y., Indraratna, B., Rujikiatkamjorn, C., and Heitor, A. (2021). “Behavior of a Mixture of Coal Wash and Rubber Crumbs under Cyclic Loading.” *J. Mater. Civ. Eng.,* 33, 04021054.

Tennakoon, N.C. (2012). “Geotechnical study of engineering behaviour of fouled ballast.” Doctoral Dissertation, Univ. of Wollongong, Australia.

Thakur, P.K., Vinod, J.S. and Indraratna, B. (2013). “Effect of confining pressure and frequency on the deformation of ballast.” *Géotechnique,* 63(9), pp.786-790.

Tian, Y., Kasyap, S. S. and Senetakis, K. (2021). “Influence of loading history and soil type on the normal contact behavior of natural sand grain-elastomer composite interfaces.” *Polymers,* 13, 1830.

Tian, Y. and Senetakis, K. (2021). “Influence of creep on the small-strain stiffness of sand–rubber mixtures.” *Géotechnique,* 1-12.

Thakur, P.K., Vinod, J.S. and Indraratna, B., (2013). “Effect of confining pressure and frequency on the deformation of ballast”. *Géotechnique,* 63(9), 786-790.

Trinch, V.N., Tang, A.M., Cui, Y.J., Dupla, J.C., Canou, J., Calon, N., Lambert, L., Robinet, A. and Schoen, O. (2012). “Mechanical characterisation of the fouled ballast in ancient railway track substructure by large-scale triaxial tests.” *Soils. found,* 52, 511-523.

Tyre Stewardship Australia. (2020). Used tyres supply chain and fate analysis. Randell Environmental Consulting Pty Ltd. Victria, Australia.

Ueng, T.S. and Chen, T.J. (2000). “Energy aspects of particle breakage in drained shear of sands.” *Géotechnique,* 50, 65-72.

Varadarajan, A., Sharma, K., Venkatachalam, K. and Gupta, A. (2003). “Testing and modeling two rockfill materials.” *J. Geotech. Geoenv. Eng.,* 129, 206-218.

Wettschureck, G., Heim, M. and Tecklenburg, M. (2002). “Long-term properties of Sylomer® ballast mats installed in the rapid transit railway tunnel near the Philharmonic Hall of Munich, Germany.” *Rail engineering international*, 31(4), pp.6-11.

Werkmeister, S., Dawson, A. R., and Wellner, F., (2005). “Permanent deformation behaviour of granular materials.” *Road. Mater. Pavement Des.,* 6(1), 31–51.

Xu, M. and Song, E. (2009). “Numerical simulation of the shear behavior of rockfills.” *Comput. Geotech.,* 36**,** 1259-1264.

Youwai, S. and Bergado, D.T. (2003). “Strength and deformation characteristics of shredded rubber tire sand mixtures”. *Can. Geotech. J.,* 40, 254-264.

APPENDIX A: Calculation of Material Quantities for the Specimens

The specific gravity of RIBS (G_s)

$$G_s = \frac{1}{\left(\frac{(1 - R_b\%)}{G_B}\right) + \frac{R_b\%}{G_R}} \tag{A.1}$$

where $G_B = 2.8$ and $G_R = 1.15$ are the specific gravity of ballast and rubber respectively. $R_b\%$ is the percentage of rubber by weight of the RIBS mix.

The particle dry density γ_d is defined as:

$$\gamma_d = \frac{G_s \gamma_w}{(1 + e)} \tag{A.2}$$

where γ_w and e are density of water and the initial void ratio of the mix.

The total mass of the RIBS mix (m_t) can be calculated from Equation A.3

$$m_t = \gamma_d V_t \tag{A.3}$$

where V_t is the volume of the 300 mm diameter and 600 mm high specimen

Firstly, a pure ballast specimen was prepared with sufficient compaction. Then the total pure ballast aggregate weight of the sample (m_b) was measured. Then the initial void ratio e was calculated ($e = 0.824$). Required mass of the rubber aggregates (m_r) and mass of the ballast aggregates (m_b) for RIBS specimens with different $R_b\%$ were back

calculated using above equations by maintaining $e = 0.824$ same as the pure ballast specimens.

The calculated masses of rubber and ballast aggregates in each specimen, density and the specific gravities of the mixtures were presented in Table A.1.

Table A.1 Initial specific gravity, density and masses of aggregates

R_b%	G_s	m_b (kg)	m_r (kg)	m_t (kg)	γ_d (kg/m^3)	e
0	2.8	65.1	0	65.1	1535	0.824
5	2.61	57.7	3.04	60.8	1432	0.824
10	2.45	51.3	5.7	57.0	1342	0.824
15	2.30	45.6	8.04	53.6	1263	0.824

APPENDIX B: Design Calculations of RIBS Track

B.1 Track design parameters

Track design is performed according to the book, Ballast railroad design-SMART approach by Indraratna and Ngo (2018). Table B.1 shows the design parameters used in the design based on test data and also the site investigation.

Table B.1 Design parameters

Track Detail	Parameters
Sleepers	Width = 0.25 m, Length =2.5 m, Height= 0.23 m Spacing (S)=0.6 m
Ballast	Density =1560 kg/m^3, Friction angle = 48°, $E_{Ballast}$=250 MPa, Resilient modulus = 275 MPa, Layer thickness = 0.25 m
RIBS	Density =1442 kg/m^3, Friction angle = 47.5°, E_{RIBS}=150 MPa, Resilient modulus=200MPa, Layer thickness=0.25m
Subballast (Capping)	Density =1670 kg/m^3, Friction angle = 35°, $E_{subballast}$=115 MPa, Layer thickness = 0.2 m,
Subgrade	Density =1730 kg/m^3, Friction angle = 20°, $E_{subgrade}$ = 25 MPa, c =10 kPa, Layer thickness = 1.5 m, Subgrade soil compressive strength = 85 kPa, Allowable subgrade plastic strain, ε_p=2%, Allowable settlement = 0.025 m
Loading condition	Wheel dia(D) =1.016 m, Axle load = 25 t, Train speed (V) = 80 Km/h, Number of cycles used for the design (N) = 4000,000, Axle spacing=1.9 m

B.2 Design of RIBS section

B.2.1 Bearing capacity check for RIBS

$$K_p = \frac{1+\sin(47.5)}{1-\sin(47.5)} = 6.613$$

$$N_q = K_p \times e^{(\pi tan\varphi)} = 203.86$$

$$N_\gamma = (N_q - 1)\tan(1.4\varphi) = 466.54$$

Shape factor, $S_\gamma = 1 + 0.1\, K_p \times (\mathrm{B/L}) = 1 + 0.1 \times 6.613 \times \frac{0.25}{2.5} = 1.066$

Therefore, the ultimate bearing capacity, (q_{ult});

$$q_{ult} = 0.5\gamma B N_\gamma S_\gamma = 0.5 \times 14.32 \times 0.25 \times 466.54 \times 1.066 = 896.55 \text{ kPa}$$

Stresses on ballast;

Dynamic amplification factor, $IF = 1 + 5.21\, V/D = 1 + 5.21 \times 80/1016 = 1.41$

Input axle load, $P_s = 9.81 \times (25/2) \times 1000 = 122.63\ kN$

Dynamic wheel load, $P = P_s \times IF = 1.41 \times 122.63 = 172.93\ kN$

$$D_f = 0.45 + 5.77 \times 10^{-4} \times S = 0.45 + 5.77 \times 10^{-4} \times 600 = 0.7962$$

Rail seat load, $q_r = D_f \times P = 0.7962 \times 172.9 = 137.69\ kN$

Effective sleeper area $= Sleeper\ width \times Sleeper\ length\ /3$

$$= 0.25 \times 2.5/3 = 0.2083$$

Equivalent dynamic stress = $137.69/0.2083 = 660.9\ kPa$

Check for the factor of safety for the bearing capacity, (FoS);

$FoS = Ultimate\ bearing\ capacity/Equivalent\ dynamic\ stress$

$$FoS = 896.55/660.9 = 1.36 > 1.2; Satisfied$$

B.2.2 Granular layer thickness for RIBS section

Calculations are made to determine the minimum thickness of granular layers

(RIBS layer thickness + Subballast layer thickness)

Design Axle load= $25\ t$

Static wheel load= $122.63\ kN$

Number of load cycles; $N = 4000{,}000$

Parameters for plastic shear strain (According to Li and Selig (1998)),

Table B.2 Parameters for plastic shear strain (Adopted from Li and Selig (1998))

Soil type	a	b	m
CH (fat clay)	1.20	0.18	2.40
CL (lean clay)	1.10	0.16	2.00
MH (elastic silt)	0.84	0.13	2.00
ML (silt)	0.64	0.10	1.70

Method 1

Based on the conducted laboratory tests, the subgrade soil is on the border of CL-ML.

For ML type soil,

$a = 0.64, b = 0.1, m = 1.7$

Subgrade soil type = (ML type) uncontrolled fill, Soil thickness $= 1.5\ m,\ \varepsilon_p = 2\%$

Subgrade compressive strength,(σ_s)

$$\sigma_s\ =\ 85\ kPa$$

Allowable deviator stress on subgrade (σ_{da}),

$$\sigma_{da}=\sigma_s\ \left[\left(\frac{\varepsilon_p}{aN^b}\right)^{1/m}\right] = 85 \times \left[\left(\frac{2}{0.64\times 4000000^{0.1}}\right)^{1/1.7}\right] =\ 67.9\ kPa$$

Train speed, (V)

$$V = 80\ km/hr$$

Design dynamic wheel load, $P_d = (1 + \frac{5.2V}{D})P_s = (1 + \frac{5.2\times80}{1016}) \times 122.63 = 173\ kN$

Area factor $= 0.645$

Strain influence factor, $I_\varepsilon = \frac{\sigma_{da}}{p_d} = \frac{67.9}{173} \times 0.645 = 0.252$

Resilient modulus of RIBS $= 250\ MPa$

Subgrade modulus $=\ 25\ MPa$

Referring the design chart for prevailing progressive shear failure by Li and Selig (1998)

$$H/L = 2.5, L = Length\ factor = 0.152$$

$$H = 2.5 \times 0.152 = 0.38\ m\ = 380\ mm$$

Calculation for granular layer thickness (Method 2)

S_a=allowable settlement $= 25\ mm$

Influence factor, $I_{pa} = \left[\frac{\frac{S_a}{L}}{a\left(\frac{P_d}{\sigma_S A}\right)^m N^b}\right] \times 100 = \left[\frac{\frac{0.025}{0.152}}{0.64\left(\frac{173}{67.9\times0.645}\right)^{1.7} \times 4000000^{0.1}}\right] \times 100 =\ 0.798$

Referring the design chart for granular layer thickness, preventing excessive plastic deformations by Li and Selig (1998);

Subgrade thickness $= 1.5\ m$

$$T/L = 1.5/0.152 =\ 9.87$$

$$H/L =\ 1$$

$$H = 1 \times 0.152 = 152\ mm$$

H (design)= maximum of H from Method 1 and Method 2 is 380 mm

Required minimum granular layer thickness $=\ 380\ mm$

Provided granular layer thickness= RIBS layer thickness + Subballast layer thickness

$$= 250 + 200\ mm\ = 450\ mm\ >\ 380; Satisfied$$

B.2.3 Elastic settlement of granular layer of the RIBS section

Elastic settlement of ballast and subballast layers

$$\bar{E} = \frac{H_b + H_c}{\frac{H_b}{E_b} + \frac{H_c}{E_c}} = 132.13\ MPa$$

Equivalent dynamic stress at sleeper ballast interface $= 660.89\ kPa$

Average strain of substructure $\varepsilon_{avg} = \sigma_{dyn}/E_{eq} = 0.5\%$

Settlement of the ballast and subballast layers $= 0.5 \times (250 + 200)/100 = 2.25\ mm$

B.3 Subgrade analysis

B.3.1 Bearing capacity check for subgrade

For the bearing capacity check, a half-track in the transverse direction is considered due to the symmetry of the track (Figure B.1)

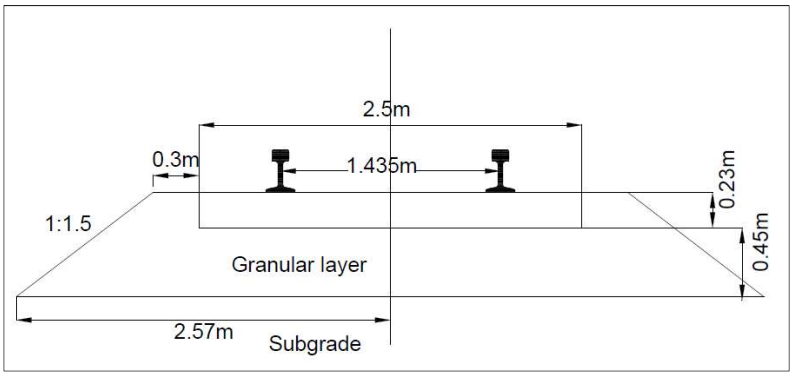

Figure B.1 Track symmetry and width of the subgrade loading

$$K_p = \frac{1 + sin(20)}{1 - sin(20)} = 2.04$$

$$N_q = K_p \times e^{(\pi tan\varphi)} = 6.4$$

$$N_\gamma = (N_q - 1)tan\ (1.4\varphi) = 2.87$$

$$N_c = (N_q - 1)tan\ (\varphi) = 14.8$$

Shape factor $S_\gamma = 1 + 0.1\ K_p(B/L)\ = 1 + 0.1 \times 6.79 \times \frac{0.25}{2.5} = \ 1.52$

Width of the loading $= 2.57\ m$

Therefore, the ultimate bearing capacity:

$$q_{ult} = cNc + 0.5\gamma BN_\gamma S_\gamma = \ 0.5 \times 17.3 \times 2.57 \times 2.87 \times 1.52 = \ 245.6\ kPa$$

Stresses on subgrade;

Stresses on top of the subgrade include vertical stresses by superstructure components and the vertical stress by train dynamic loads (Figure B.2).

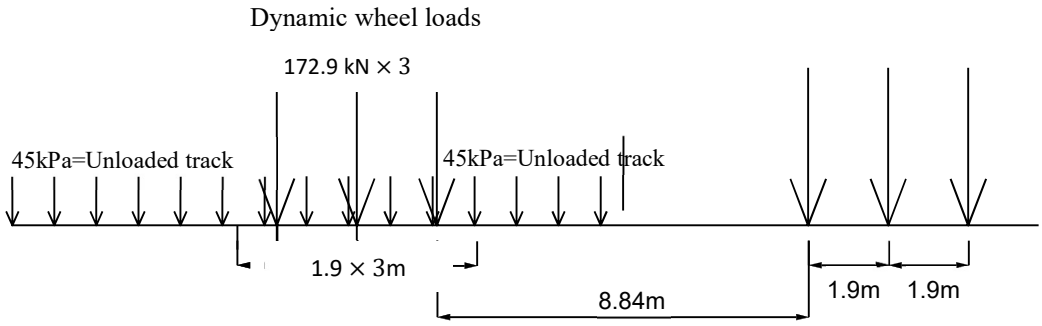

Figure B.2 Diagram of loads (track section from the longitudinal direction)

Vertical stresses caused by superstructure components (unloaded track) $= 45\ kPa$ (Lackenby, 2006)

Design dynamic wheel load, $P_d\ = \ (1 + \frac{5.2V}{D})P_S\ = \ (1 + \frac{5.2\times80}{1016}) \times 122.63 = 172.9\ kN$

Axle spacing $= 1.9\ m$

Dynamic load per meter run $= (172.9 \times 3)/(1.9 \times 3)\ = \ 91\ kN/m$

Load bearing subgrade width (considering symmetry) $= \ 2.57\ m$ (Figure A.4)

Stress due to the wheel loads on the subgrade $= \ 91/2.57\ = 35.41\ kPa$

Total stress on top of the subgrade $= \ (45 + 35.41)\ = 80.41\ kPa$

Figure A.6 shows the vertical stress distribution diagram from the FEM analysis.

Total stress on top of the subgrade from the FEM analysis, $= 75.2\ kPa$

Calculations and the FEM analysis gives comparable values for the total stress on the subgrade tope ($80.41kPa$ and $75.21\ kPa$).

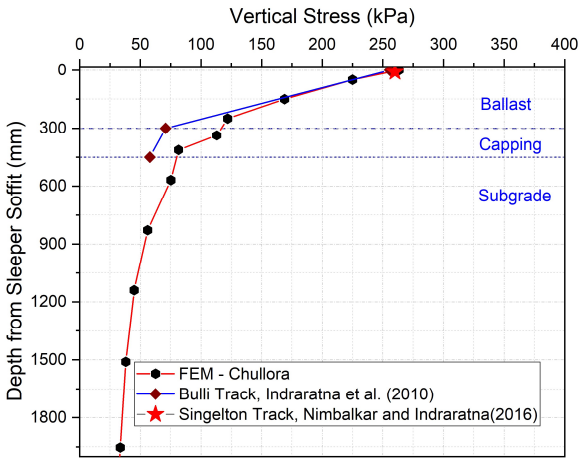

Figure B.3 Vertical stress distribution under the track

Check for the factor of safety for the bearing capacity

$$FoS = Ultimate\ bearing\ capacity/\ Maximum\ vertical\ stresses\ on\ \ subgrade$$

$$FoS\ =\ 245.6/80.41 = 3.0\ ;\ Satisfied$$

Note that soil compaction and surcharge loading during the construction will further increase the subgrade properties.

B.3.2 Elastic settlement of the subgrade

Stress on the subgrade, $\sigma_{sub}\ = 80.1\ kPa$

Elastic modulus $= 25\ MPa$

Using the Boussinesq chart (Figure B.4) for continuous loading (Figure A.8);

When the loading width is 'B';

$$B/2 = 2.57m$$

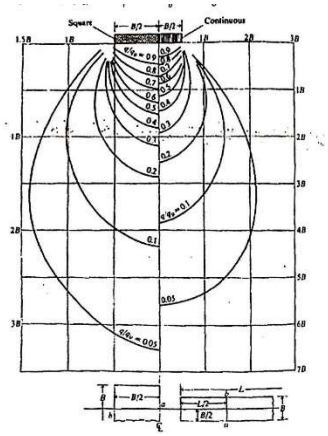

Figure B.4 Boussinesq stress contours under the square and continues loading

1.5 m of subgrade thickness was considered for the analysis (Considering Borehole data). 1.5 m below the subgrade is stiff weathered shale.

Table B.3 Boussinesq parameters and elastic settlement

	Thickness(m)	**Z (m)**	**z/B**	**I**	**σ_z=I×σ**	**ε %**	**Elastic settlement**
Subgrade	1.5	0.75	0.292	0.8	64.33	0.257	3.86 mm

Here, Z, I and ε represent the depth from the ground level, impact factor and the elastic strain respectively.

B.3.3 Predicted long-term settlement of conventional ballast track and RIBS track

Here the logarithmic relationship proposed by Salim, (2004) is used for settlement analysis of ballast track.

S= $a + b \times ln(N)$, here $a = 2.94$ and b=0.56 for unreinforced ballast.

Table B.4 Long-term settlements

Number of cycles (*N*)	**Settlement (mm)**
100	5.5
1000	6.8
10,000	8.1
100,000	9.4
500,000	10.3
4,000,000	11.5

According to the design calculations, the control section is constructed with conventional ballast and the RIBS track is safe for bearing capacity and settlements.